Electronic Supplementary Material (ESI) for Chemical Communications.

Supporting Information

Appropriation of Group II Metals: Synthesis and Characterisation of the first Alkaline Earth Metal supported Transition Metal Carbonite Complexes

Siad Wolff, Annabelle Ponsonby, André Dallmann, Christian Herwig, Beatrice Cula, Fabian Beckmann, Christian Limberg

Table of content

1. General Considerations.

All manipulations were carried out under an argon atmosphere using Schlenk techniques or in glove boxes under either dinitrogen or argon atmospheres maintained below 1 ppm of O_2 and H_2O. Glassware was heated under vacuum for approx. 10 min using a heat gun at 650 °C prior to use. Solvents were used purified from an MBraun solvent purification system (SPS). C_6D_6 and THF-d_8 were stored in a glove box and dried over 3 Å molecular sieves. NMR Spectra were recorded on Bruker NMR spectrometers (Avance DPX 300 MHz, Avance 400 MHz, Avance III 500 MHz). Chemical shifts are referenced to residual C_6D_5H (δ = 7.16 ppm) or THF-d_7 (δ = 5.32 ppm), labelled by '*' in the spectra unless otherwise stated. IR spectra were recorded on a Bruker ALPHA spectrometer with an ATR sampling unit. Elemental analyses were performed with a HEKA Euro 3000 elemental analyser.

All materials were obtained from commercial vendors as ACS reagent-grade or better and used as received, if not stated otherwise.

[L$^{t\text{Bu}}$NiCO$_2$Na], **I$^{\text{Na}}$**, was synthesised in-situ prior to use via mixing of [L$^{t\text{Bu}}$NiOOCH] and NaN(^{i}Pr)$_2$ in THF and used without further purification.[1] [L$^{t\text{Bu}}$NiOOCH],[2] [L$^{\text{Mes}}$Mg(Et$_2$O)I],[3] [L$^{\text{Dipp}}$Ca(Et$_2$O)I][3] and NaN(^{i}Pr)$_2$ [4-5] were prepared according to literature procedures. ^{13}C-labelled derivatives of the reported complexes were synthesised starting from [L$^{t\text{Bu}}$NiOO^{13}CH].[2]

For most of the presented complexes carbon values, collected during elemental analysis, were reproducibly below the range usually considered as acceptable, although crystalline material was analysed. The presented complexes are highly sensitive and quickly undergo decomposition, which may impede appropriate data collection. We refer to a recent study that is questioning the reasonableness of narrow deviation guidelines for elemental analysis.[6]

Table S1: Collected spectroscopic features of the carbonite ligands within the presented complexes.

	$\delta^{13}C_{CO2}$ (C_6D_6)	$\delta^{13}C_{CO2}$ (THF-d_8)	ν_{CO2}
1	172.5	168.8	1580
1´	-	169.4	-
2	172.8	171.0	1580
2´	-	171.2	-
2-18C6	171.4	-	1603
3	175.8	175.7	1577
4	-	171.0	-

2. Synthetic procedures

2.1 Synthesis of $[Mg(THF)_4(L^{tBu}NiCO_2)_2]$, 1

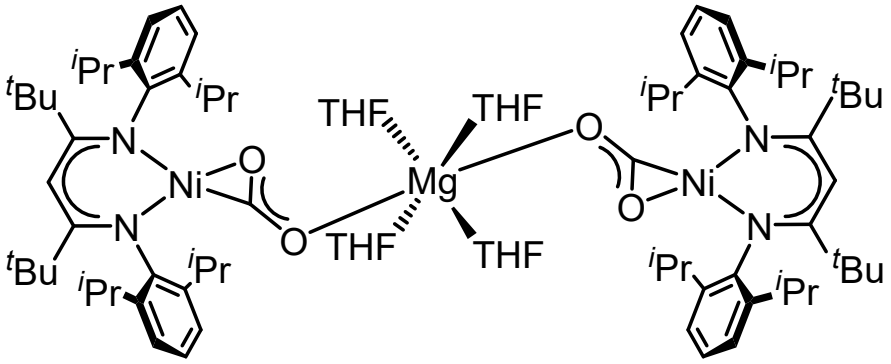

A mixture of [L^{tBu}NiOOCH] (72.6 mg, 0.12 mmol) and NaN(^{i}Pr)$_2$ (19.2 mg, 0.16 mmol) was dissolved in 3 mL of THF and stirred for 20 min. After evaporation of the solvent MgI_2 (33.4 mg, 0.12 mmol) was added together with 3 mL of THF. The suspension was stirred for another 15 min followed by removal of the solvent *in vacuo.* The remaining residue was extracted with hexane until the extracts became colourless. The combined organic phases were concentrated to approximately 2 mL. Storage at –30 °C caused formation of orange needle-like crystals of $[Mg(THF)_4(L^{tBu}NiCO_2)_2]$, **1**, (25.3 mg, 28%).

The obtained crystalline material was suitable for single crystal X-ray diffraction.

^{1}H-NMR (500 MHz, C_6D_6): δ (ppm) = 6.94-6.85 (m, 12 H, Ar-**H**), 5.38 (s, 2 H, C**H**$_{backbone}$), 4.12 (sept, J = 6.8 Hz, 4 H, C**H**$(CH_3)_2$), 4.03 (sept, J = 6.8 Hz, 4 H, C**H**$(CH_3)_2$), 3.20 (m, 16 H, THF), 1.82 (d, J=6.8 Hz, 12 H, CH(C**H**$_3)_2$), 1.74 (d, J=6.8 Hz, 12 H, CH(C**H**$_3)_2$), 1.46 (d, J=6.8 Hz, 12 H, CH(C**H**$_3)_2$), 1.44 (d, J=6.8 Hz, 12 H, CH(C**H**$_3)_2$), 1.34 (m, 16 H, THF), 1.28 (s, 18 H, C(C**H**$_3)_3$), 1.16 (s, 18 H, C(C**H**$_3)_3$).

^{1}H-NMR (600 MHz, THF-d_8): δ (ppm) = 6.74-6.64 (m, 12 H, Ar-**H**), 5.00 (s, 2 H, C**H**$_{backbone}$), 3.75 (sept, J = 6.8 Hz, 4 H, C**H**$(CH_3)_2$), 6.63 (sept, J = 6.9 Hz, 4 H, C**H**$(CH_3)_2$), 1.70 (d, J=6.9 Hz, 12 H, CH(C**H**$_3)_2$), 1.51 (d, J=6.8 Hz, 12 H, CH(C**H**$_3)_2$), 1.27 (d, J=6.9 Hz, 12 H, CH(C**H**$_3)_2$), 1.23 (d, J=6.9 Hz, 12 H, CH(C**H**$_3)_2$), 1.05 (s, 18 H, C(C**H**$_3)_3$), 0.9 (s, 18 H, C(C**H**$_3)_3$).

^{13}C NMR (125 MHz, C_6D_6): δ (ppm) = 172.50 (**C**O_2), 167.45 (N**C**-^{t}Bu), 166.09 (N**C**-^{t}Bu), 154.65 (Ar-**C**), 148.68 (Ar-**C**), 141.79 (Ar-**C**), 140.28 (Ar-**C**), 123.31 (Ar-**C**), 122.28 (Ar-**C**), 122.07 (Ar-**C**), 96.91 (γ-**C**), 68.70 (THF), 42.72 (**C**$(CH_3)_3$), 42.35 (**C**$(CH_3)_3$), 33.80 (C(**C**$H_3)_3$), 33.24 (C(**C**$H_3)_3$), 28.46 (**C**$H(CH_3)_2$), 28.26 (CH(**C**$H_3)_2$), 26.21 (CH(**C**$H_3)_2$), 25.23 (THF), 24.61 (CH(**C**H_3)2), 23.78 (CH(**C**$H_3)_2$), 23.63 (CH(**C**$H_3)_2$), 23.07 (CH(**C**$H_3)_2$).

^{13}C NMR (125 MHz, THF-d_8): δ (ppm) = 168.81 (**C**O_2), 166.90 (N**C**CH_3), 166.05 (N**C**CH_3), 155.56 (Ar-**C**), 149.66 (Ar-**C**), 141.78 (Ar-**C**), 140.63 (Ar-**C**), 123.27 (Ar-**C**), 123.17 (Ar-**C**), 122.73 (Ar-**C**), 122.37 (Ar-**C**), 96.98 (γ-**C**), 43.18 (**C**$(CH_3)_3$), 42.86 (**C**$(CH_3)_3$), 34.00 (C(**C**$H_3)_3$), 33.48 (C(**C**$H_3)_3$), 28.86 (**C**$H(CH_3)_2$), 28.72 (CH(**C**$H_3)_2$), 26.53 (CH(**C**$H_3)_2$), 26.43 (CH(**C**H_3)2), 23.92 (CH(**C**$H_3)_2$), 23.81 (CH(**C**$H_3)_2$).

ATR-IR (solid obtained from C_6D_6 solution): ν (cm^{-1}) = 3052 (w), 2957 (m), 2927 (w), 2903 (w), 2867 (w), 1580 (br, ν_{CO}), 1536 (w), 1512 (m), 1461 (w), 1433 (m), 1404 (s), 1366 (s) 1321 (s), 1251 (w), 1211 (m), 1195 (w), 1180 (w), 1161 (w), 1098 (m), 1031 (m), 935 (w), 919 (w), 883 (w), 803 (m), 759 (m), 496 (w).

Elemental analysis calc. (%) for $C_{88}H_{138}MgN_4Ni_2O_8$ (1521,78 g*mol^{-1}): C 69.46, H 9.14, N 3.79; found: C 66.10, H 8.87, N 3.68.

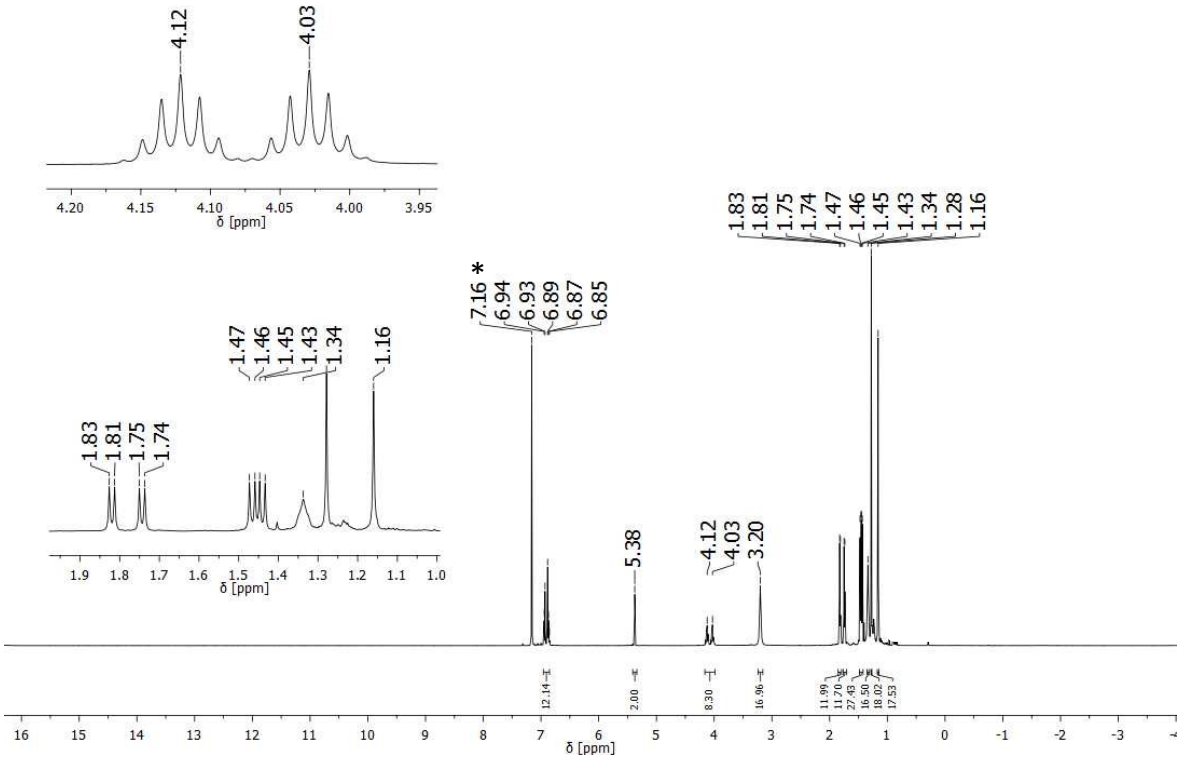

Figure S1: ^{1}H NMR (500.13 MHz, C_6D_6) spectrum of **1**.

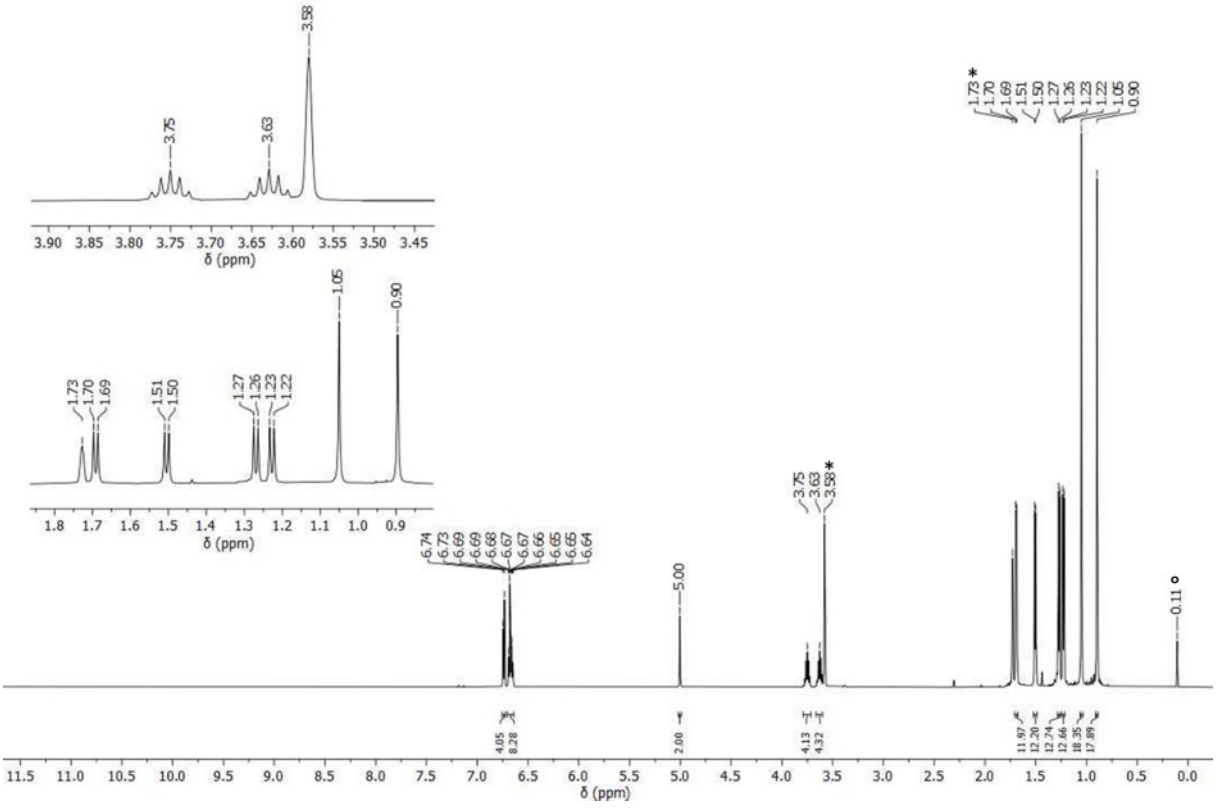

Figure S2: ^{1}H NMR (599.89 MHz, THF-d_8) spectrum of **1** (° = impurity of silicon grease).

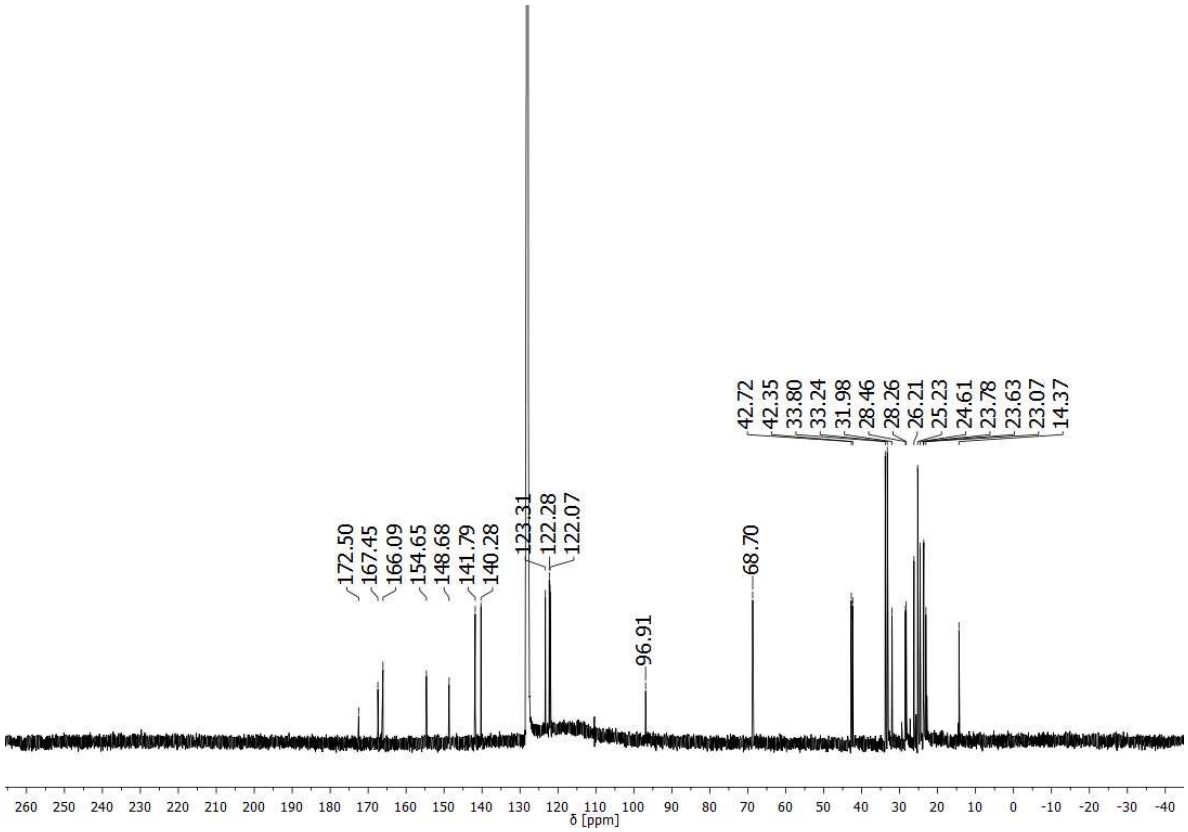

Figure S3: ^{13}C NMR (125.77 MHz, C_6D_6) spectrum of **1**.

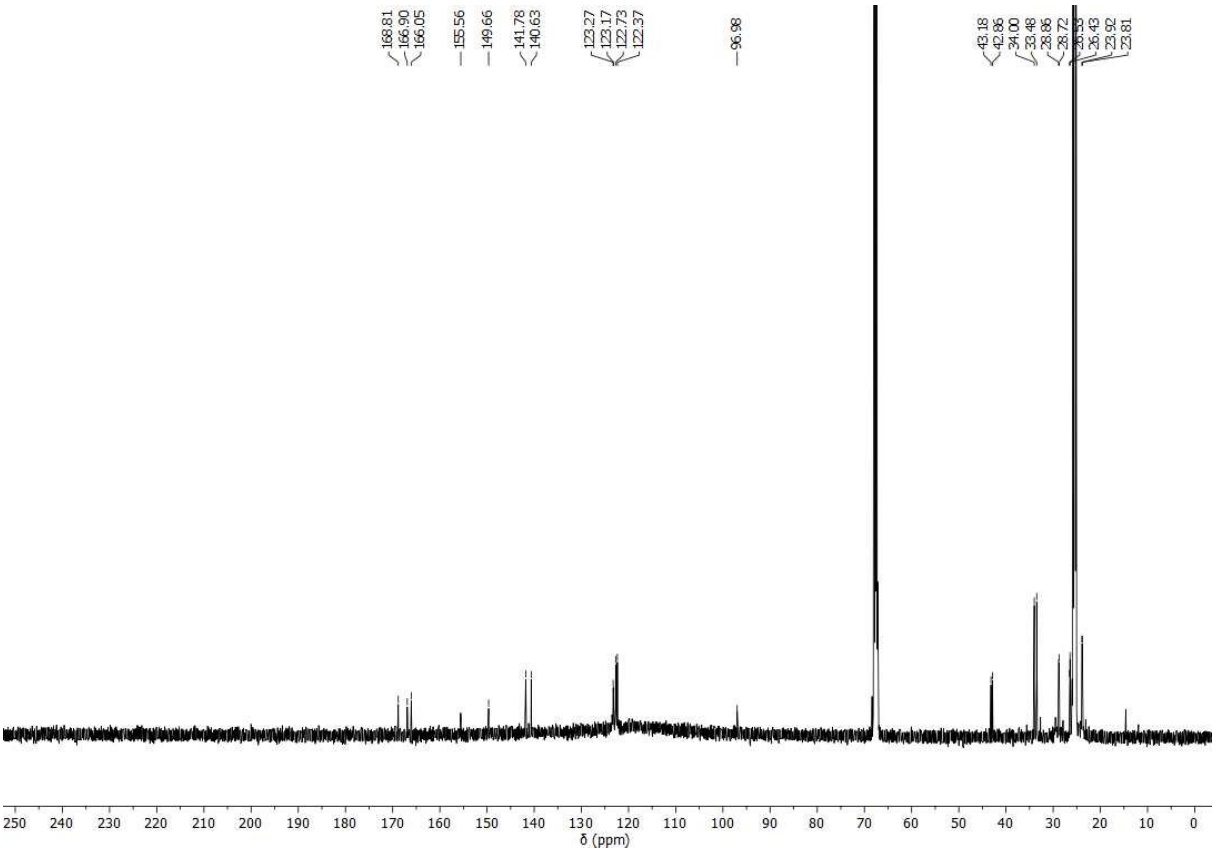

Figure S4: ^{13}C NMR (125.77 MHz, THF-d_8) spectrum of **1**.

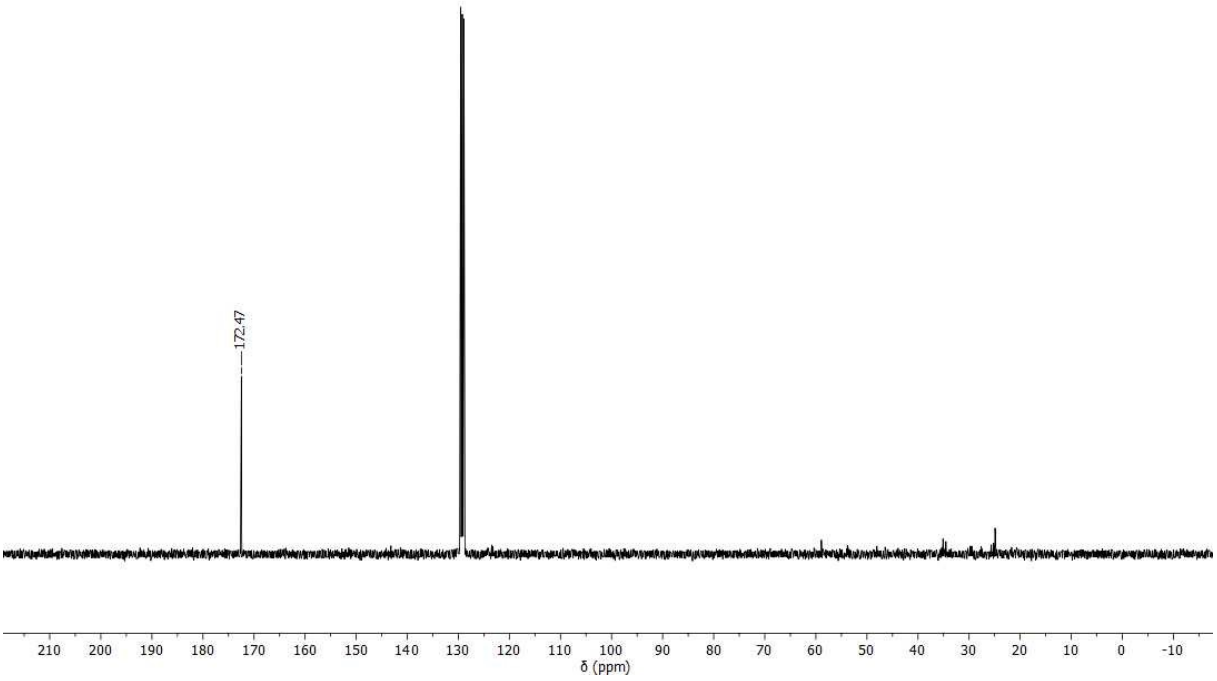

Figure S5: ^{13}C NMR (75.76 MHz, C_6D_6) spectrum of ^{13}**1**.

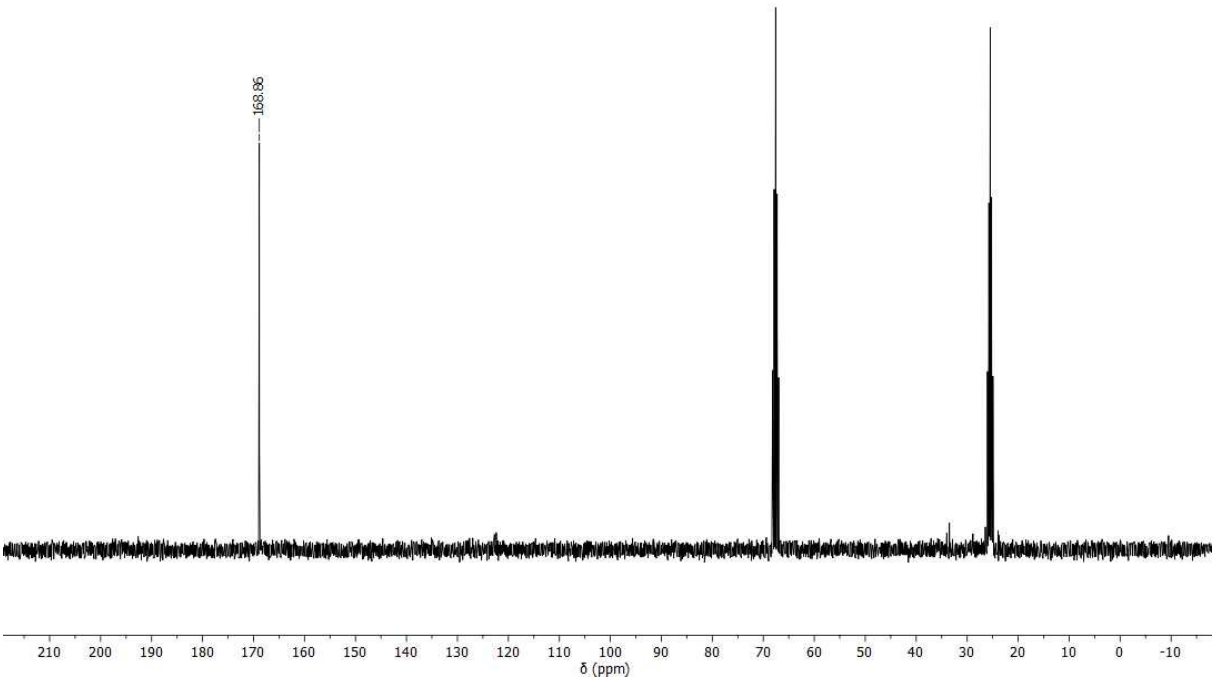

Figure S6: ^{13}C NMR (75.76 MHz, THF-d_8) spectrum of ^{13}**1**.

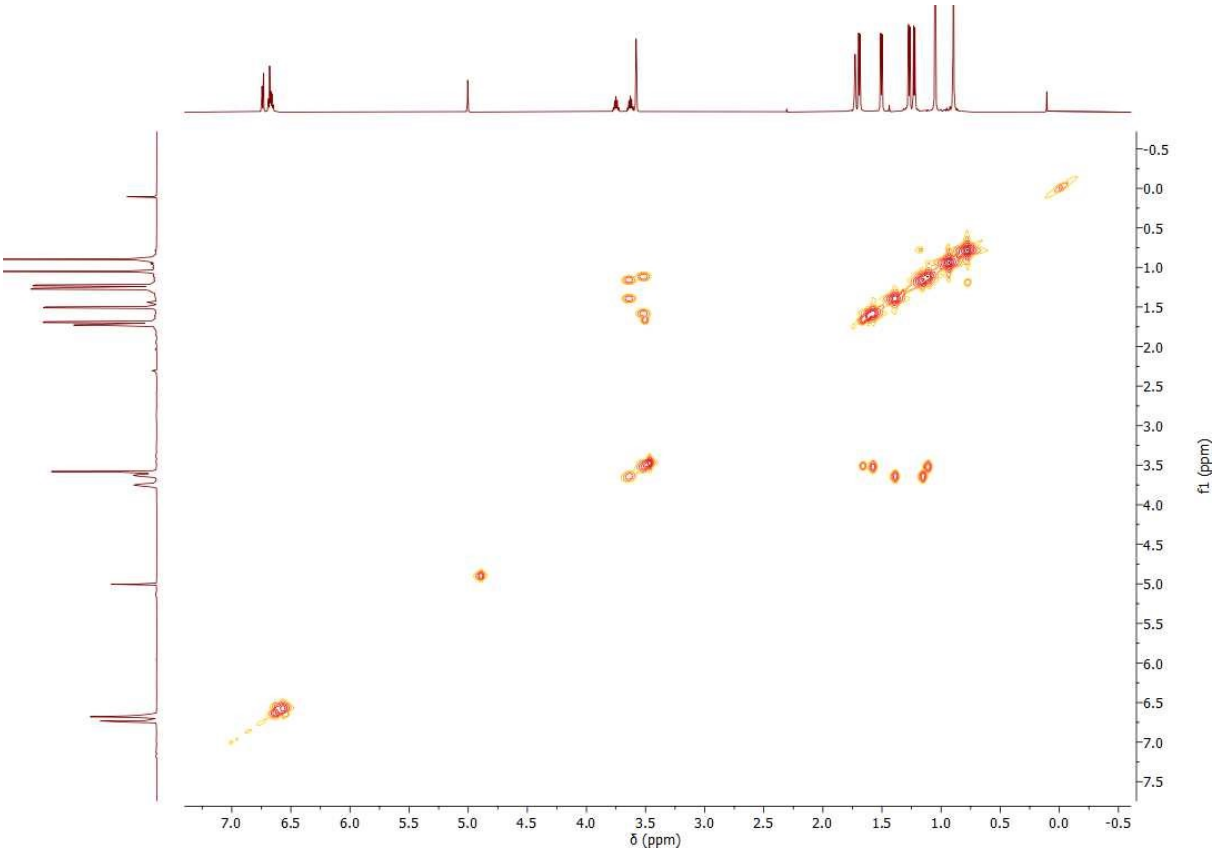

Figure S7: ^{1}H-^{1}H COSY NMR (500.13 MHz, THF-d_8) spectrum of **1**.

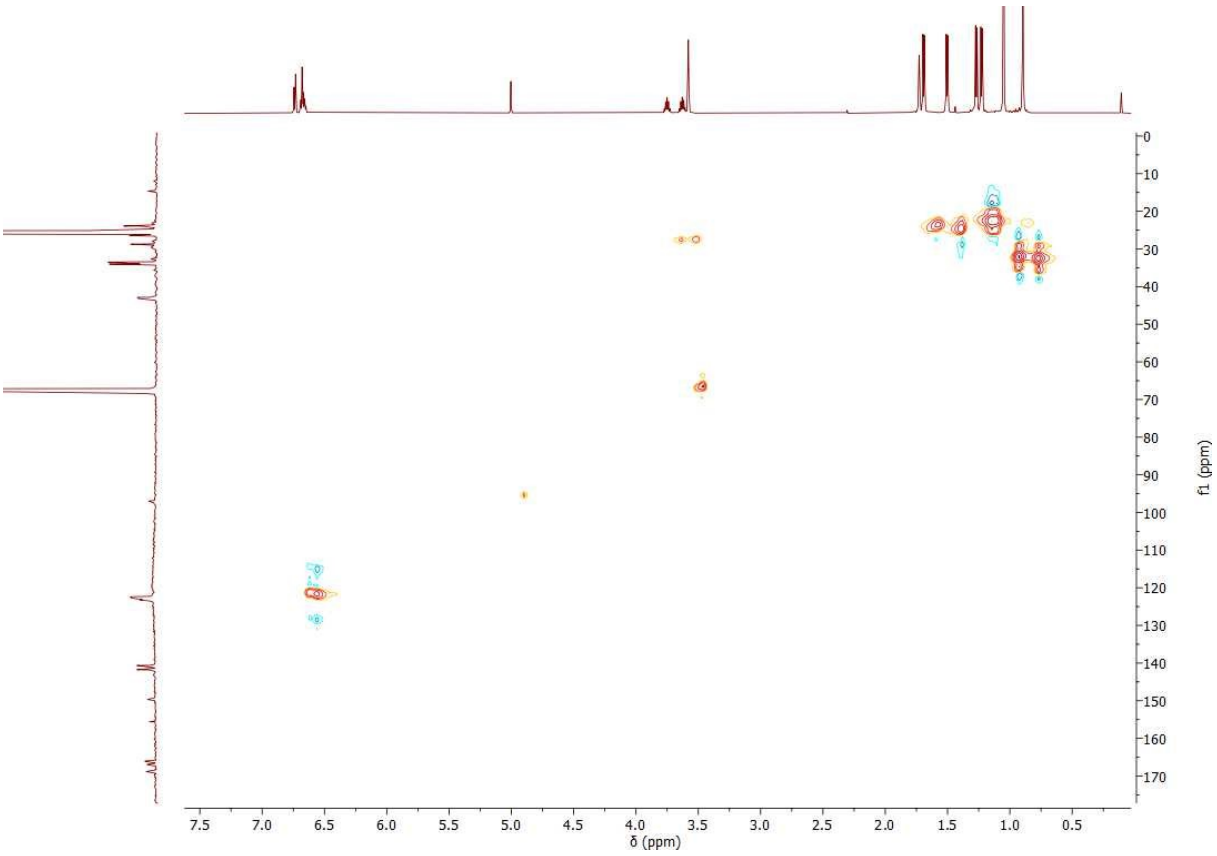

Figure S8: ^{1}H-^{13}C HSQC NMR (500.13 MHz, THF-d_8) spectrum of **1**.

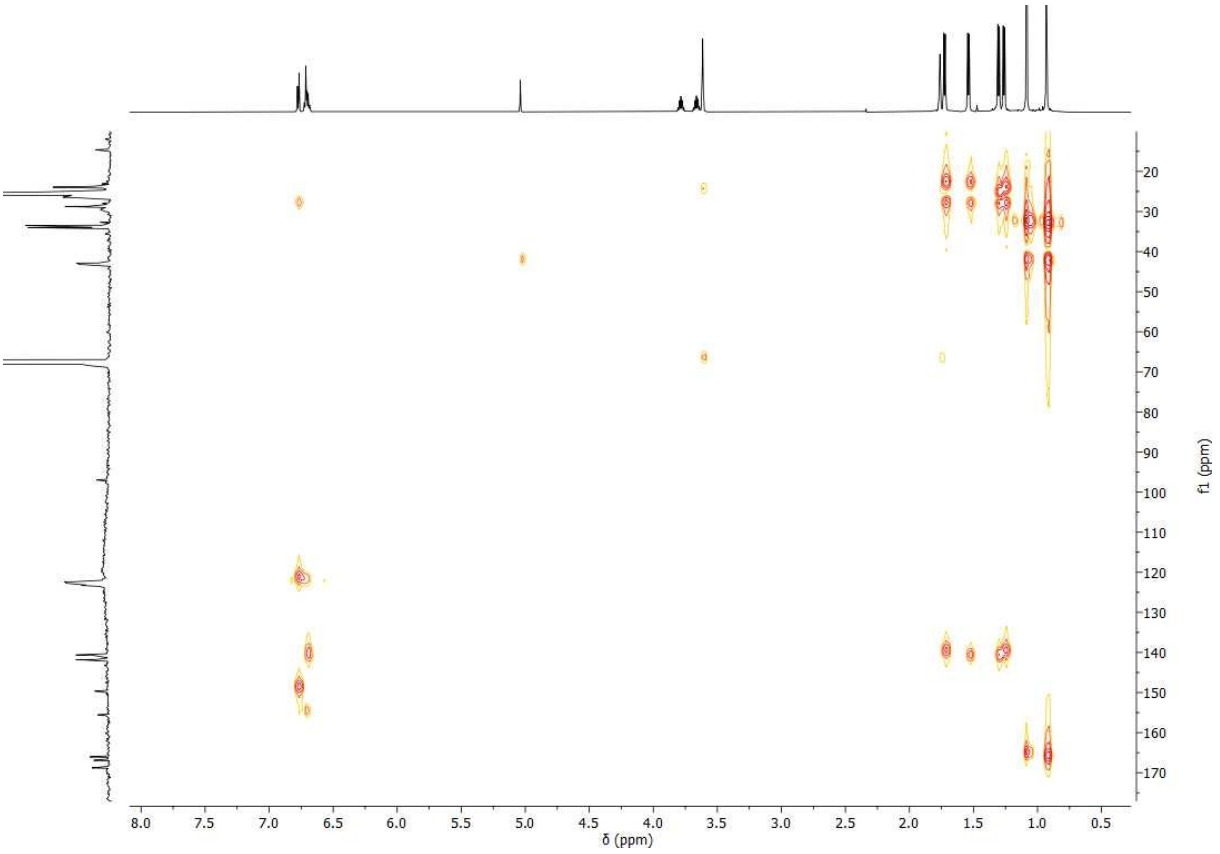

Figure S9: ^{1}H-^{13}C HMBC NMR (500.13 MHz, THF-d_8) spectrum of **1**.

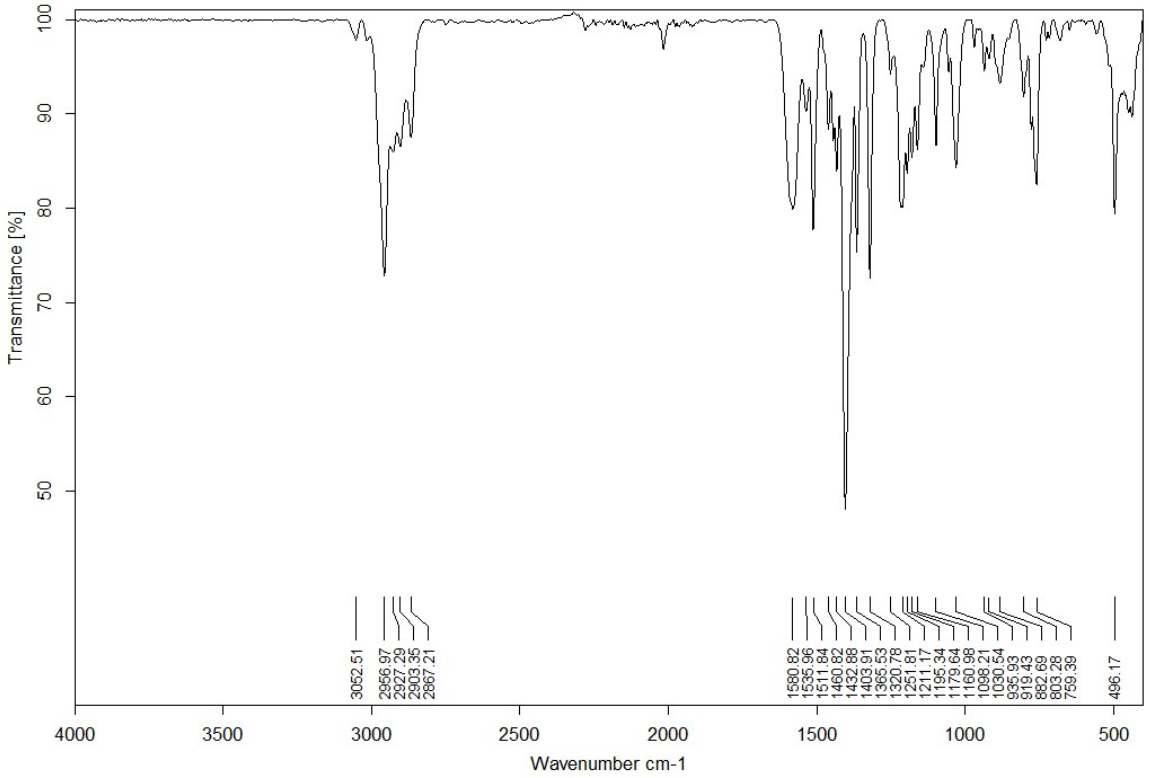

Figure S10: ATR-IR spectrum of **1** (solid obtained from C_6D_6 solution).

2.2 Synthesis of $[Ca(THF)_4(L^{tBu}NiCO_2)_2]$, 2

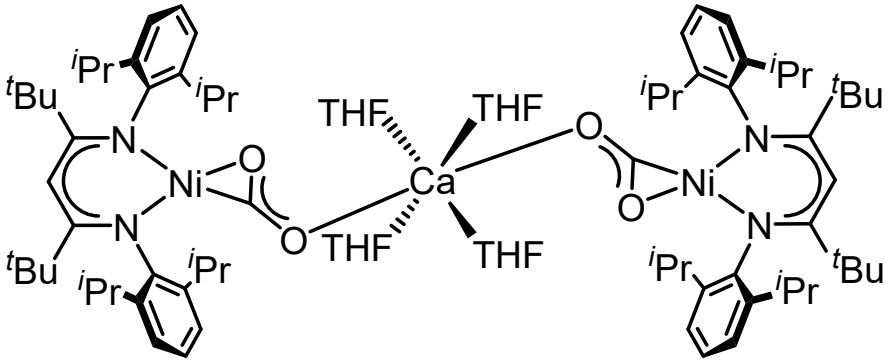

A mixture of [L^{tBu}NiOOCH] (72.6 mg, 0.12 mmol) and NaN(^{i}Pr)$_2$ (19.2 mg, 0.16 mmol) was dissolved in 3 mL of THF and stirred for 20 min. After evaporation of the solvent CaI_2 (35.3 mg, 0.12 mmol) was added together with 3 mL of THF. The suspension was stirred for another 15 min followed by removal of the solvent *in vacuo.* The remaining residue was extracted with hexane until the extracts became colourless. The combined organic phases were evaporated to dryness and were treated with 1 mL of THF causing the formation of an orange crystalline solid. Washing of the solid with hexane (three times 1 mL) followed by drying under reduced pressure afforded $[Ca(THF)_4(L^{tBu}NiCO_2)_2]$, **2**, as an orange solid (34.7 mg, 38%).

Crystals suitable for single crystal X-ray diffraction were grown via recrystallisation from hot THF.

Note: 2 exhibits a very poor solubility in organic solvents. Therefore, preparation of NMR samples of appropriate concentration was impeded. In case of THF-d_8 solubility was sufficient to record a ^{13}C NMR spectrum. However, some signals suffer from bad signal-to-noise ratios. 2D NMR experiments were conducted in order to ensure a correct assignment of all signals.

^{1}H-NMR (600 MHz, THF-d_8): δ (ppm) = 6.74-6.62 (m, 12 H, Ar-**H**), 5.00 (s, 2 H, C**H**$_{backbone}$), 3.77 (sept, J = 6.6 Hz, 4 H, C**H**$(CH_3)_2$), 3.72 (sept, J = 6.6 Hz, 4 H, C**H**$(CH_3)_2$), 1.59 (d, J=6.6 Hz, 12 H, CH(C**H**$_3)_2$), 1.51 (d, J=6.6 Hz, 12 H, CH(C**H**$_3)_2$), 1.28 (d, J=6.6 Hz, 12 H, CH(C**H**$_3)_2$), 1.24 (d, J=6.6 Hz, 12 H, CH(C**H**$_3)_2$), 1.06 (s, 18 H, C(C**H**$_3)_3$), 1.08 (s, 18 H, C(C**H**$_3)_3$).

^{1}H-NMR (500 MHz, C_6D_6): δ (ppm) = 6.95-6.86 (m, 12 H, Ar-**H**), 5.39 (s, 2 H, C**H**$_{backbone}$), 4.16 (sept, J = 6.8 Hz, 4 H, C**H**$(CH_3)_2$), 4.02 (sept, J = 6.8 Hz, 4 H, C**H**$(CH_3)_2$), 3.27 (m, 16 H, THF), 1.85 (d, J=6.8 Hz, 12 H, CH(C**H**$_3)_2$), 1.77 (d, J=6.8 Hz, 12 H, CH(C**H**$_3)_2$), 1.48 (d, J=6.8 Hz, 12 H, CH(C**H**$_3)_2$), 1.44 (d, J=6.8 Hz, 12 H, CH(C**H**$_3)_2$), 1.38 (m, 16 H, THF), 1.28 (s, 18 H, C(C**H**$_3)_3$), 1.19 (s, 18 H, C(C**H**$_3)_3$).

^{13}C NMR (125 MHz, THF-d_8): δ (ppm) = 170.96 (**C**O_2), 167.01 (N**C**-^{t}Bu), 165.76 (N**C**-^{t}Bu), 154.45 (Ar-**C**), 149.59 (Ar-**C**), 141.01 (Ar-**C**), 140.76 (Ar-**C**), 123.26 (Ar-**C**), 123.18 (Ar-**C**), 122.52 (Ar-**C**), 122.28 (Ar-**C**), 43.09 (**C**$(CH_3)_3$), 42.84 (**C**$(CH_3)_3$), 34.03 (C(**C**$H_3)_3$), 33.49 (C(**C**$H_3)_3$), 28.93 (**C**$H(CH_3)_2$), 28.65 (CH(**C**$H_3)_2$), 26.48 (CH(**C**$H_3)_2$), 25.98 (CH(**C**$H_3)_2$), 23.94 (CH(**C**$H_3)_2$), 23.86 (CH(**C**$H_3)_2$).

^{13}C NMR (76 MHz, C_6D_6): δ (ppm) = 172.78(^{13}**C**O_2).

ATR-IR (solid obtained from THF-d_8 solution): ν (cm^{-1}) = 3052 (w), 2957 (m), 2927 (w), 2904 (w), 2864 (w), 2244 (w, THF-d_8), 2079 (w, THF-d_8), 1580 (br, ν_{CO}), 1534 (w), 1510 (m), 1460 (w), 1433 (m), 1404 (s), 1364 (s) 1321 (s), 1259 (w), 1218 (m), 1195 (w), 1180 (w), 1176 (w), 1096 (m), 1046 (m), 935 (w), 897 (w), 800 (m), 757 (m), 544 (w).

Elemental analysis calc. (%) for $C_{88}H_{138}CaN_4Ni_2O_8$ (1537.56 g*mol^{-1}): C 68.74, H 9.05, N 3.64; found: C 65.87, H 8.76, N 3.56.

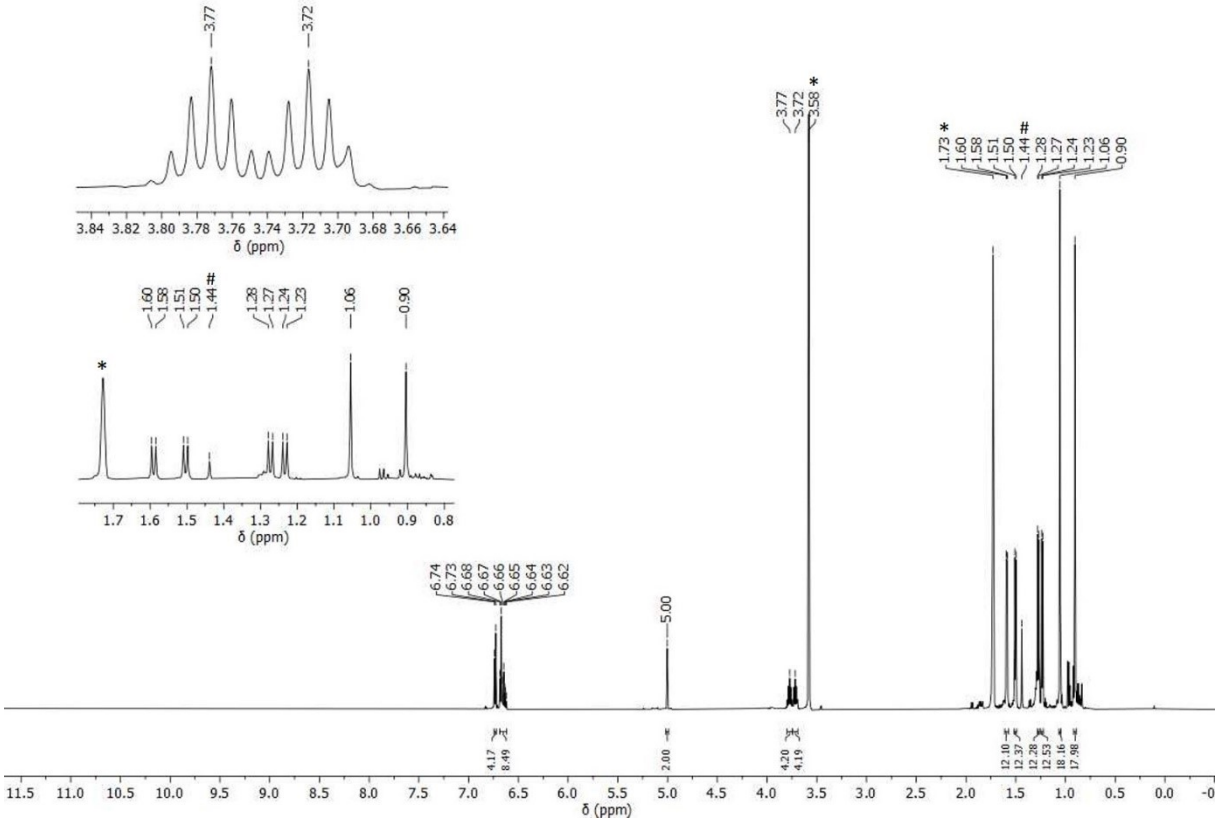

Figure S11: ^{1}H NMR (599.89 MHz, THF-d_8) spectrum of **2**.

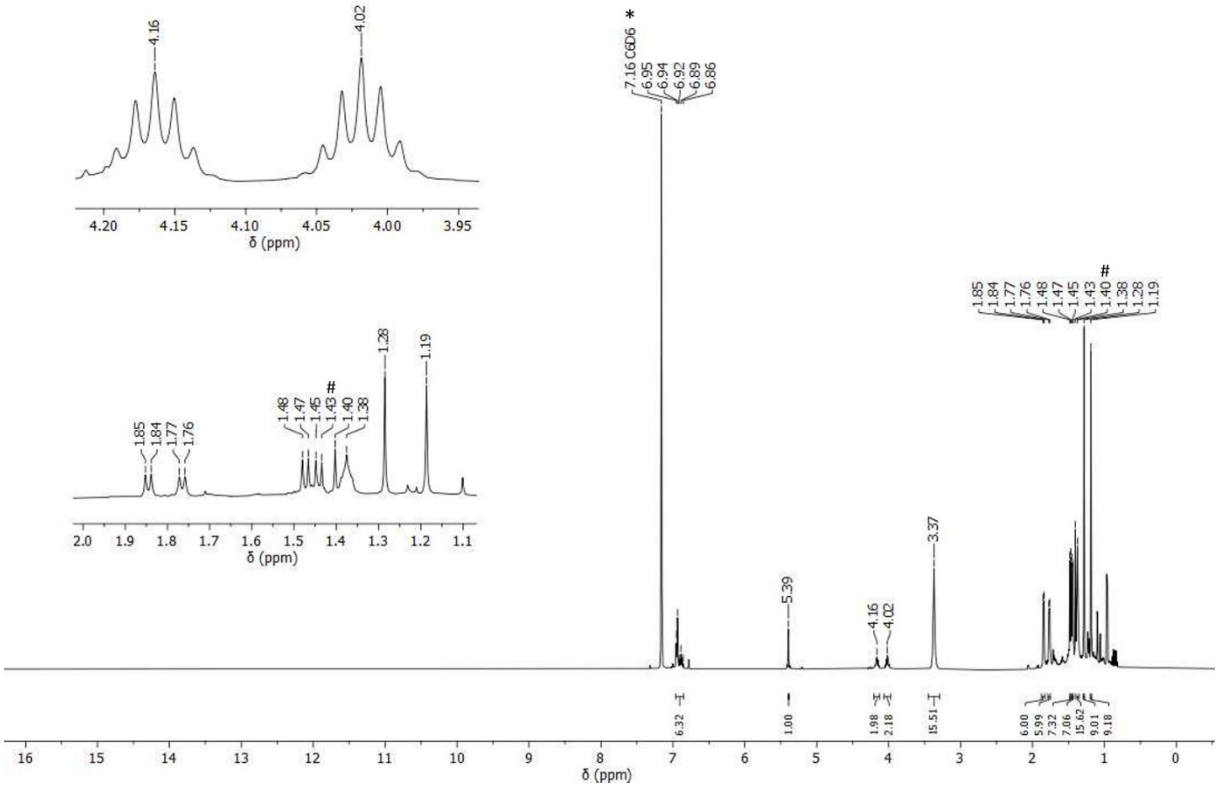

Figure S12: ^{1}H NMR (500.13 MHz, C_6D_6) spectrum of **2**.

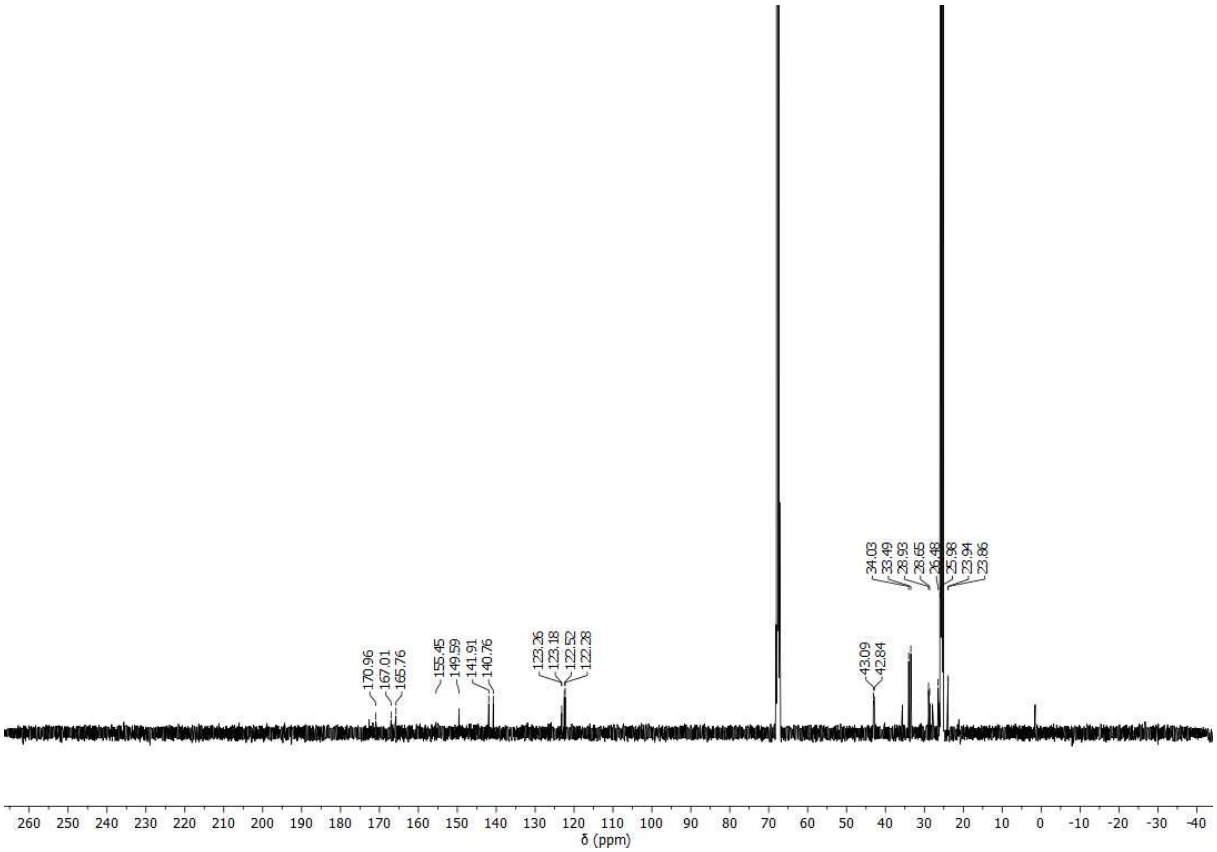

Figure S13: ^{13}C NMR (125.77 MHz, THF-d_8) spectrum of **2.**

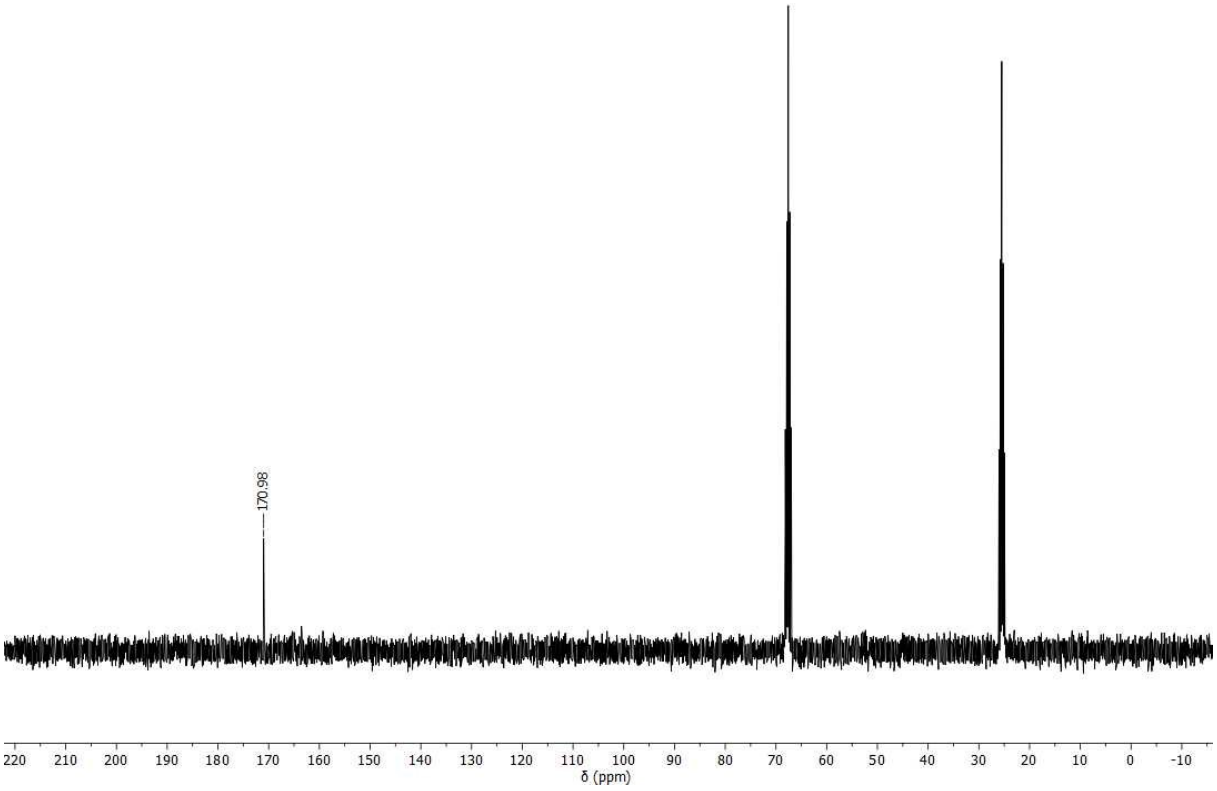

Figure S14: ^{13}C NMR (75.76 MHz, THF-d_8) spectrum of **^{13}2**.

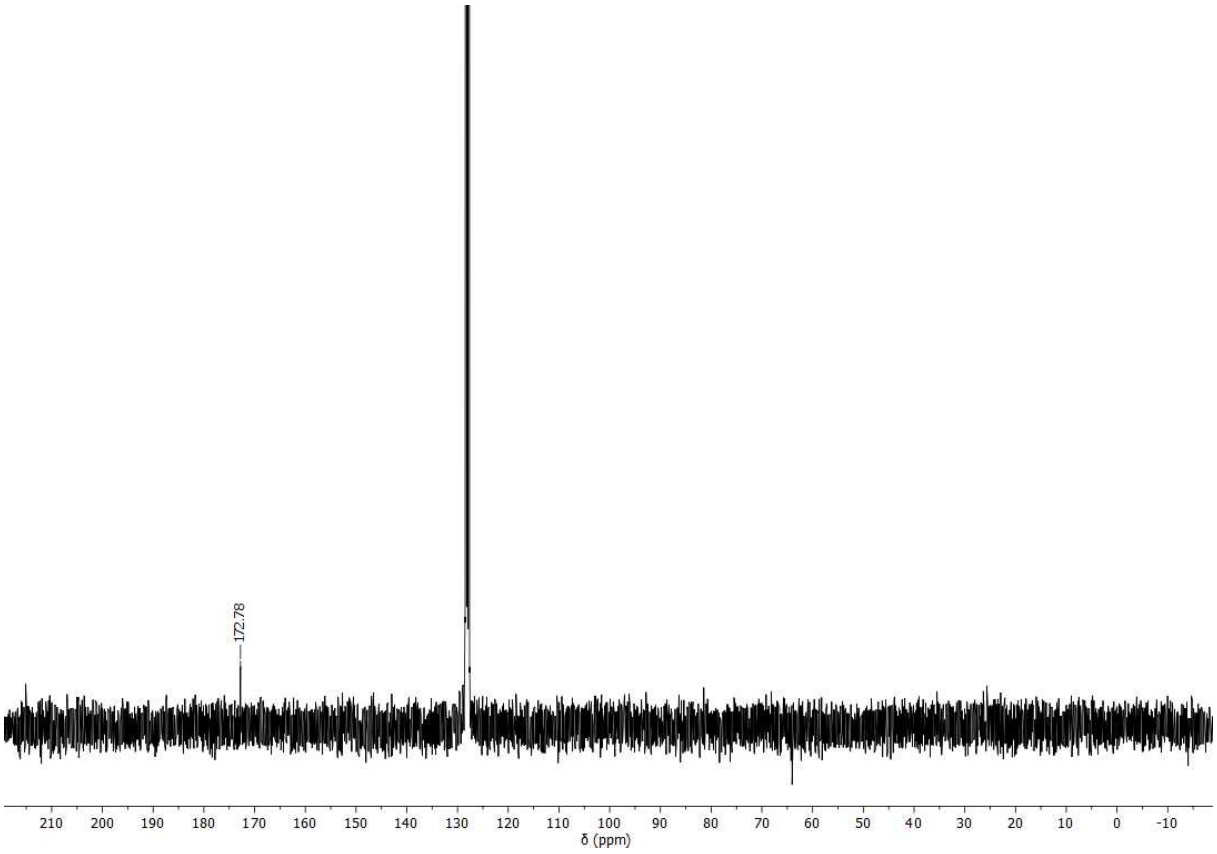

Figure S15: ^{13}C NMR (75.76 MHz, C_6D_6) spectrum of **^{13}2**.

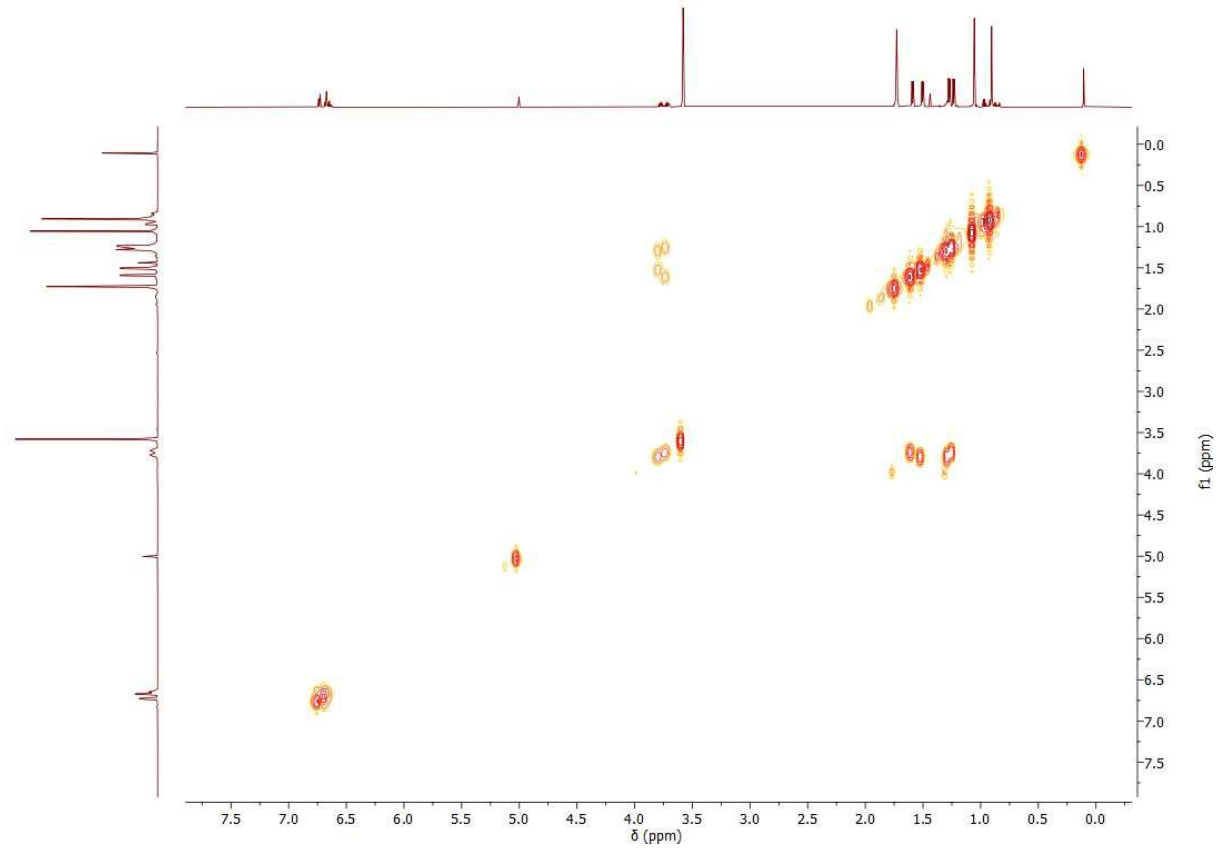

Figure S16: ^{1}H-^{1}H COSY NMR (599.89 MHz, THF-d_8) spectrum of **2**.

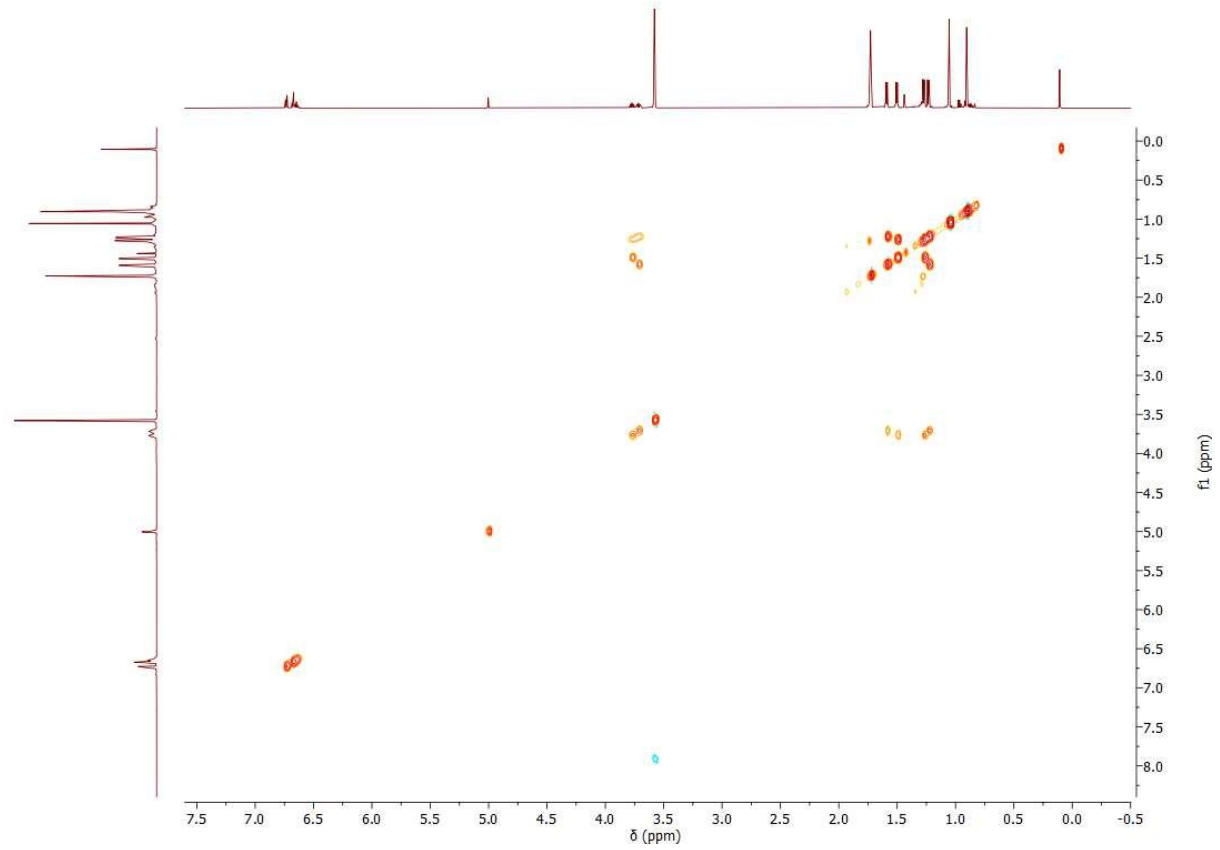

Figure S17: ^{1}H-^{1}H TOCSY NMR (599.89 MHz, THF-d_8) spectrum of **2**.

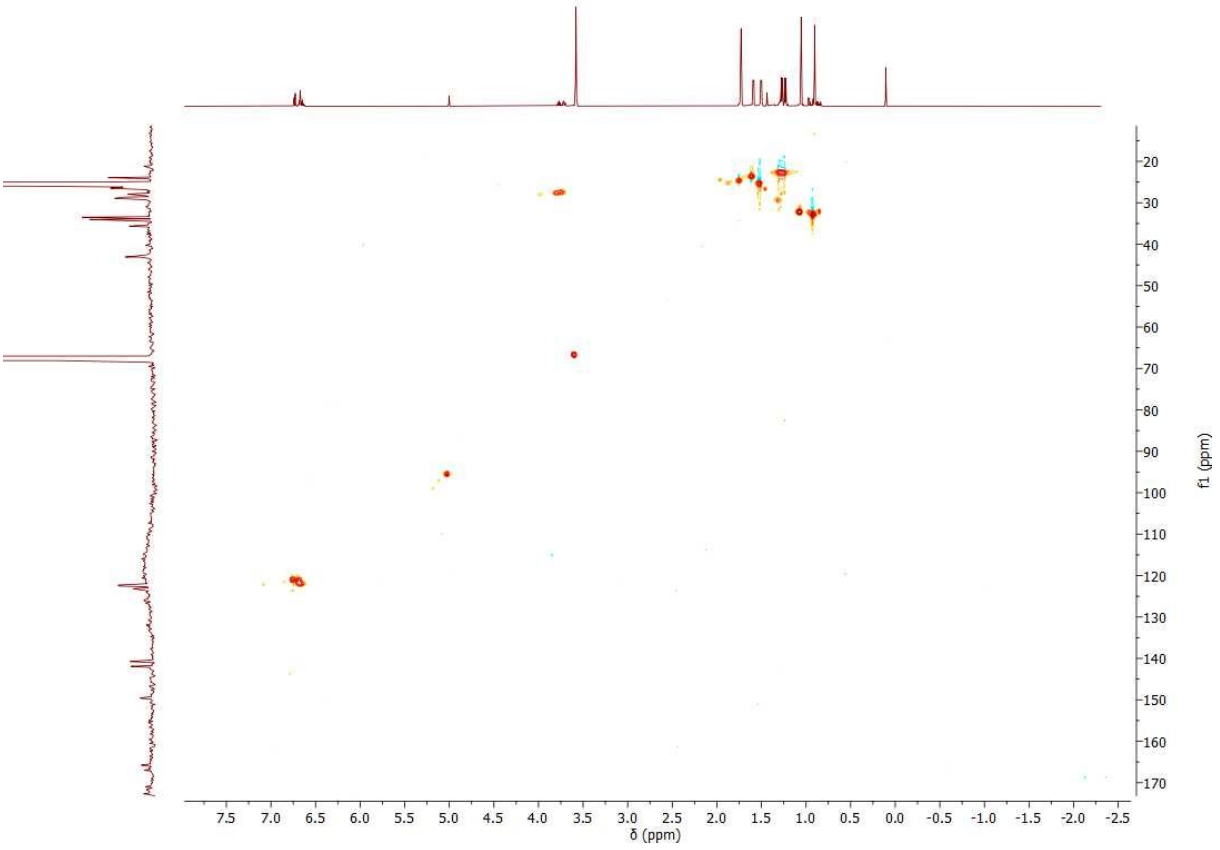

Figure S18: ^{1}H-^{13}C HSQC NMR (599.89 MHz, THF-d_8) spectrum of **2**.

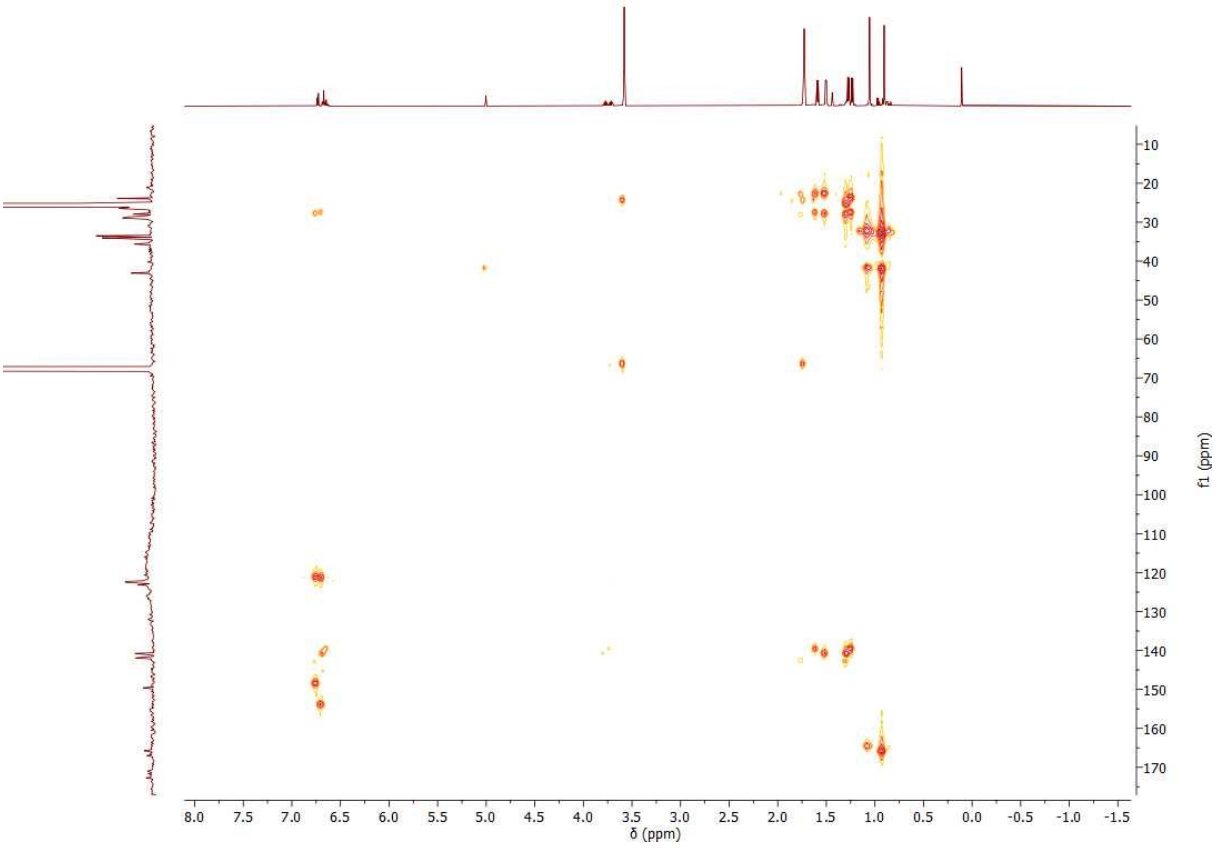

Figure S19: ^{1}H-^{13}C HMBC NMR (599.89 MHz, THF-d_8) spectrum of **2**.

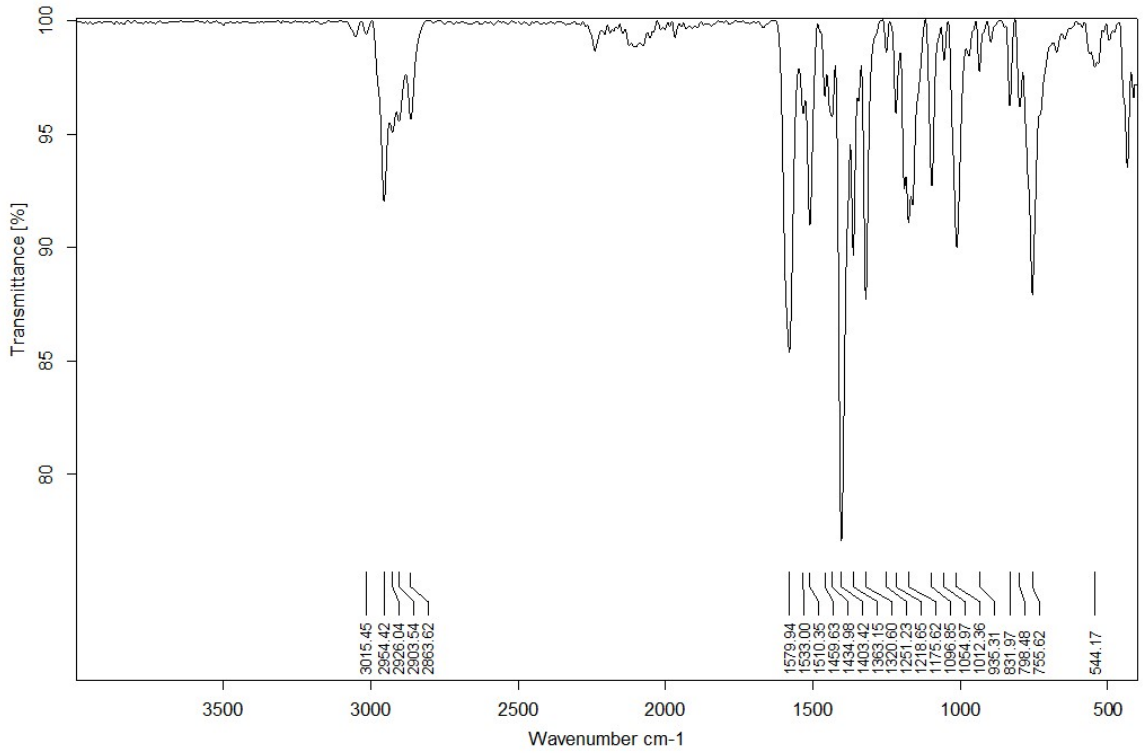

Figure S20: ATR-IR spectrum of **2** (solid obtained from THF-d_8 solution).

2.3 Synthesis of [Ca(18C6)($L^{tBu}NiCO_2)_2$], 2-18C6

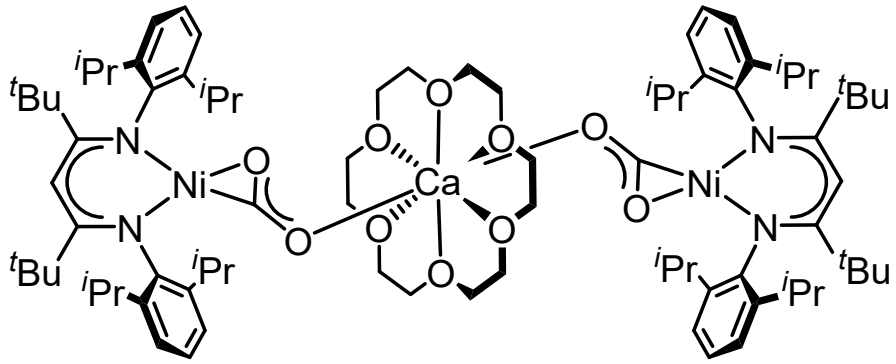

A mixture of **2** (25 mg, 0.02 mmol) and 18-crown-6 (4.3 mg, 0.02 mmol) was suspended in C_6D_6 (0.6 mL) and shaken for about 1 min until all solid material was solubilised. Subsequent analysis by NMR spectroscopy indicated a quantitative conversion giving [Ca(18C6)($L^{tBu}NiCO_2)_2$], **2-18C6**, as the sole product.

Single crystals suitable for X-ray diffraction were grown by slow evaporation of a hexane/Et_2O mixture.

^{1}H-NMR (500 MHz, C_6D_6): δ (ppm) = 6.93-6.77 (m, 12 H, Ar-**H**), 5.38 (s, 2 H, C**H**$_{backbone}$), 4.15 (sept, J = 6.8 Hz, 4 H, C**H**$(CH_3)_2$), 4.09 (sept, J = 6.8 Hz, 4 H, C**H**$(CH_3)_2$), 2.84 (s, 24 H, 18C6), 1.75 (d, J=6.8 Hz, 12 H, CH(C**H**$_3)_2$), 1.72 (d, J=6.8 Hz, 12 H, CH(C**H**$_3)_2$), 1.50 (d, J=6.8 Hz, 12 H, CH(C**H**$_3)_2$), 1.48 (d, J=6.8 Hz, 12 H, CH(C**H**$_3)_2$), 1.35 (s, 18 H, C(C**H**$_3)_3$), 1.23 (s, 18 H, C(C**H**$_3)_3$).

^{13}C NMR (125 MHz, C_6D_6): δ (ppm) = 171.37 (**C**O_2), 166.87 (N**C**-^{t}Bu), 165.31 (N**C**-^{t}Bu), 154.43 (Ar-**C**), 149.25 (Ar-**C**), 141.64 (Ar-**C**), 140.24 (Ar-**C**), 122.67 (Ar-**C**), 122.37 (Ar-**C**), 121.97 (Ar-**C**), 121.91 (Ar-**C**), 96.20 (γ-**C**), 69.01 (18C6), 42.76 (**C**$(CH_3)_3$), 42.48 (**C**$(CH_3)_3$), 33.87 (C(**C**$H_3)_3$), 33.31 (C(**C**$H_3)_3$), 28.41 (**C**H$(CH_3)_2$), 28.13 (CH(**C**$H_3)_2$), 26.18 (CH(**C**$H_3)_2$), 24.69 (CH(**C**$H_3)_2$), 24.00 (CH(**C**$H_3)_2$), 23.77 (CH(**C**$H_3)_2$).

ATR-IR (solid obtained from C_6D_6 solution): ν (cm^{-1}) = 3052 (w), 2957 (m), 2920 (m), 2904 (w), 2864 (w), 1663 (w), 1603 (br, ν_{CO}), 1534 (w), 1510 (m), 1461 (w), 1432 (m), 1406 (s), 1364 (s) 1321 (s), 1259 (w), 1218 (m), 1195 (w), 1180 (w), 1176 (w), 1096 (m), 1046 (m), 1014 (s), 795 (m), 757 (m), 495 (w).

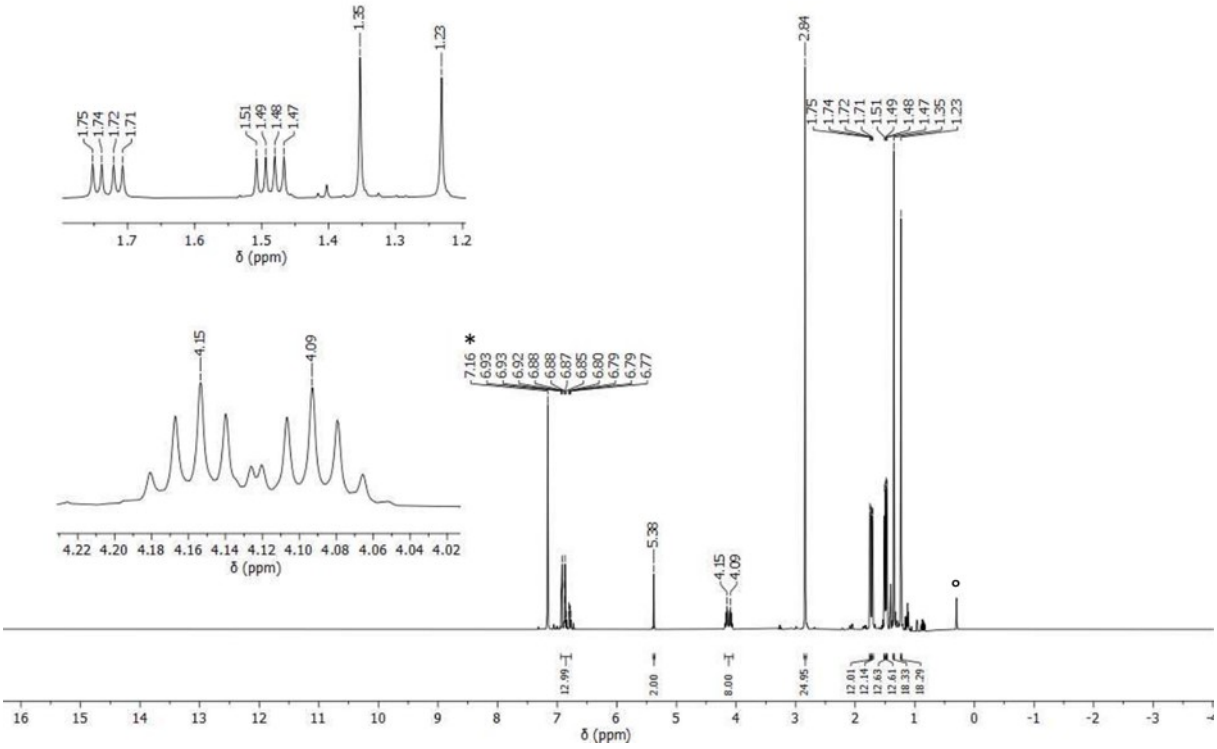

Figure S21: ^{1}H NMR (500.13 MHz, C_6D_6) spectrum of **2-18C6** (° = impurity of silicon grease).

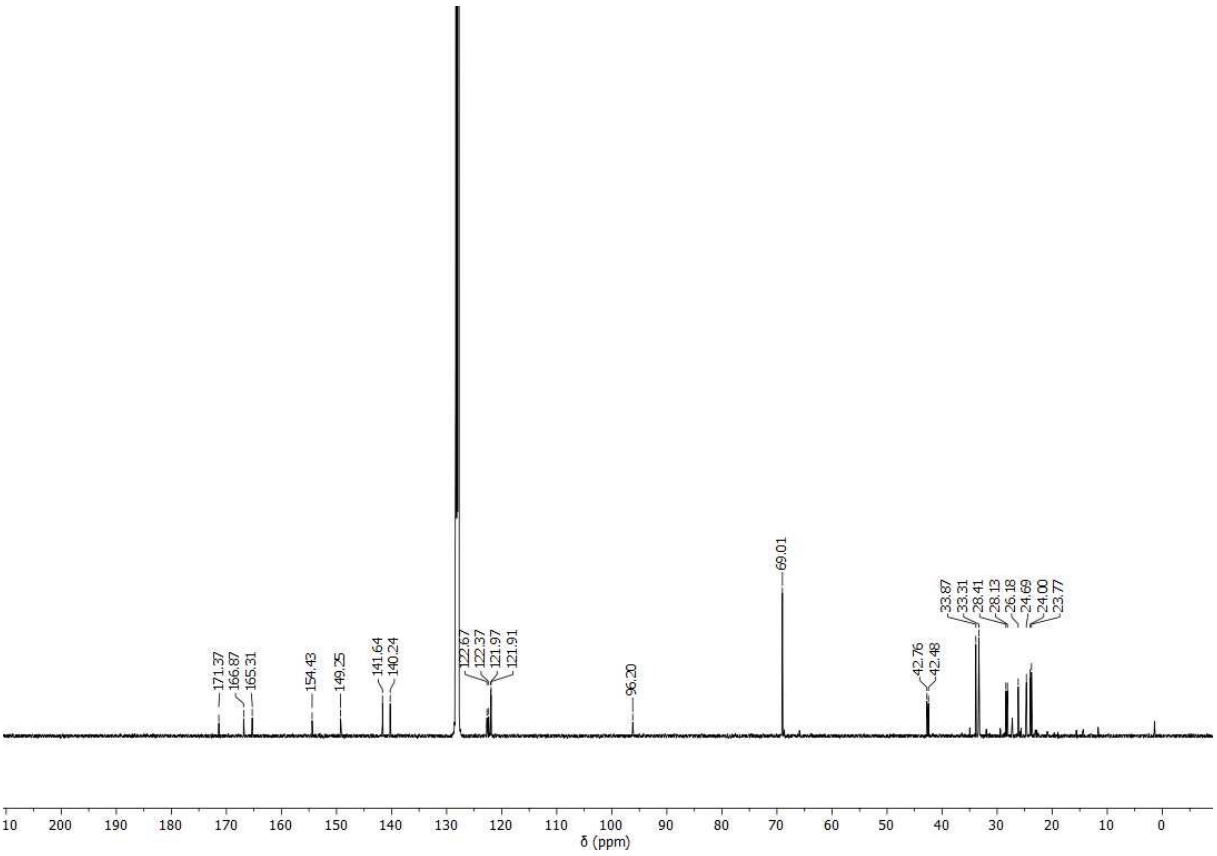

Figure S22: ^{13}C NMR (125.77 MHz, C_6D_6) spectrum of **2-18C6.**

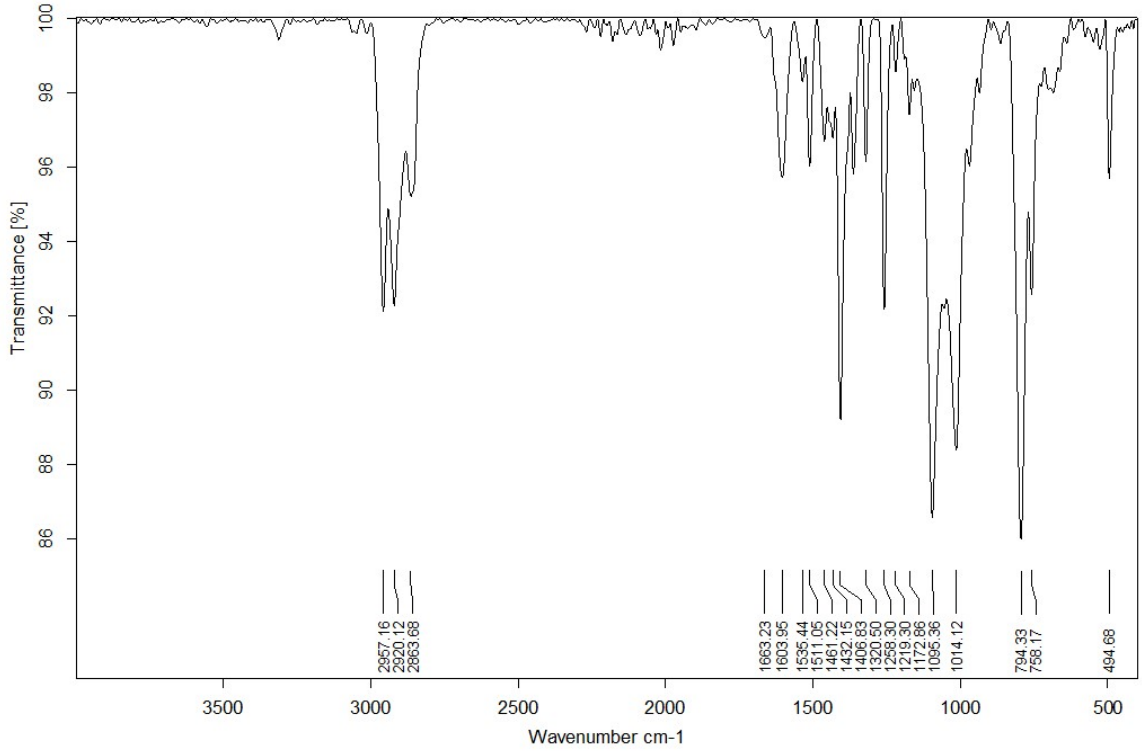

Figure S23: ATR-IR spectrum of **2-18C6** (solid obtained from THF-d_8 solution).

2.4 Synthesis of [$L^{tBu}NiCO_2Mg(THF)L^{Mes}$], 3

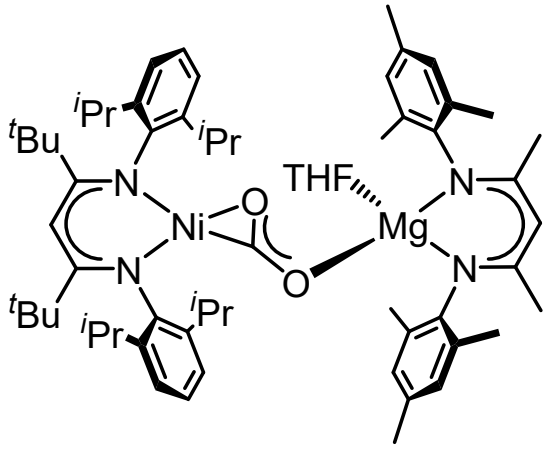

A mixture of [L^{tBu}NiOOCH] (72.6 mg, 0.12 mmol) and NaN(^{i}Pr)$_2$ (19.2 mg, 0.16 mmol) was dissolved in 3 mL of THF and stirred for 20 min. After evaporation of the solvent [L^{Mes}Mg(Et_2O)I] (66.9 mg, 0.12 mmol) was added together with 3 mL of THF. The suspension was stirred for another 15 min followed by removal of the solvent *in vacuo.* The remaining residue was extracted with Et_2O until the extracts became colourless. The combined organic phases were concentrated to approximately 1 mL. Storage at –30 °C caused formation of orange block shaped crystals of [$L^{tBu}NiCO_2Mg(THF)L^{Mes}$]•$Et_2O$, **3**, (62.1 mg, 0.06 mmol, 34%).

The isolated crystalline material was suitable for single crystal X-ray diffraction. The molecular structure thus determined revealed the presence of one equivalent of non-coordinated Et_2O per molecule of **3**. This finding was consistent with the recorded NMR data of the dried crystalline material.

^{1}H-NMR (500 MHz, C_6D_6): δ (ppm) = 6.91-6.81 (m, overlapping signals of L^{tBu} and L^{Mes}, 10 H, Ar-**H**), 5.34 (s, 1 H, L^{tBu}-C**H**$_{backbone}$), 4.69 (s, 1 H, L^{Mes}-C**H**$_{backbone}$), 4.08 (sept, J = 6.8 Hz, 2 H, L^{tBu}-C**H**$(CH_3)_2$), 3.95 (sept, J = 6.8 Hz, 2 H, L^{tBu}-C**H**$(CH_3)_2$), 3.16 (m, 4 H, THF), 2.29 (s, 6 H, L^{Mes}-*p*-C**H**$_3$), 2.00 (br, 12 H, L^{Mes}-*o*-C**H**$_3$), 1.67 (d, J=6.8 Hz, 6 H, L^{tBu}-CH(C**H**$_3)_2$), 1.56 (d, J=6.8 Hz, 6 H, L^{tBu}-CH(C**H**$_3)_2$), 1.51 (s, 6 H, L^{Mes}-NC**C**H$_3$), 1.44 (d, J=6.8 Hz, 6 H, L^{tBu}-CH(C**H**$_3)_2$), 1.41 (d, J=6.8 Hz, 6 H, L^{tBu}-CH(C**H**$_3)_2$), 1.24 (s, 9 H, L^{tBu}-C(C**H**$_3)_3$), 1.17 (m, 4 H, THF), 1.11 (s, 9 H, L^{tBu}-C(C**H**$_3)_3$).

^{13}C NMR (125 MHz, C_6D_6): δ (ppm) = 175.80 (**C**O_2), 168.45 (L^{Mes}-N**C**CH$_3$), 167.53 (L^{tBu}-N**C**-^{t}Bu), 166.02 (L^{tBu}-N**C**-^{t}Bu), 154.47 (L^{tBu}-Ar-**C**), 148.07 (L^{tBu}-Ar-**C**), 145.04 (L^{Mes}-Ar-**C**), 142.14 (L^{tBu}-Ar-**C**), 140.10 (L^{tBu}-Ar-**C**), 133.24 (L^{Mes}-Ar-**C**), 131.61 (L^{Mes}-Ar-**C**), 129.57 (L^{Mes}-Ar-**C**), 123.58 (L^{tBu}-Ar-**C**), 123.51 (L^{tBu}-Ar-**C**), 122.42 (L^{tBu}-Ar-**C**), 122.09 (L^{tBu}-Ar-**C**), 96.80 (L^{tBu}-γ-**C**), 94.83 (L^{Mes}-γ-**C**), 69.29 (THF), 42.61 (L^{tBu}-**C**$(CH_3)_3$), 42.20 (L^{tBu}-**C**$(CH_3)_3$), 33.77 (L^{tBu}-C(**C**H$_3)_3$), 33.19 (L^{tBu}-C(**C**H$_3)_3$), 28.52 (L^{tBu}-**C**H$(CH_3)_2$), 28.23 (L^{tBu}-**C**H$(CH_3)_2$), 26.56 (L^{tBu}-CH(**C**H$_3)_2$), 25.15 (THF), 24.07 (L^{tBu}-CH(**C**H$_3)_2$), 23.86 (L^{tBu}-CH(**C**H$_3)_2$), 23.66 (L^{tBu}-CH(**C**H$_3)_2$), 23.13 (L^{Mes}-NC**C**H$_3$), 21.02 (L^{Mes}-Ar-*p*-**C**H$_3$), 18.79 (L^{Mes}-Ar-*o*-**C**H$_3$).

^{13}C NMR (75 MHz, THF-d_8): δ (ppm) = 175.73 (**C**O_2).

ATR-IR (solid obtained from C_6D_6 solution): ν (cm^{-1}) = 3052 (w), 2956 (m), 2922 (w), 2905 (w), 2866 (w), 2280 (w, C_6D_6), 1577 (w, ν_{CO}), 1537 (m), 1512 (m), 1445 (m), 1433 (m), 1393 (s), 1365 (s), 1320 (m), 1259 (m), 1217 (m), 1197 (w), 1181 (w), 1160 (w), 1147 (w), 1098 (m), 1019 (m), 970 (w), 958 (w), 935 (w), 857 (m), 804 (w), 758 (m), 516 (w), 495 (s), 438 (w).

Elemental analysis calc. (%) for $C_{63}H_{90}MgN_4NiO_3$•$C_4H_{10}O$ (1108,56 g*mol^{-1}): C 72.59, H 9.09, N 4.98; found: C 70.25, H 8.79, N 5.05.

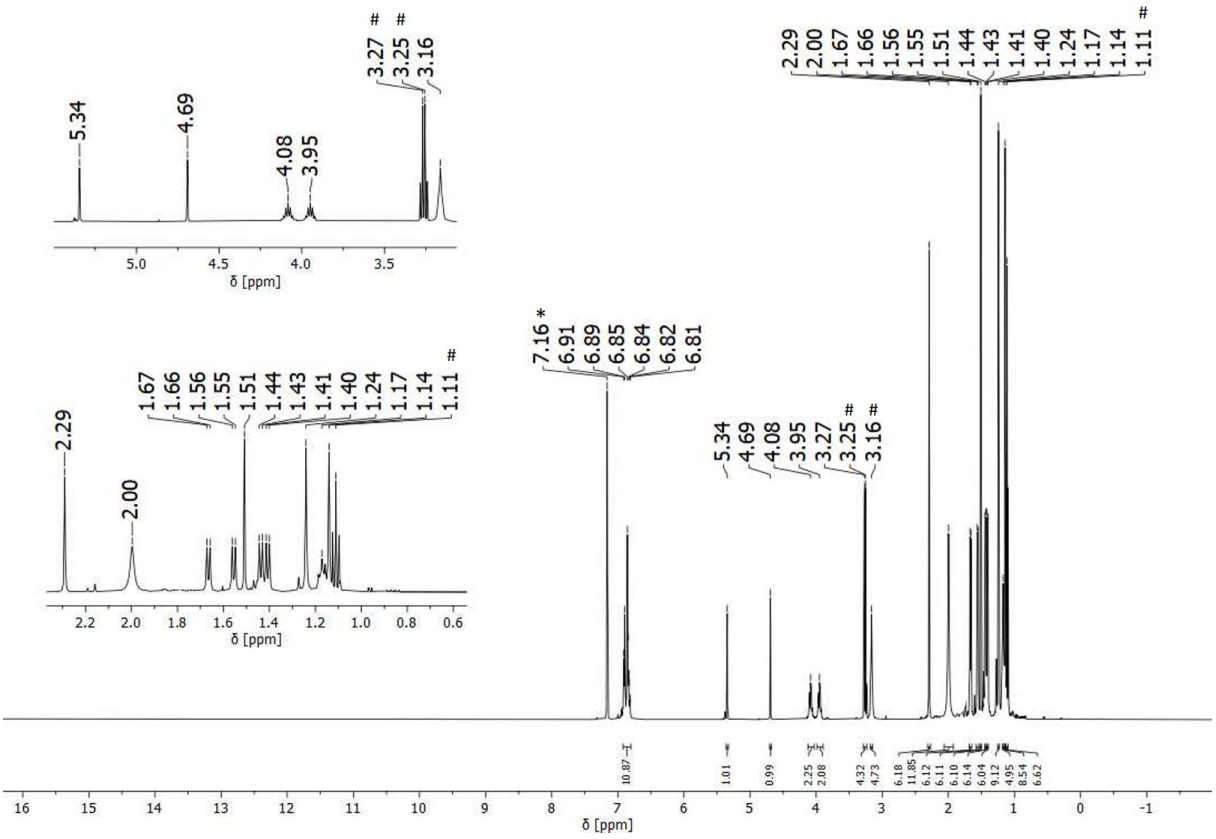

Figure S24: ^{1}H NMR (500.13 MHz, C_6D_6) spectrum of **3** (# = Et_2O).

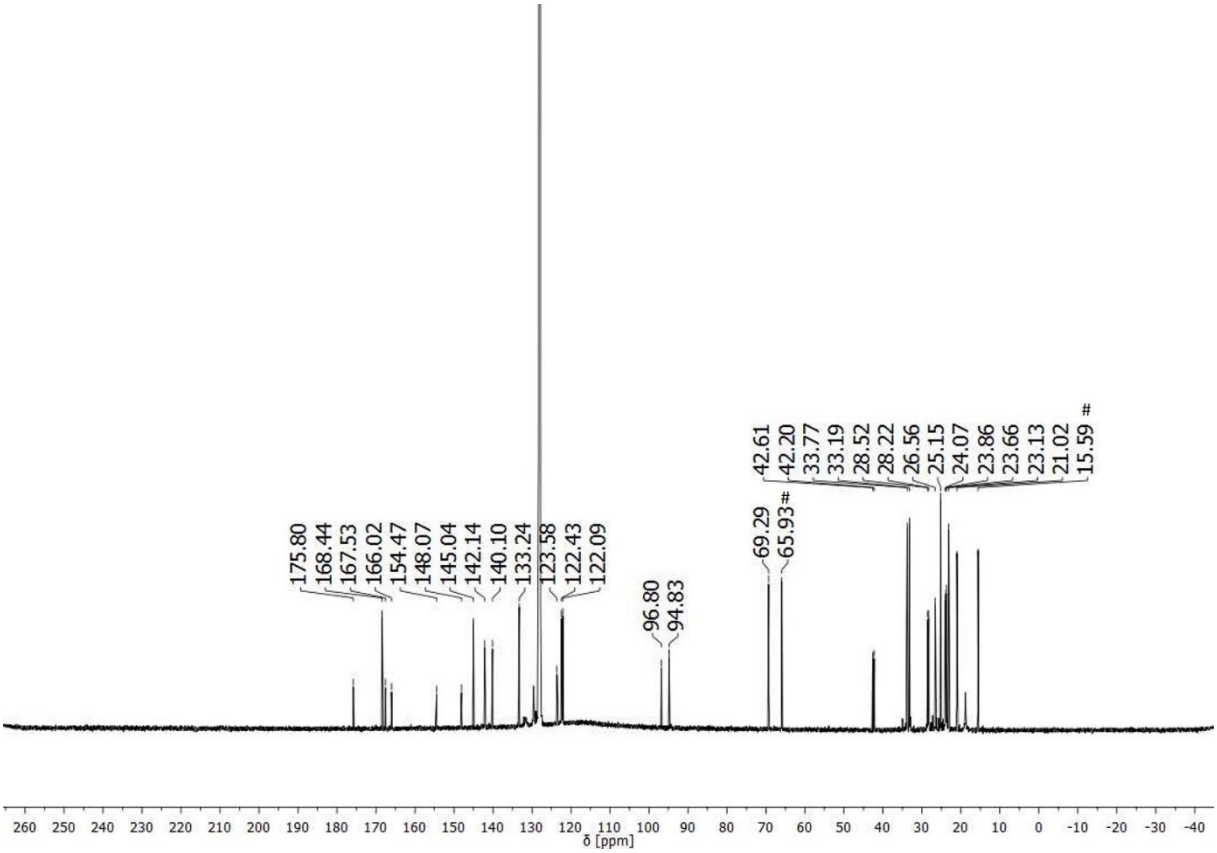

Figure S25: ^{1}H NMR (125.77 MHz, C_6D_6) spectrum of **3**. (# = Et_2O)

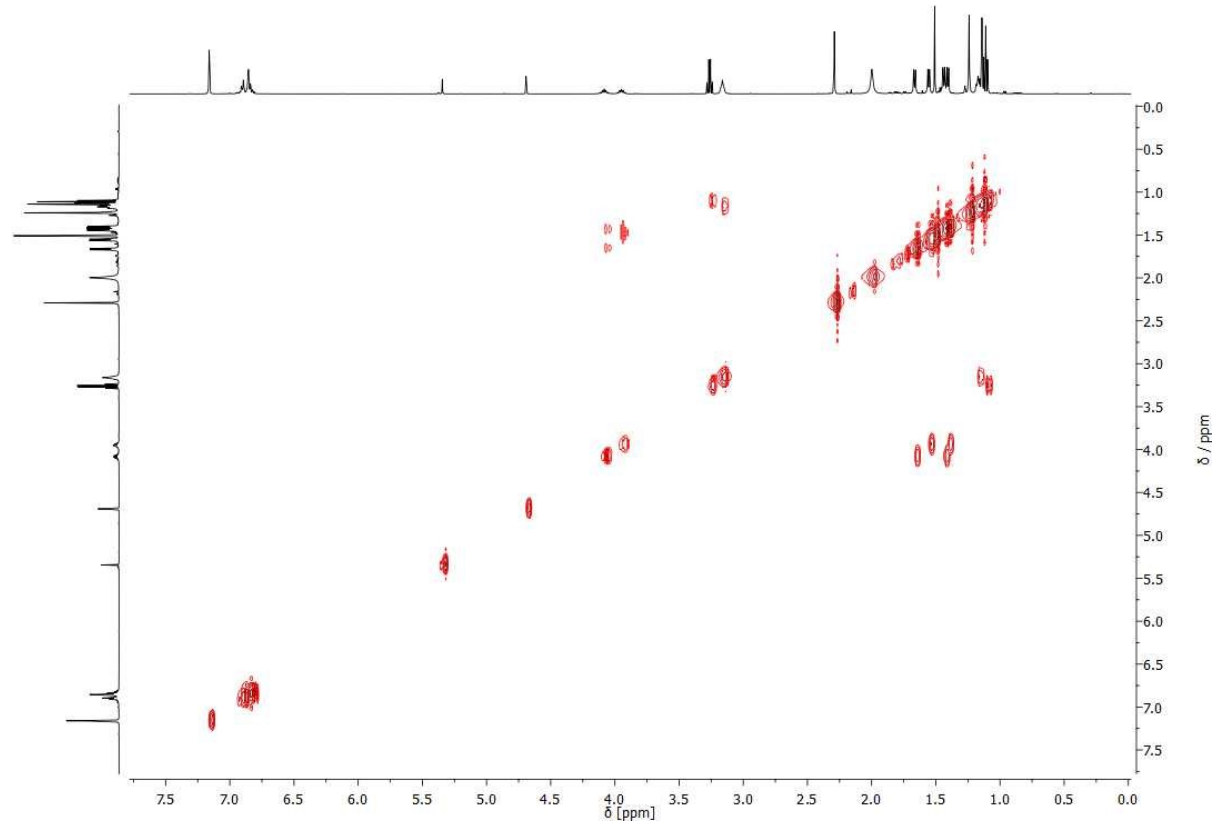

Figure S26: ^{1}H-^{1}H COSY NMR (500.13 MHz, C_6D_6) spectrum of **3**.

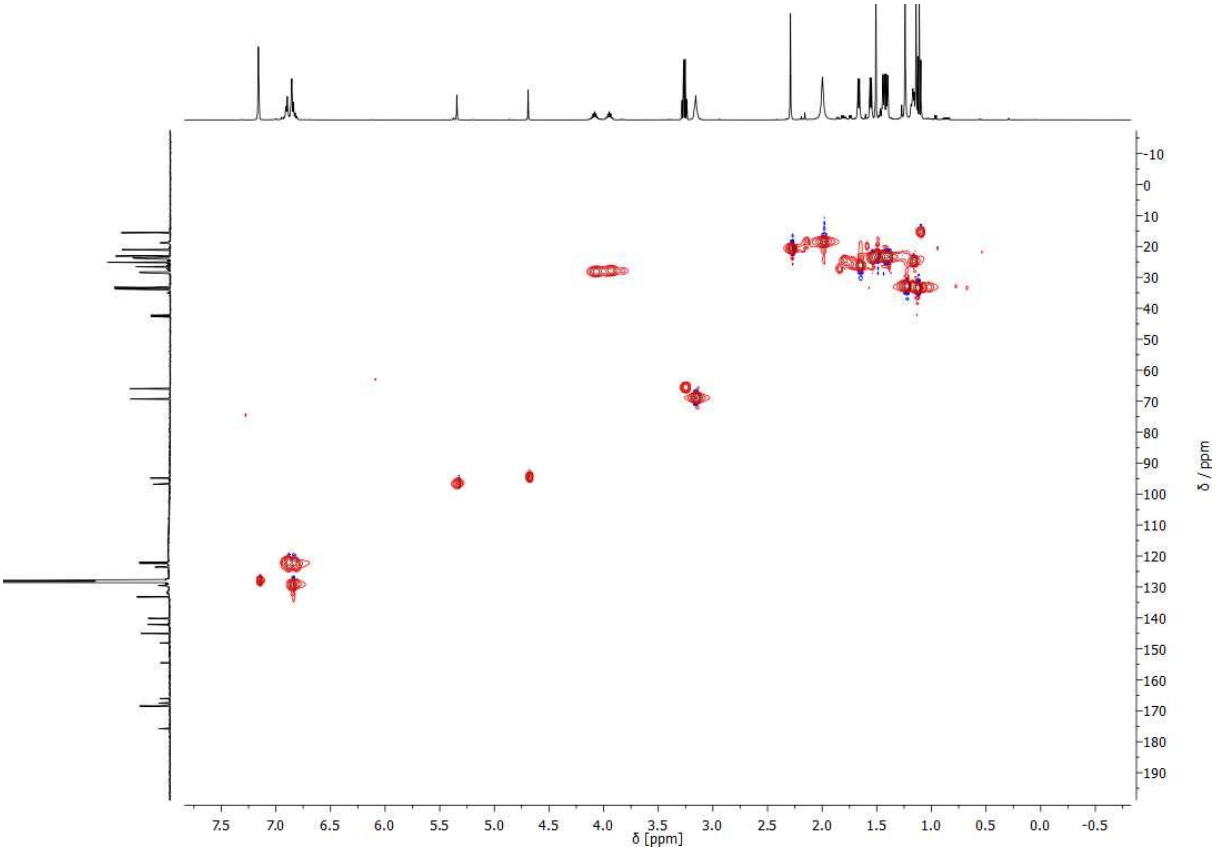

Figure S27: ^{1}H-^{13}C HSQC NMR (500.13 MHz, C_6D_6) spectrum of **3**.

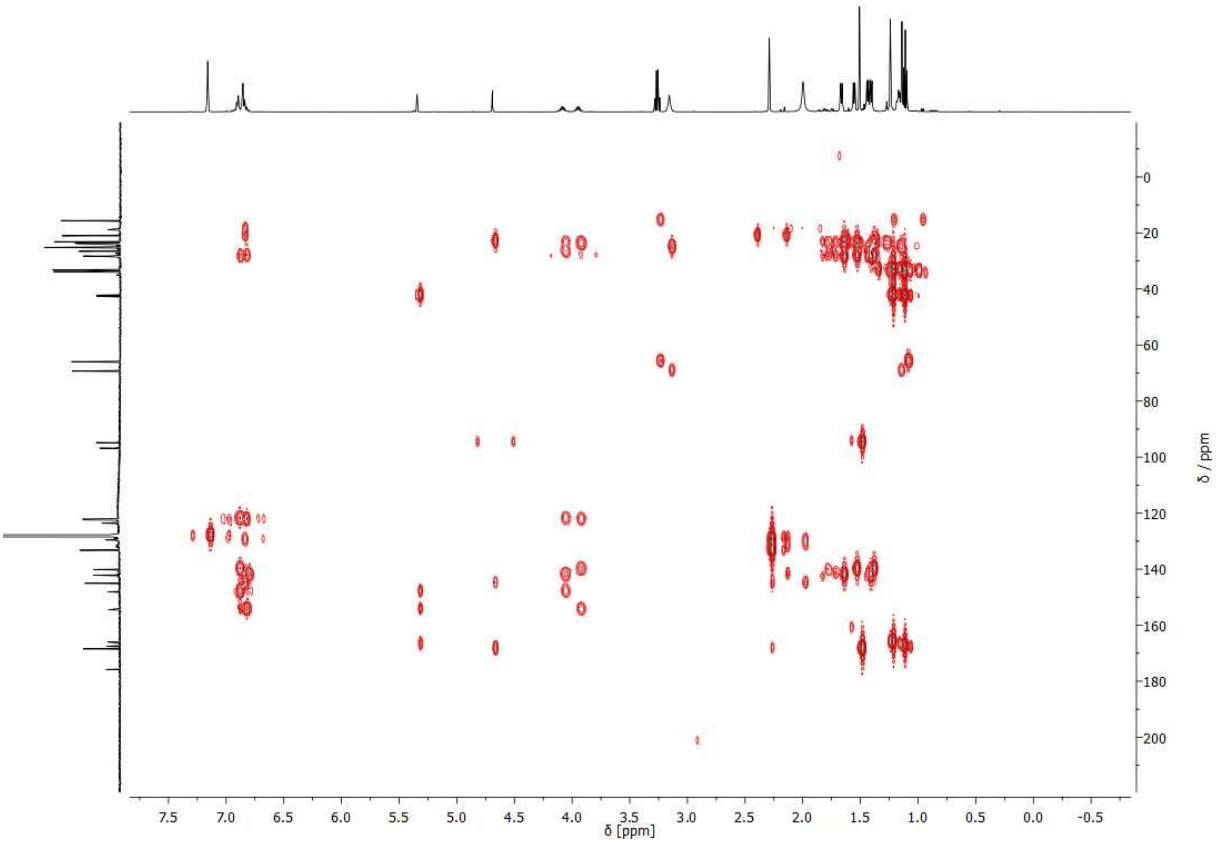

Figure S28: ^{1}H-^{13}C HMBC NMR (500.13 MHz, C_6D_6) spectrum of **3**.

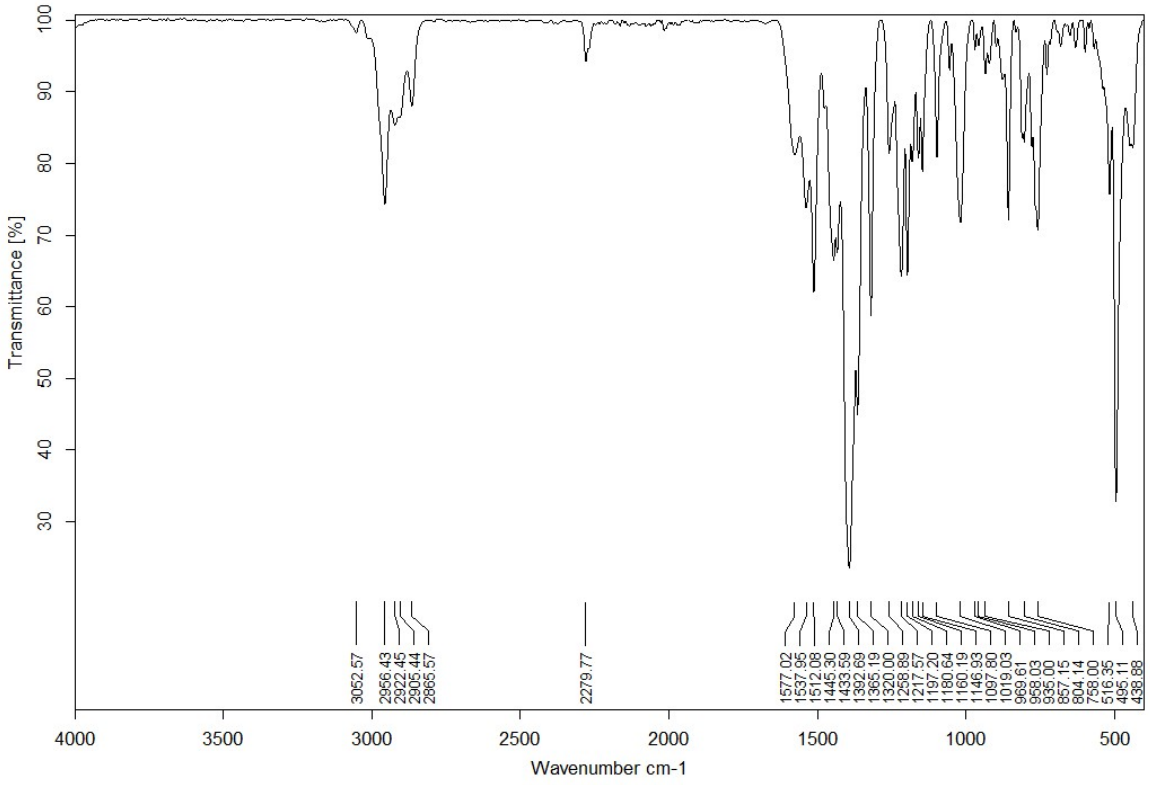

Figure S29: ATR-IR spectrum of **3** (solid obtained from C_6D_6 solution).

2.5 Reaction of [$L^{tBu}NiCO_2Na$] with [$L^{Dipp}Ca(Et_2O)I]_2$

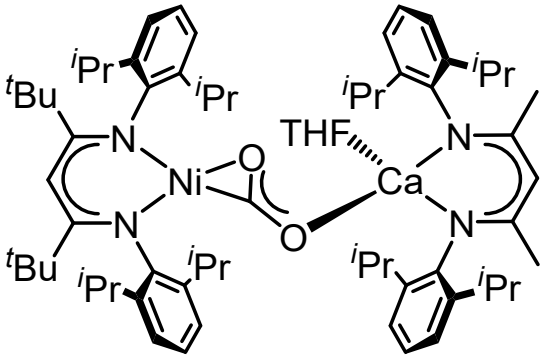

A scintillation vial was charged with **I^{Na}** (18.8 mg, 0.03 mmol), [$L^{Dipp}CaI(Et_2O)$] (19.7 mg, 0.03 mmol) and 0.6 mL of THF-d_8. After shaking for 1 min **2** precipitated as orange crystalline solid (10.1 mg, 0.01 mmol, 44%) which was filtered off. The solution was analysed by NMR spectroscopy. The ^{1}H NMR spectrum showed the formation of **2´** and the homoleptic complex [$(L^{Dipp})_2Ca$] (signals of **2** were only found in small traces as most of the complex precipitated from solution). Additionally, another set of signals was found which was assigned to the newly formed complex [$L^{tBu}NiCO_2Ca(THF)L^{Dipp}$], **4**. Repeating the experiment with [$L^{tBu}Ni^{13}CO_2Na$], **$^{13}I^{Na}$**, allowed the use of ^{13}C NMR spectroscopy for reaction control. The ^{13}C NMR spectrum of the reaction confirmed formation of two $^{13}CO_2$ species (see Figure S31, **2´**: 171.30 ppm, **4**: 170.95 ppm).
Attempts to isolate complex **4** failed as the complex undergoes dissociation towards **2** and [$(L^{Dipp})_2Ca$].

Note: DOSY measurements of the reaction mixture were conducted to substantiate the formation of **4** (see section 4.2).

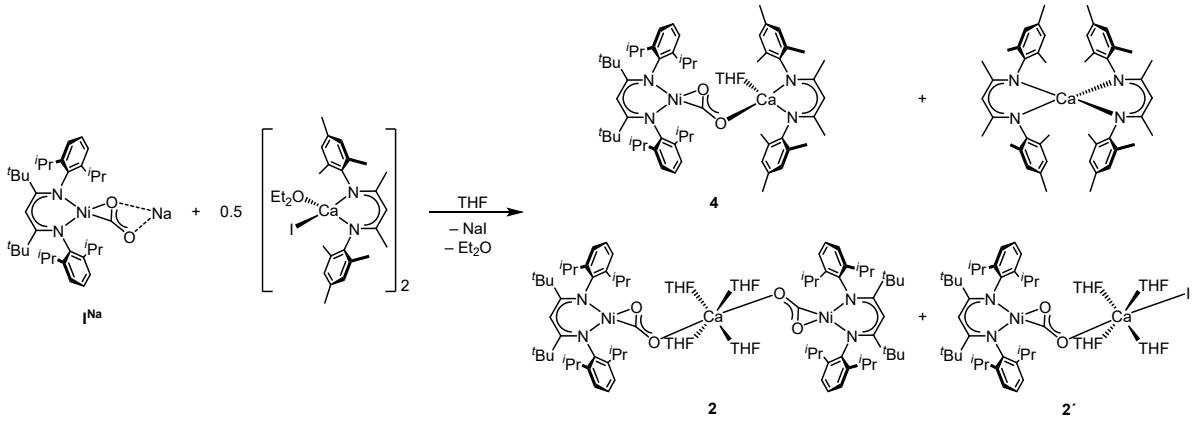

Scheme S1: Salt metathesis reaction between **I^{Na}** and [$L^{Dipp}CaI(Et_2O)$] accompanied by ligand exchange reactions around the Ca^{2+} centre.

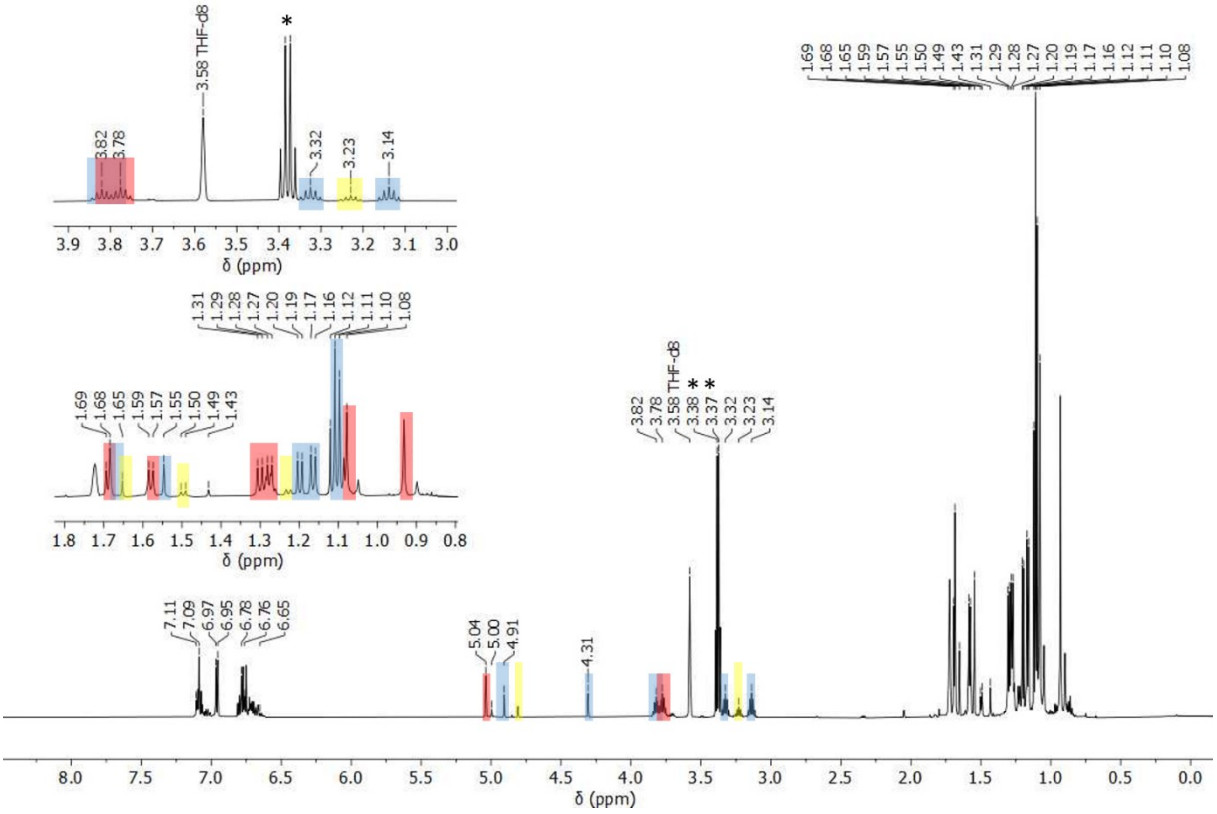

Figure S30: ^{1}H NMR (600.13 MHz, THF-d_8) spectrum of the reaction between $\mathbf{I^{Na}}$ and [L^{Dipp}CaI] (red label: **2´**, blue label: **4**, yellow label: [(L^{Dipp})$_2$Ca], * = Et_2O).

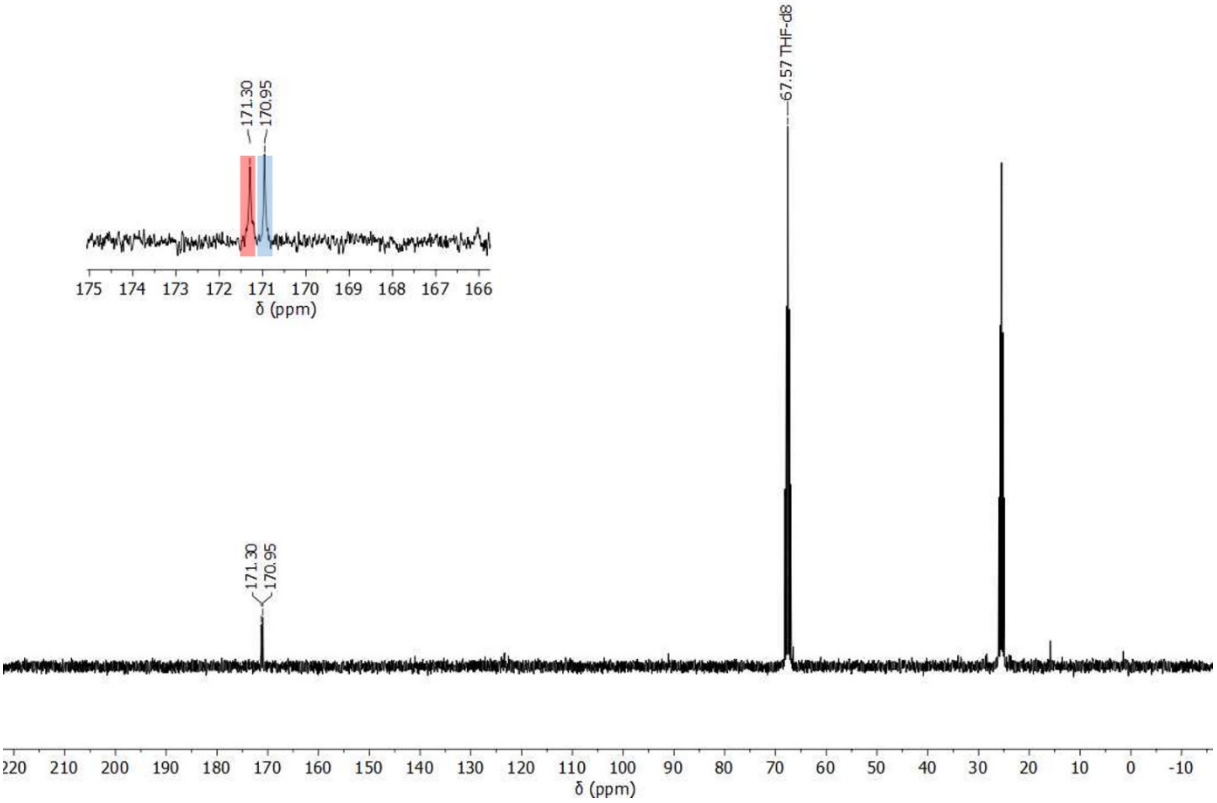

Figure S31: ^{13}C NMR (75.76 MHz, THF-d_8) spectrum of the reaction between $\mathbf{I^{Na}}$ and [L^{Dipp}CaI] (red label: **2´**, blue label: **4**).

2.6 Reactivity towards propylene oxide

A J Young NMR tube was charged with **2-18C6** (12 mg, 0.01 mmol) in C_6D_6 and 15 µL of propylene oxide (0.2 mL, 20 eq) were added. After 1 min of shaking the samples was stored for 24 h and subsequently analysed by ^{1}H NMR spectroscopy. The spectrum indicated complete conversion of **2-18C6** into [Ca(18C6)($L^{tBu}NiCO_3$)$_2$], **5^{Ca}-18C6** accompanied by the formation of 1 equiv. of propylene (see Figure S33). After removal of the excessive propylene oxide under vacuum **5^{Ca}-18C6** was recrystalised from hot MeCN solutions to obtain crystalline material suitable for single crystal X-ray diffraction (see Figure S32).

Reactions using **1** or **2** as a starting material proceeded in an analogous fashion to yield [Mg(THF)$_4$($L^{tBu}NiCO_3$)$_2$], **5^{Mg}**, or [Ca(THF)$_4$($L^{tBu}NiCO_3$)$_2$], **5^{Ca}** (NMR signals of all three AE carbonates appeared only slightly shifted towards each other).

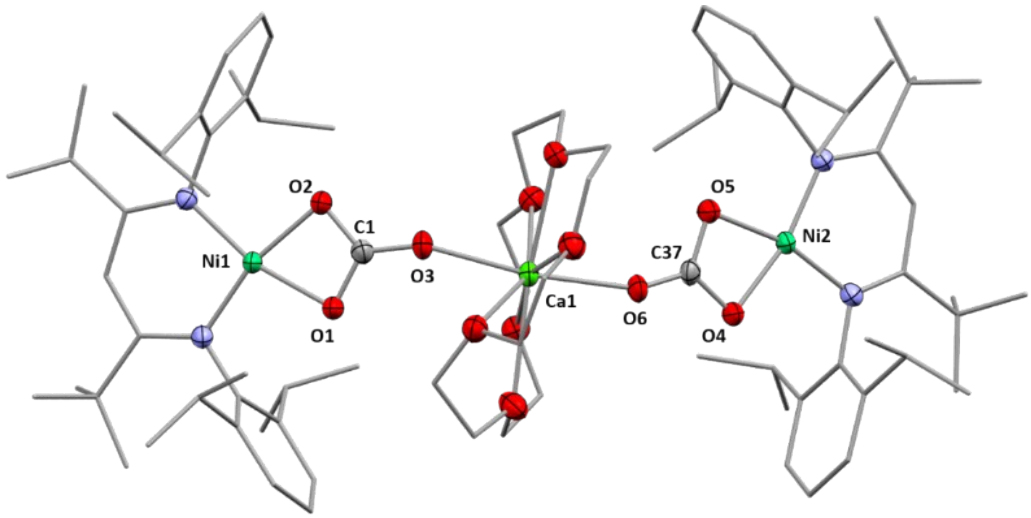

Figure S32: Molecular structures of **5^{Ca}-18C6**. H atoms and co-crystallised solvent molecules omitted for clarity. Selected bond lengths (Å): Ni1-O1 1.908(1), Ni1-O2 1.899(1), C1-O1 1.298(3), C1-O2 1.299(3), C1-O3 1.253(2), O3-Ca1 2.248(1), Ni2-O4 1.906(1), Ni2-O5 1.913(2), C37-O4 1.296(3), C37-O5 1.305(2), C37-O6 1.254(2), O6-Ca1 2.256(1).

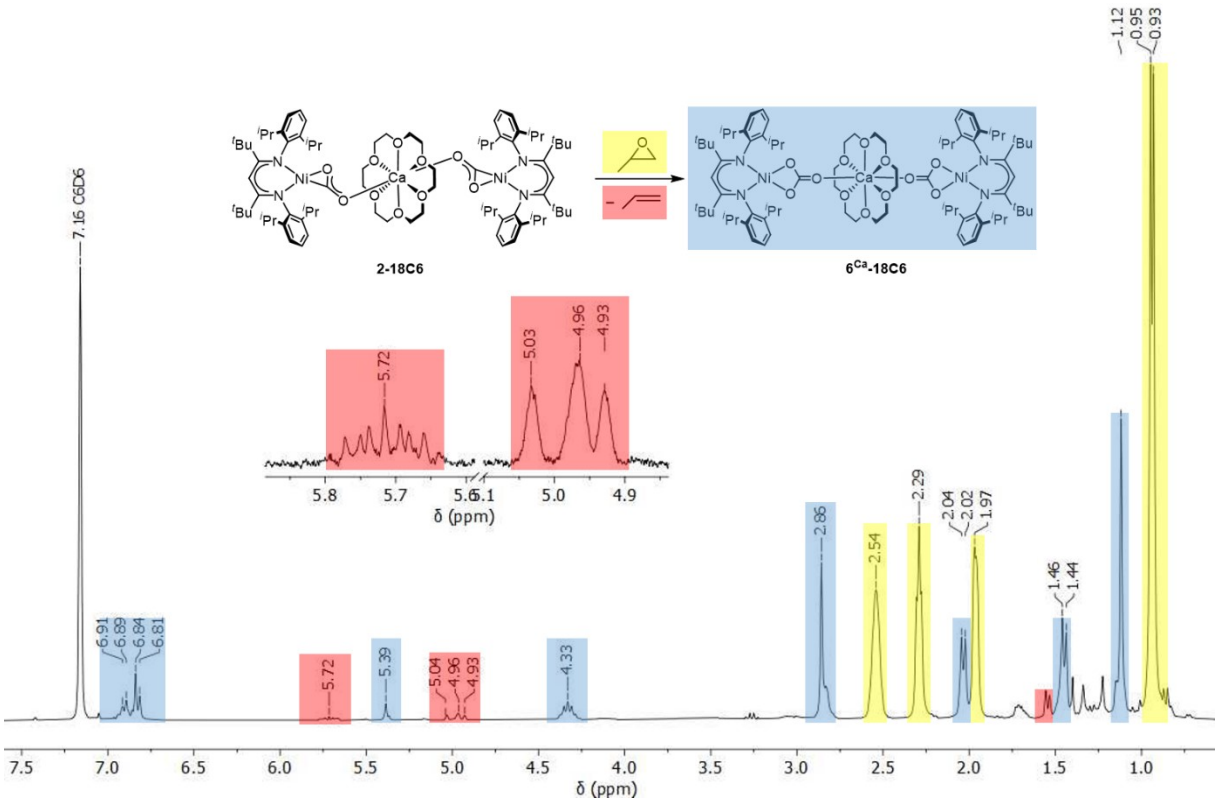

Figure S33: ^{1}H NMR (300.13 MHz, C_6D_6) spectrum of the reaction between **2-18C6** and C_3H_6O (red label: C_3H_6, blue label: **6^{Ca}-18C6**, yellow label: C_3H_6O).

2.7 Reaction of 1 with CO and isolation of $[Mg(THF)_4(L^{tBu}NiCO)_2]$, 6

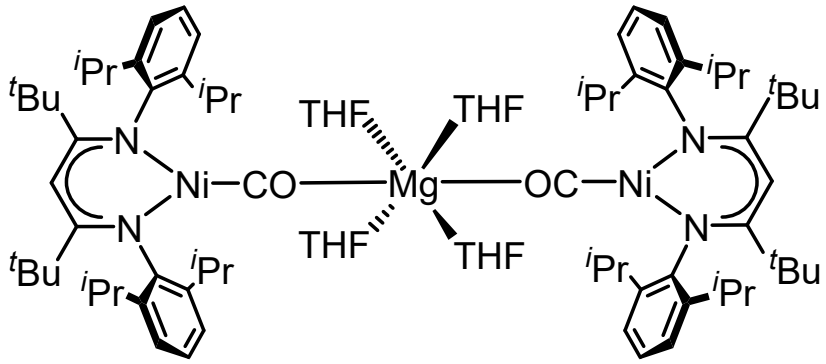

A solution of **1** (50.0 mg, 0.03 mmol) in toluene (1 mL) was put through three cycles of freeze-pump-thaw degassing. CO was added (approximately 1.3 bar) and the closed vessel was shaken a few times. Within 5 min $[Mg(THF)_4(L^{tBu}NiCO)_2]$, **6**, precipitated as yellow crystalline solid (29.4 mg, 62%).

The obtained crystalline material was suitable for single crystal X-ray diffraction.

Repeating the reaction with ^{13}C-labelled **^{13}1** allowed monitoring of the reaction by ^{13}C NMR spectroscopy. After exposure to CO the signal for the released $^{13}CO_2$ molecule (124.7 ppm) was detected.

Note: The poor solubility of the product prevented characterization by ^{1}H NMR and other solution techniques.

ATR-IR: ν (cm^{-1}) = 3053 (2), 2956 (m), 2928 (w), 2903 (w), 2867 (w), 1722 (s, ν_{CO}), 1586(w), 1535 (w), 1508 (m), 1460 (w), 1433 (m), 1430 (m), 1395 (s), 1364 (s), 1321 (s), 1253 (w), 1218 (m), 1194 (w), 1157 (w), 1097 (m), 1030 (m), 936 (w), 920 (w), 881 (w), 757 (m), 677 (w), 646 (w), 496 (w).

Elemental analysis calc. (%) for $C_{88}H_{138}MgN_4Ni_2O_6$ (1489,79 g*mol-1): C 70.95, H 9.34, N 3.76; found: C 68.39, H 8.80, N 4.02.

2.8 Reaction of 2 with CO

A solution of **2** (15.0 mg, 0.01 mmol) in C_6D_6 (0.6 mL) was put through three cycles of freeze-pump-thaw degassing. CO was added (approximately 1.3 bar) and the closed vessel was shaken a few times. Analysis by IR and NMR spectroscopy revealed formation $[L^{tBu}NiCO]$, indicating that the reaction proceeded similar to the previously investigated reaction of $\mathbf{I^{Na}}$ with CO.[7]

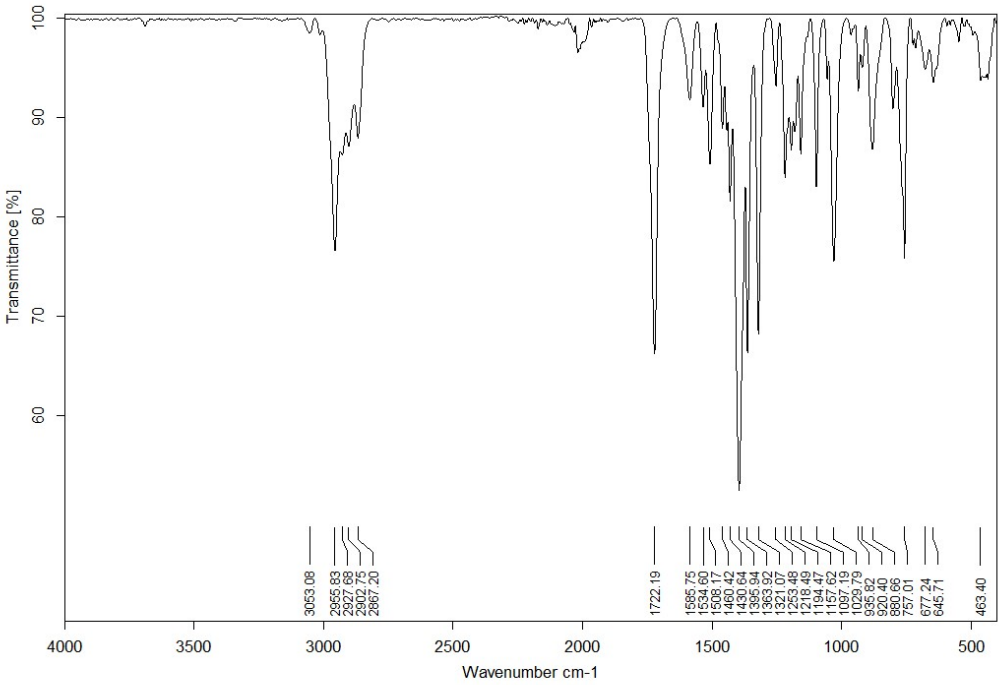

Figure S34: ATR-IR spectrum of **6** (solid obtained from C_6D_6 solution).

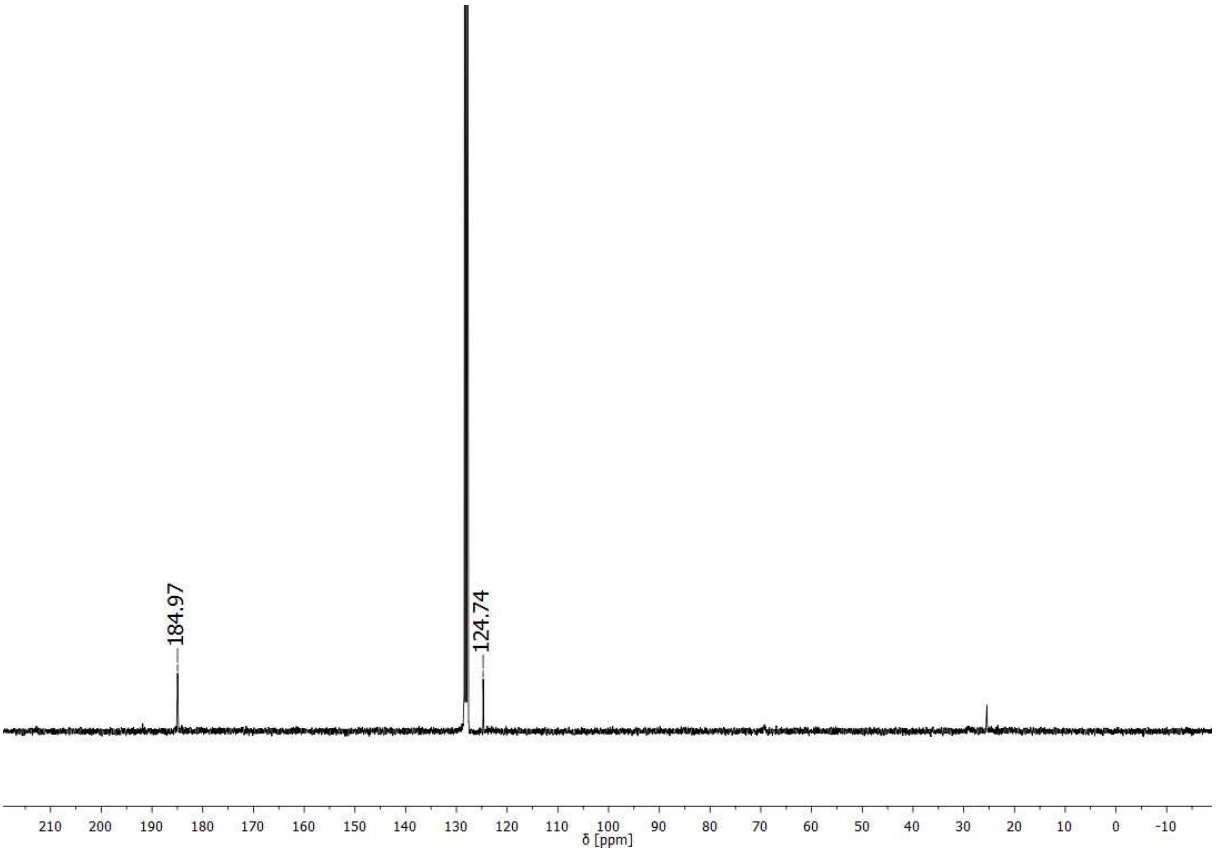

Figure S35: ^{13}C NMR (75.76 MHz, C_6D_6) spectrum of the reaction between **1** and CO.

3. NMR Investigation of the Schlenk equilibrium

3.1 In situ generation of [L^{tBu}NiCO$_2$Ca(THF)$_4$I], 2´

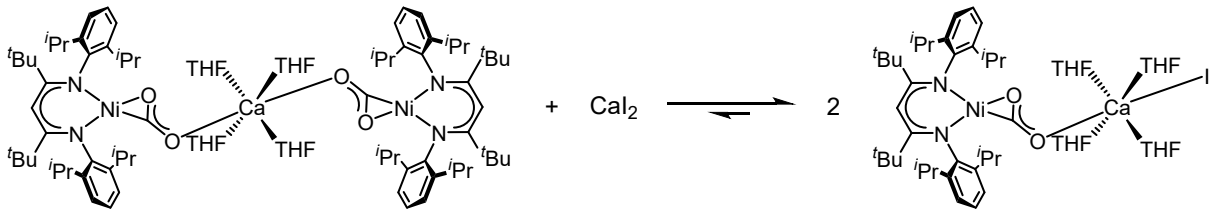

2 **2´**

Scheme S2: Schlenk equilibrium between **2** and **2´**.

A scintillation vial was charged with **I^{Na}** (18.8 mg, 0.03 mmol), CaI_2 (9.0 mg, 0.03 mmol) and 0.6 mL of THF-d_8. After shaking for 1 min the solution was filtered into a J. Young NMR tube and the sample was analysed by NMR and IR spectroscopy.

The ^{1}H NMR spectrum indicated the formation of two new complexes, the minor product of which was identified as **2**. The main product was assumed to be a heteroleptic complex CaI(THF)$_4$[L^{tBu}NiCO$_2$], **2´**. Considering the proposed structure of the main product and the presence of two L^{tBu}Ni entities in **2** a molar ratio of 93:7 was determined based on integration of the ^{1}H NMR signals (see Figure S36). Repeating the experiment with **^{13}I^{Na}** allowed for the use of ^{13}C NMR spectroscopy to monitor the reaction. The ^{13}C NMR spectrum of the reaction mixture confirmed formation of two $^{13}CO_2$ species in a comparable ratio as observed in the ^{1}H NMR spectrum (see Figure S37).

Concentration of **2** in the analysed samples was low enough to exclusively collect the ^{13}C NMR spectroscopic data of **2´**. 2D NMR experiments were performed to ensure a correct assignment of all signals.

Isolation of **2´** as a pure sample failed since all applied measures (concentration, change of solvent, cooling down etc.) caused precipitation of CaI_2 and shift of the equilibrium towards **2**.

NMR Data for 2´:

^{1}H-NMR (500 MHz, THF-d_8): δ (ppm) = 6.78-6.66 (m, 6 H, Ar-**H**), 5.03 (s, 1 H, C**H**$_{backbone}$), 3.80 (overlapping septets, 4 H, C**H**(CH$_3$)$_2$), 1.69 (d, J=6.5 Hz, 6 H, CH(C**H**$_3$)$_2$), 1.58 (d, overlapping with a doublet of **2**, J=6.5 Hz, 12 H, CH(C**H**$_3$)$_2$), 1.30 (d, J=6.5 Hz, 12 H, CH(C**H**$_3$)$_2$), 1.28 (d, overlapping with a doublet of **2**, J=6.5 Hz, 12 H, CH(C**H**$_3$)$_2$), 1.08 (s, 18 H, C(C**H**$_3$)$_3$), 0.93 (s, 18 H, C(C**H**$_3$)$_3$).

^{13}C NMR (125 MHz, THF-d_8): δ (ppm) = 171.23 (**C**O$_2$), 167.04 (N**C**-^{t}Bu), 165.82 (N**C**-^{t}Bu), 155.09 (Ar-**C**), 149.57 (Ar-**C**), 141.92 (Ar-**C**), 140.79 (Ar-**C**), 123.37 (Ar-**C**), 123.19 (Ar-**C**), 122.58 (Ar-**C**), 122.30 (Ar-**C**), 96.80 (γ-**C**), 43.07 (**C**(CH$_3$)$_3$), 42.81 (**C**(CH$_3$)$_3$), 34.00 (C(**C**H$_3$)$_3$), 33.46 (C(**C**H$_3$)$_3$), 28.94 (**C**H(CH$_3$)$_2$), 28.68 (CH(**C**H$_3$)$_2$), 26.50 (CH(**C**H$_3$)$_2$), 26.47 (CH(**C**H$_3$)$_2$), 23.92 (CH(**C**H$_3$)$_2$), 23.86 (CH(**C**H$_3$)$_2$).

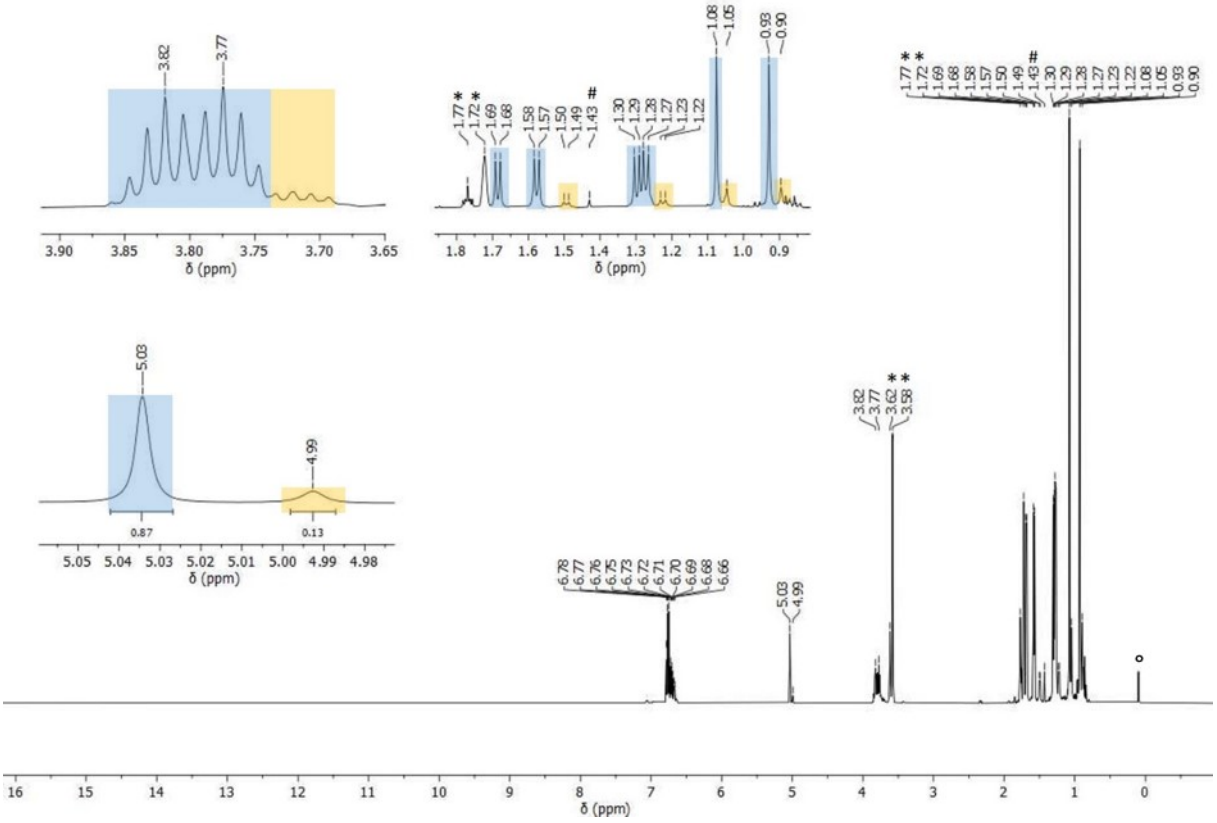

Figure S36: ^{1}H NMR (500.13 MHz, THF-d_8) spectrum of **2´** (93%, blue label) and **2** (7%, orange label) (° = impurity of silicon grease, # = unknown impurity).

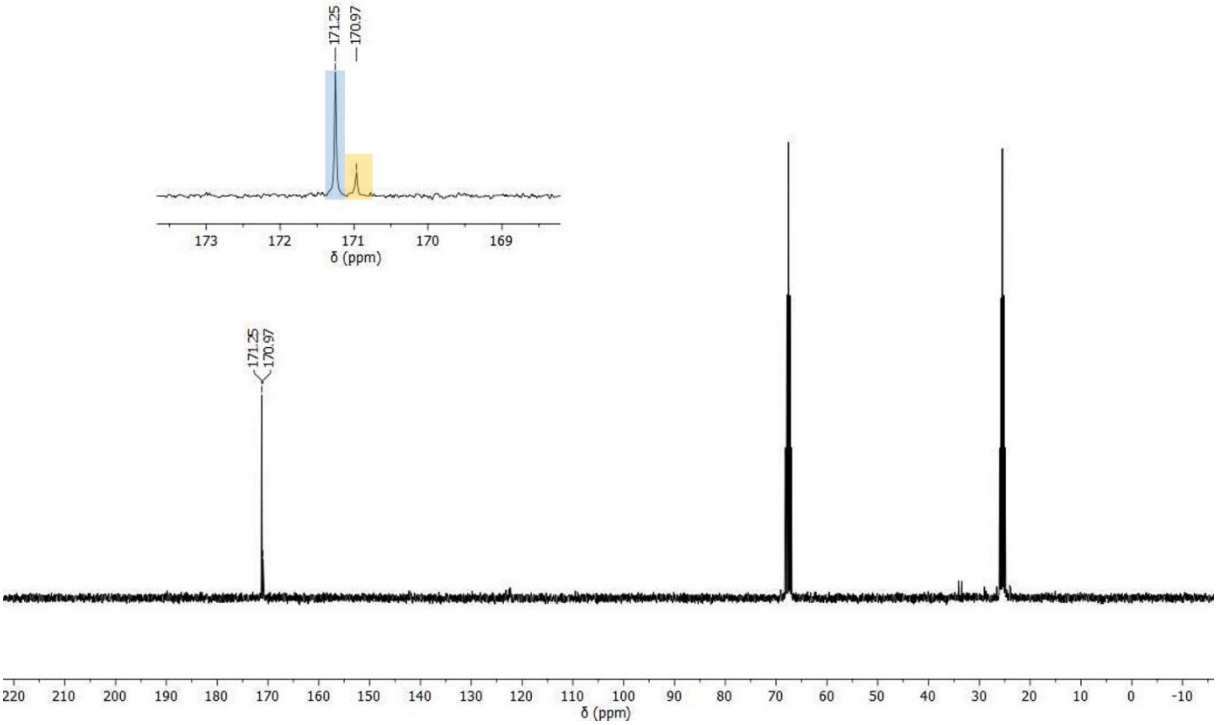

Figure S37: ^{13}C NMR (75.76 MHz, THF-d_8) spectrum of **2´** (93%, blue label) and **2** (7%, orange label).

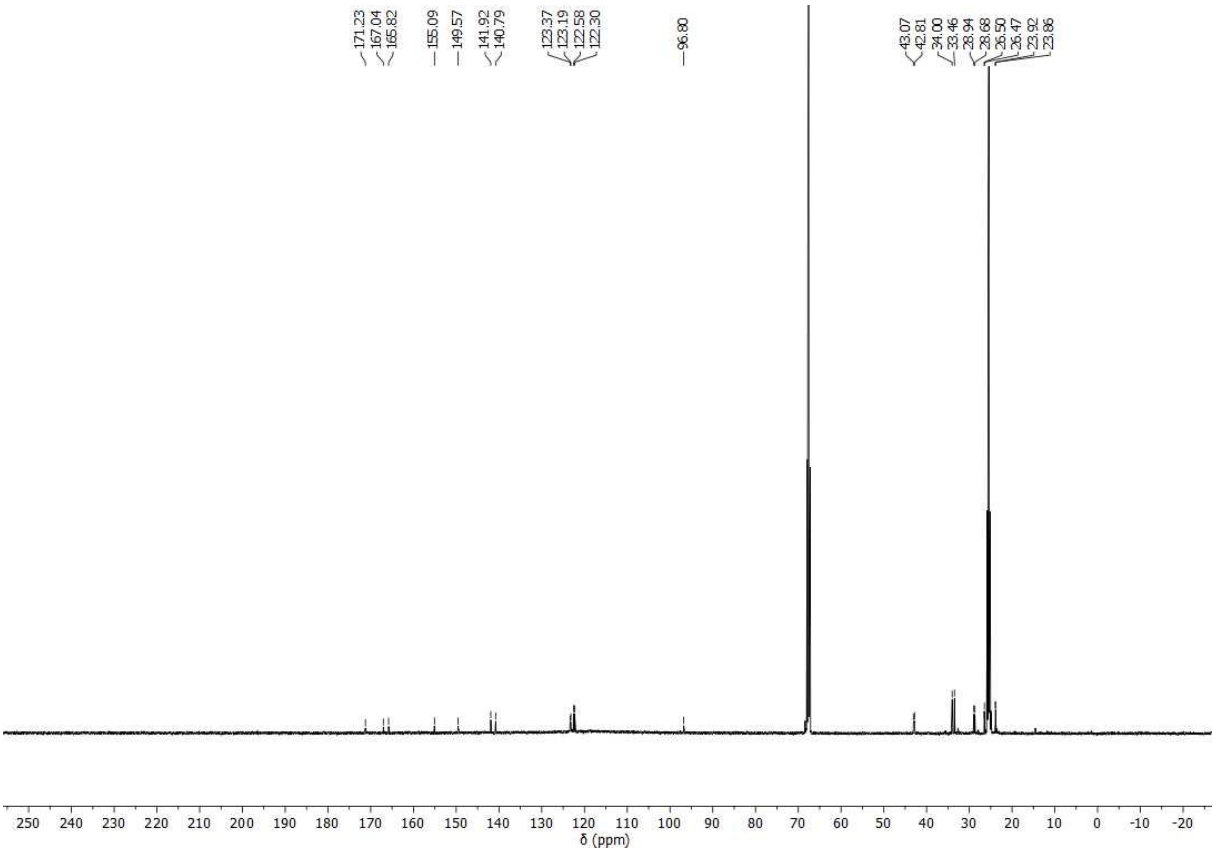

Figure S38: ^{13}C NMR (125.77 MHz, THF-d_8) spectrum of **2´** (signals of **2** were not detected due to its low concentration).

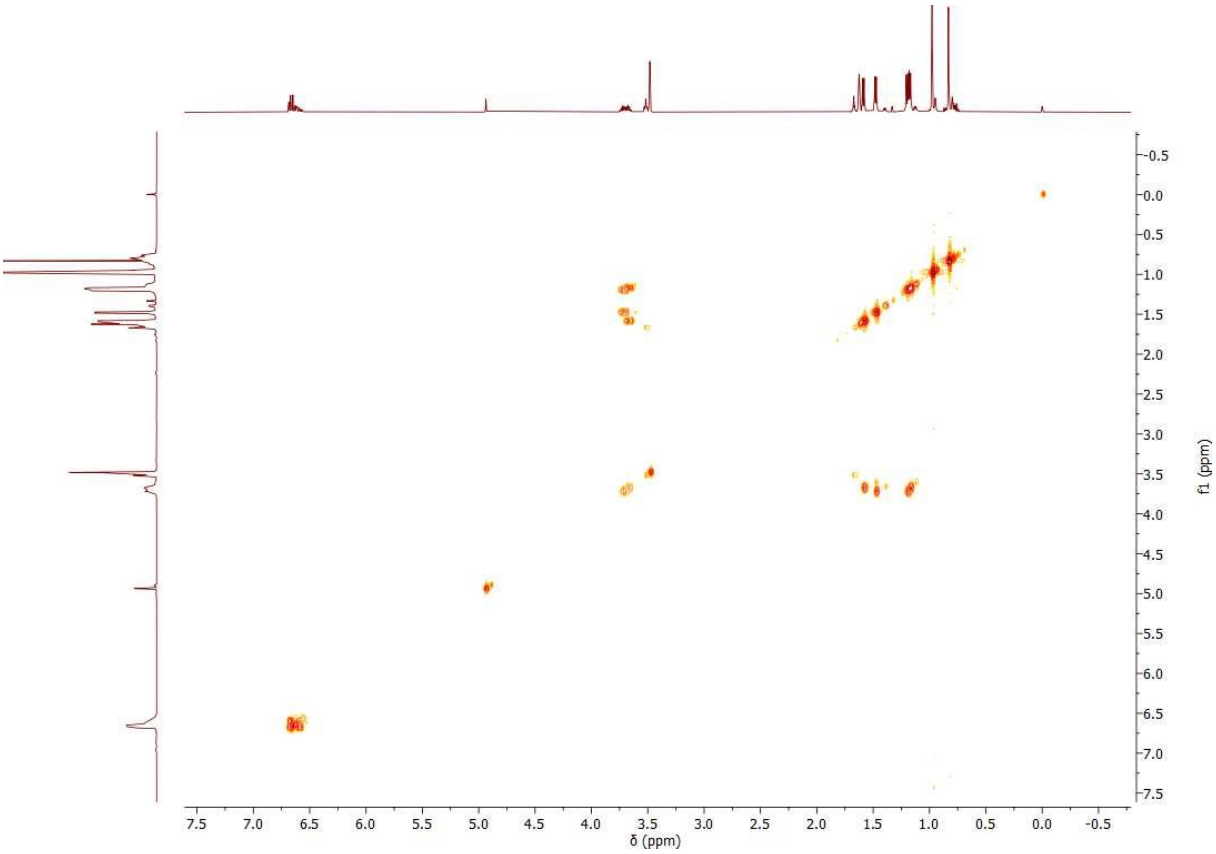

Figure S39: ^{1}H-^{1}H COSY NMR (500.13 MHz, THF-d_8) spectrum of **2´** (signals of **2** were not detected due to its low concentration).

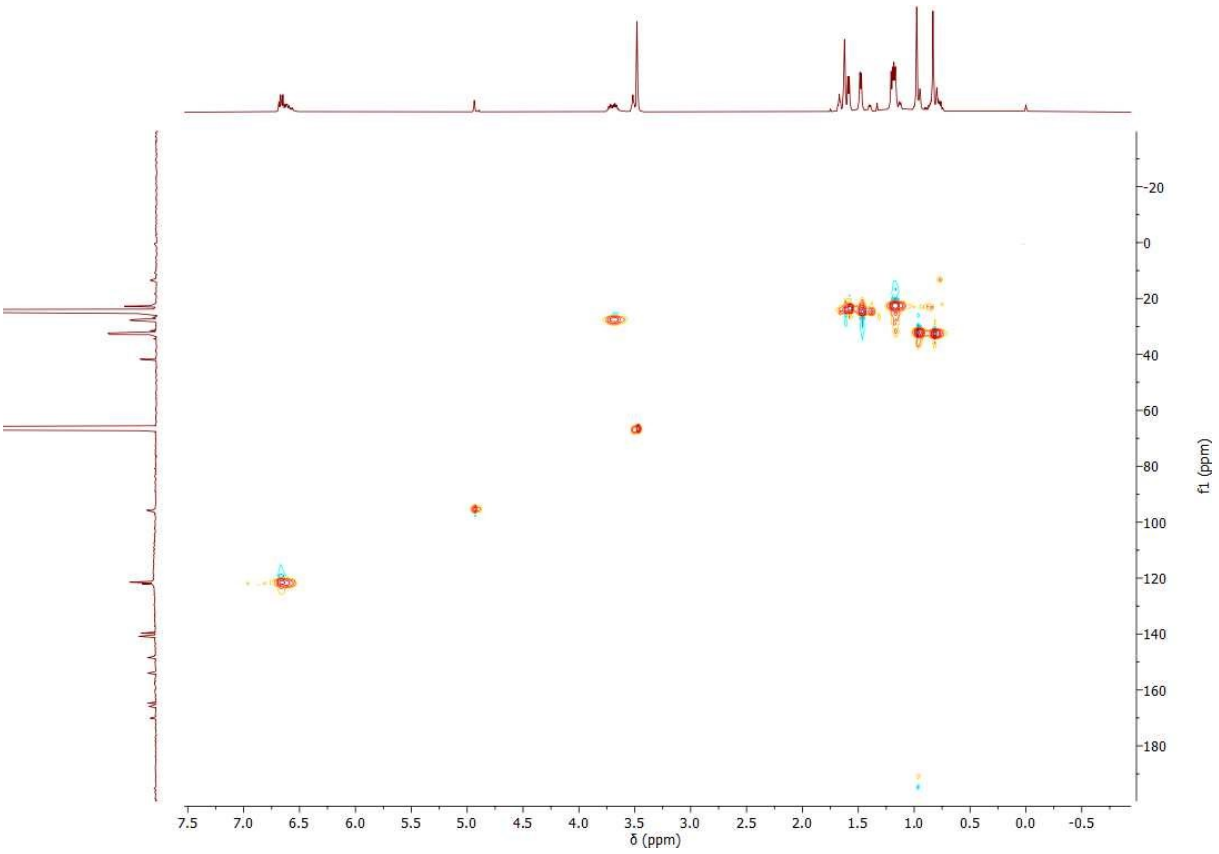

Figure S40: ^{1}H-^{13}C HSQC NMR (500.13 MHz, THF-d_8) spectrum of **2´** (signals of **2** were not detected due to its low concentration).

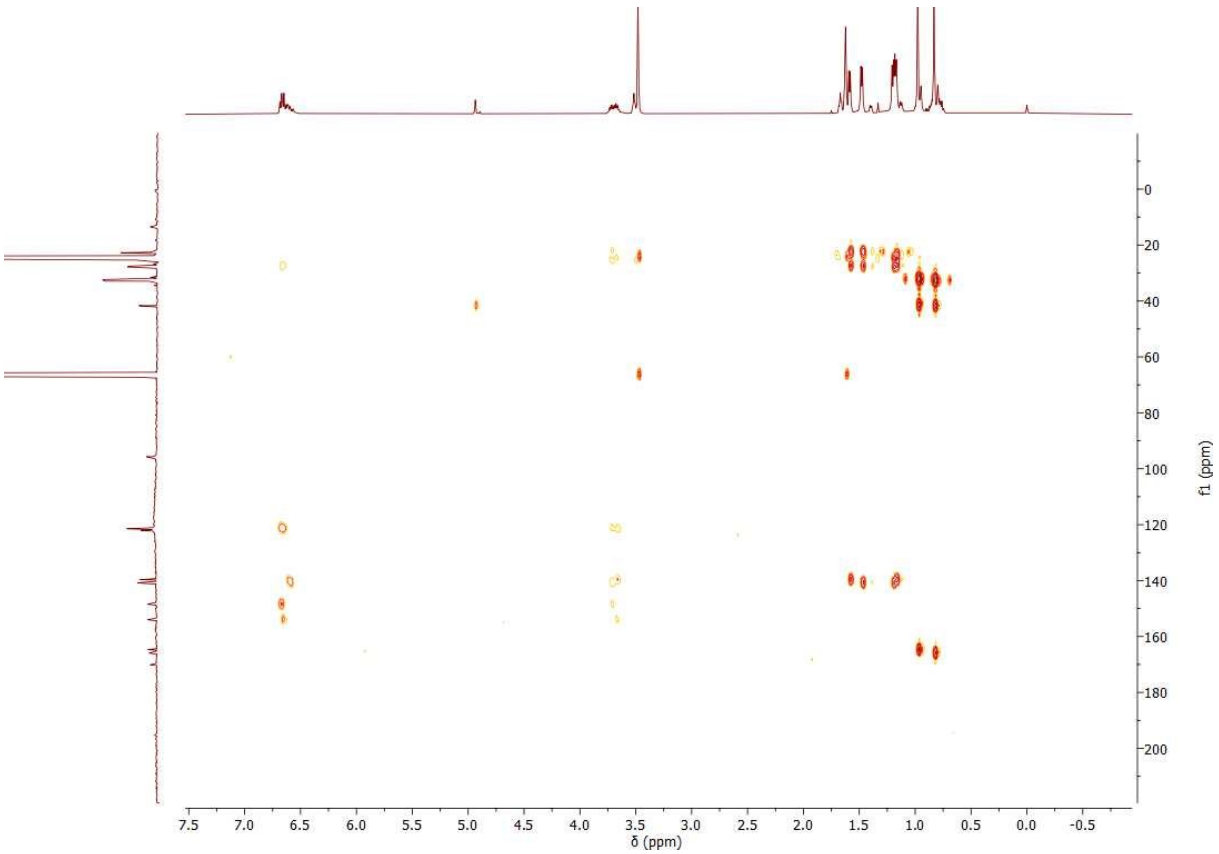

Figure S41: ^{1}H-^{13}C HMBC NMR (500.13 MHz, THF-d_8) spectrum of **2´** (signals of **2** were not detected due to its low concentration).

3.2 Generation of mixtures of 2 and 2´

A scintillation vial was charged with **I^{Na}** (18.8 mg, 0.03 mmol), CaI_2 (9.0 mg, 0.03 mmol) and 0.6 mL of THF and subsequently shaken for 1 min. The solvent was removed under reduced pressure and the residue was extracted with Et_2O. After evaporation of the solvent the residue was taken up in 0.6 mL of THF-d_8 and analysed by NMR and IR spectroscopy.

The ^{1}H NMR spectrum featured again a mixture of **2** and **2´**. The latter was still identified as the main product, however, the molar ratio had changed significantly as the concentration of **2** had increased. Considering the proposed structure of the main product and the presence of two L^{tBu}Ni entities in **2** a molar ratio of 68:32 was determined based on the integration of the ^{1}H NMR signals (see Figure S42). Repeating the experiment with **^{13}I^{Na}** allowed for the use of ^{13}C NMR spectroscopy for reaction control. The ^{13}C NMR spectrum of the reaction confirmed formation of two $^{13}CO_2$ species in a comparable ratio as observed in the ^{1}H NMR spectrum (see Figure S43).

^{1}H NMR signals of an unidentified side product were observed which was reproducibly formed during the described sample preparation (see Figure S42). Furthermore, IR spectroscopic data analysis indicated that during the sample preparation decomposition of CO_2^{2-} ligand occurred since a band for the characteristic C-O stretching vibration of [L^{tBu}Ni^{13}CO] was observed (see Figure S45).

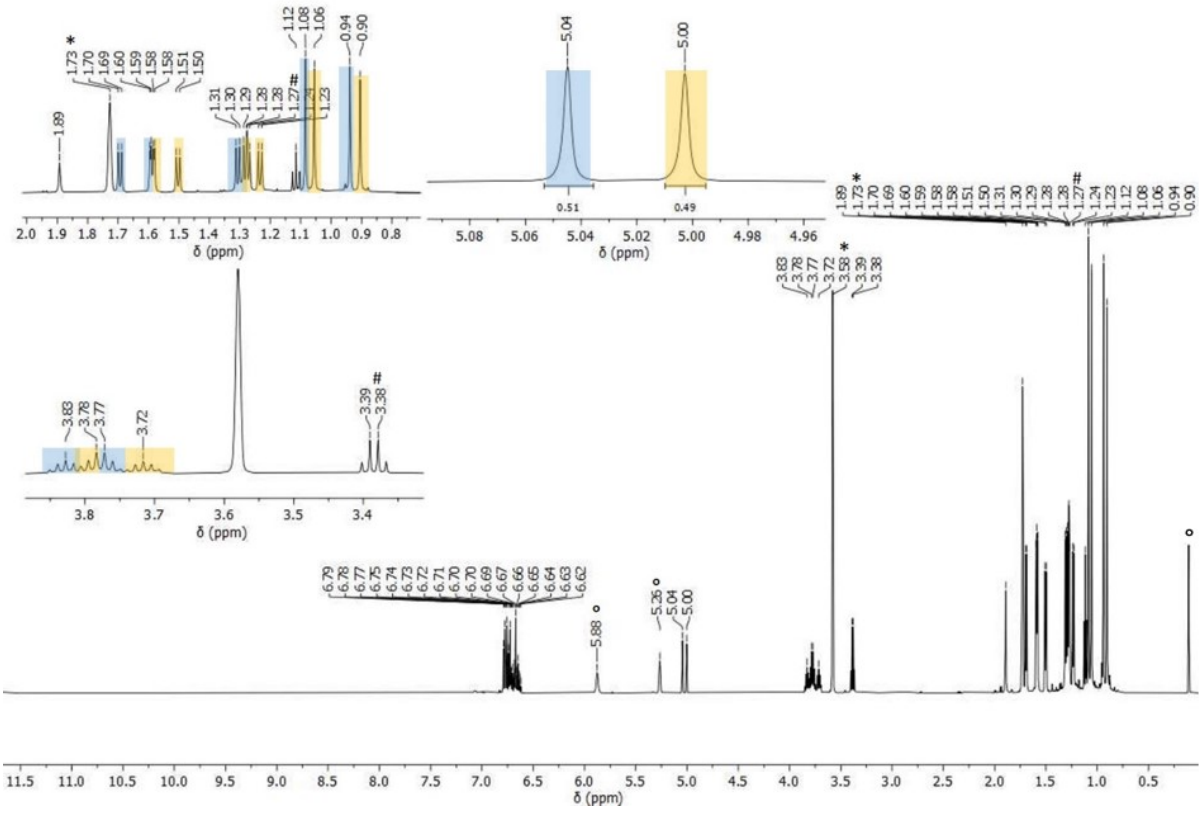

Figure S42: ^{1}H NMR (500.13 MHz, THF-d_8) spectrum of **2´** (68%, blue label) and **2** (32%, orange label). (° = impurity of silicon grease, # = Et_2O).

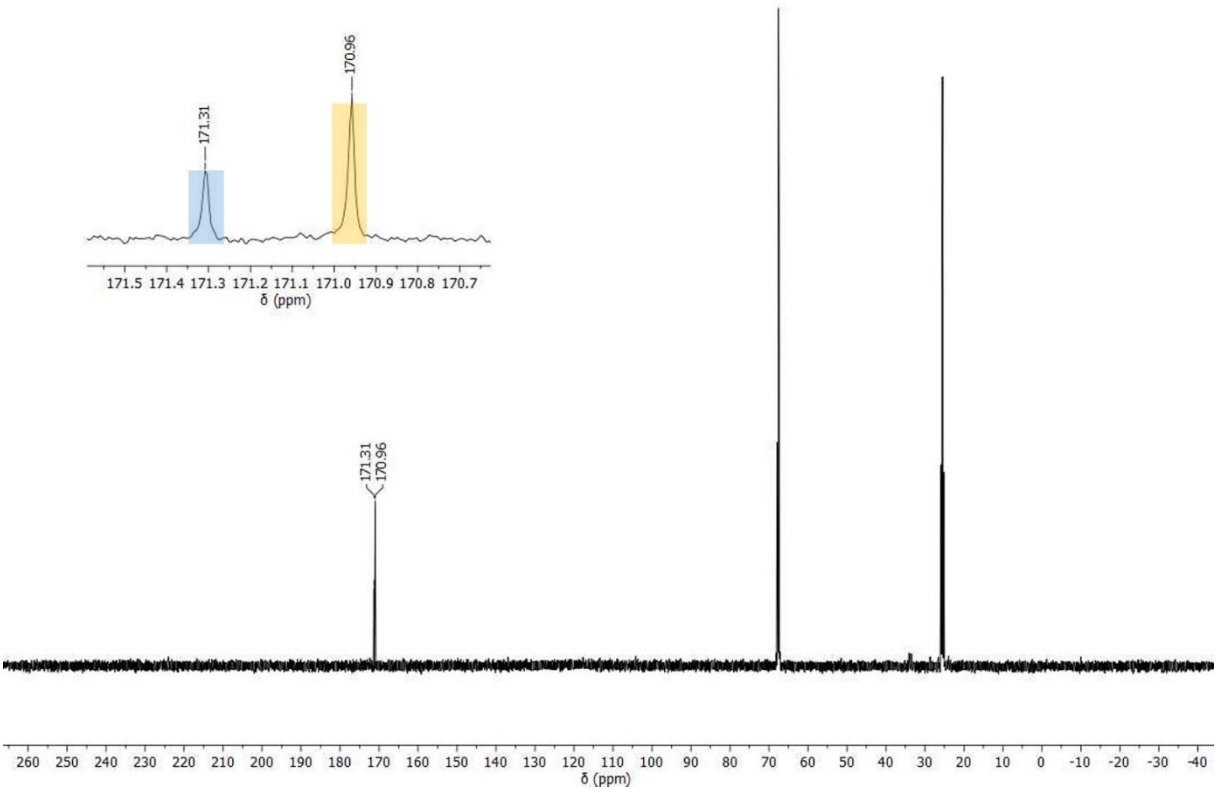

Figure S43: ^{13}C NMR (75.76 MHz, THF-d_8) spectrum of **2´** (68%, blue label) and **2** (32%, orange label).

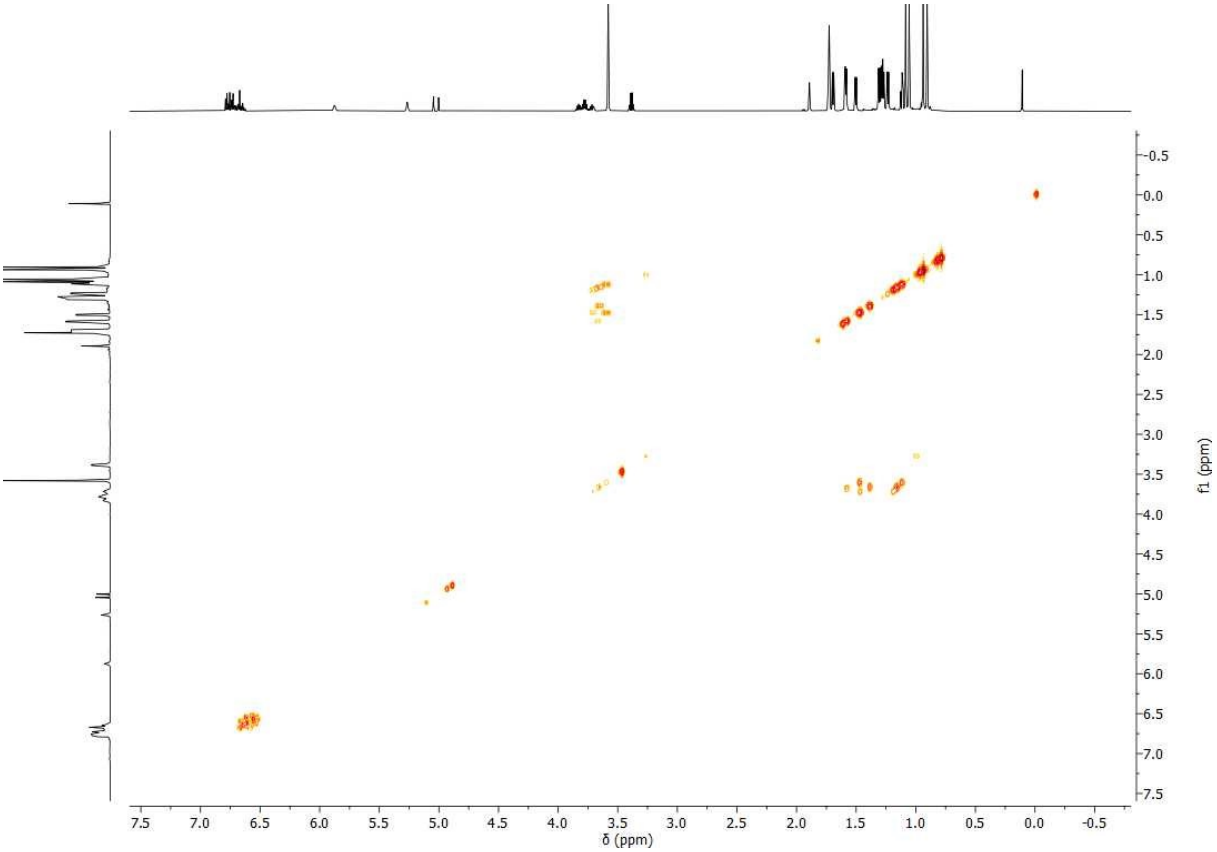

Figure S44: ^{1}H-^{1}H COSY NMR (500.13 MHz, THF-d_8) spectrum of **2´** (68%, blue label) and **2** (32%, orange label).

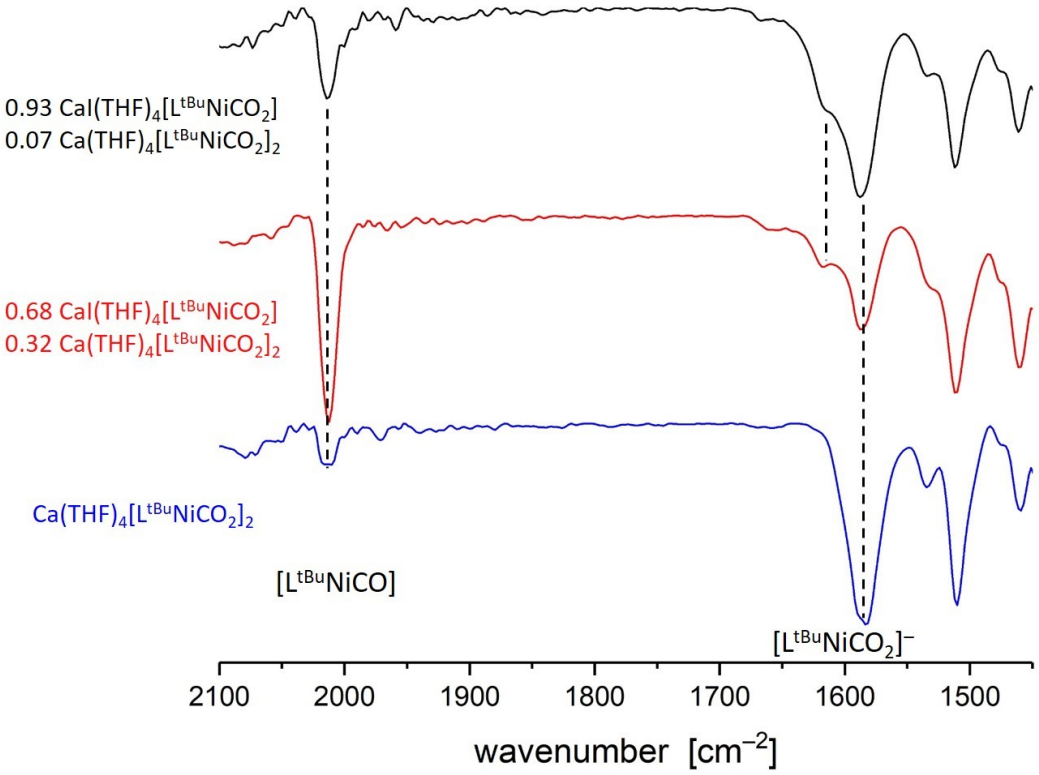

Figure S45: Comparison of the IR spectra **2, 2´** and their mixtures for the C-O stretching frequencies.

3.3 Generation of [MgI(THF)$_4$(L^{tBu}NiCO$_2$)], 1´, at elevated temperatures

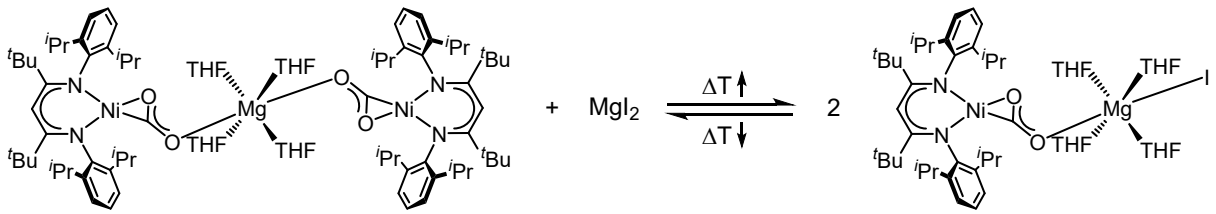

1 **1´**

Scheme S3: Temperature-dependent interconversion of **1** and **1´**.

15 mg (0.01 mmol) of ^{13}**1** together with 10 mg (0.04 mmol) of MgI_2 were suspended in 0.6 mL of THF-d_8. Afterwards the excessive MgI_2 was allowed to settle down and NMR spectra were recorded at temperatures between +55 °C and –40 °C. After heating the sample to 55 °C a new species formed which was assumed to be [MgI(THF)$_4$(L^{tBu}Ni^{13}CO$_2$)], ^{13}**1´** (see Figure S46). Considering the proposed structure of **1´**and the presence of two L^{tBu}Ni entities in ^{13}**1** a molar ratio of 40:60 was determined based on the integration of the ^{1}H NMR signals. Heating the sample for an extended period of time or even to higher temperatures did not shift the molar ratio further towards the heteroleptic complex ^{13}**1´**.

Upon cooling to –40 °C signals of ^{13}**1´** disappeared again to give back the initial sample of ^{13}**1**. However, this reaction did not proceed continuously throughout the cooling period. In between 55 °C and 0 °C no change of the sample composition was observed. Only when the sample was cooled down even further to –20°C the signals of ^{13}**1´** instantaneously disappeared.

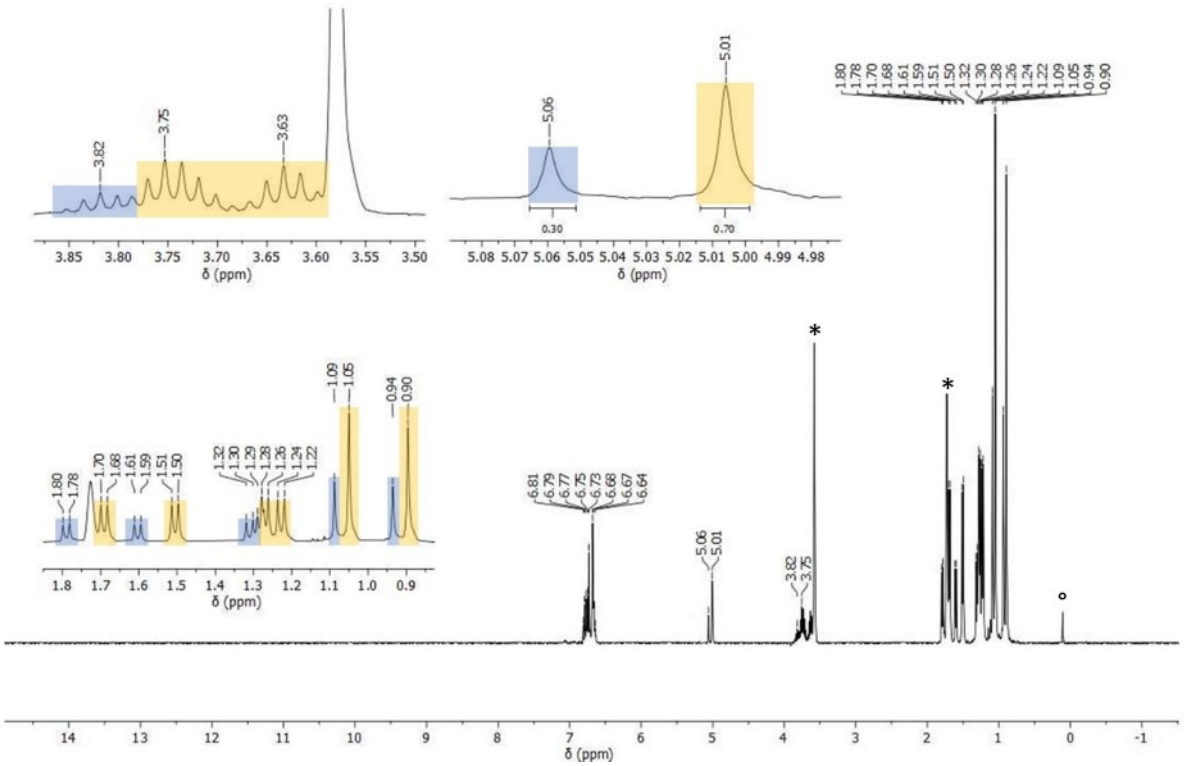

Figure S46: ^{1}H NMR (500.13 MHz, 55 °C, THF-d_8) spectrum of **1´** (40%, blue label) and **1** (60%, orange label) (° = impurity of silicon grease).

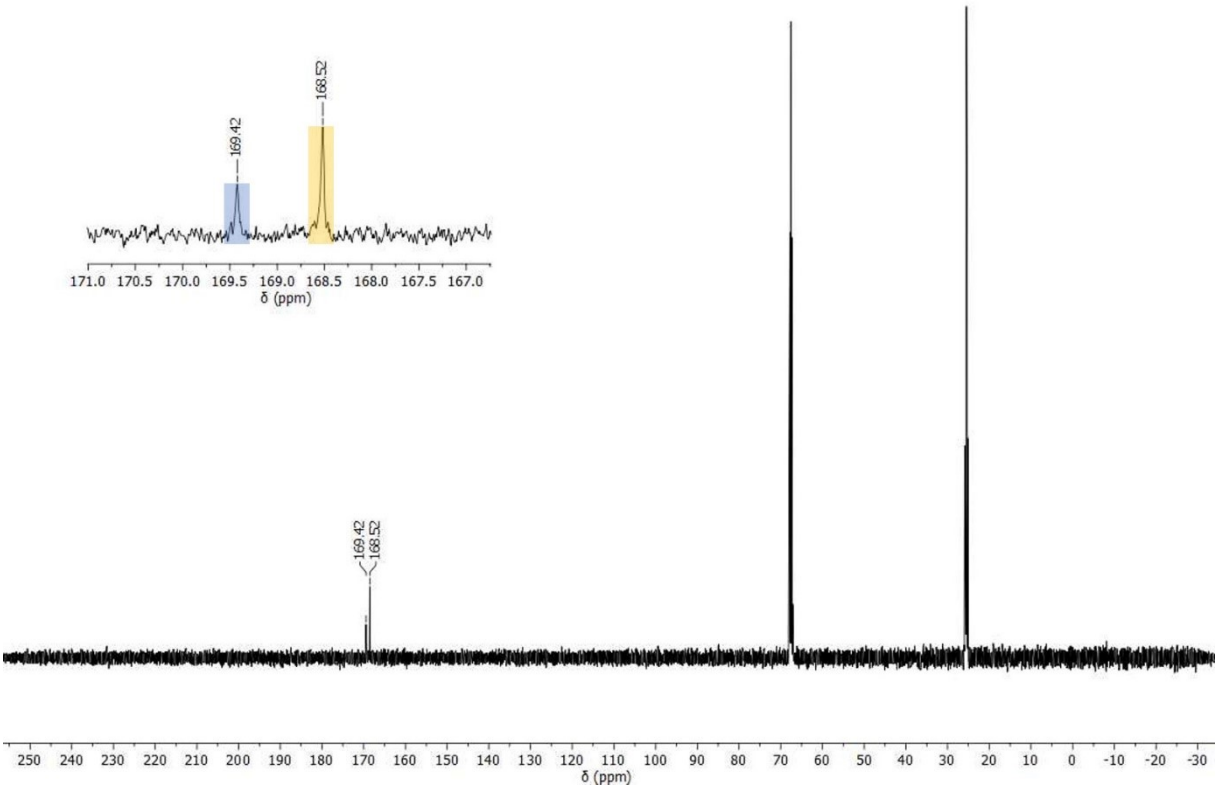

Figure S47: ^{13}C NMR (75.76 MHz, 55 °C, THF-d_8) spectrum of **^{13}1´** (40%, blue label) and **^{13}1** (60%, orange label).

4. DOSY measurement

In order to provide experimental evidence for the suggested structures of $CaI(THF)_4[L^{tBu}NiCO_2]$, **2´**, and $[L^{tBu}NiCO_2Ca(THF)_4I]$, **4**, DOSY measurements were recorded. The DOSY measurements were undertaken on a Bruker Avance 600 MHz NMR spectrometer. The corresponding spectra recorded for THF-d_8 solutions are shown below. Using the Stokes-Einstein equation the hydrodynamic radius was calculated from the diffusion coefficients.

4.1 Experiments for 1, 2 and 2´

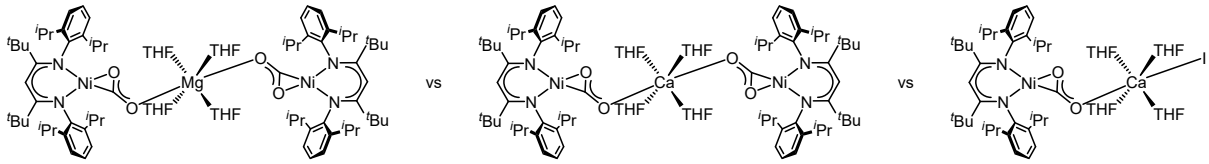

1 **2** **2´**

A pure sample of **2** and the two samples of **2´**, described in section 3.1 and 3.2, were analysed. Additionally, $Mg(THF)_4[L^{tBu}NiCO_2]_2$, **1**, was used as reference.

The DOSY spectrum of mixture of **2** and **2´** indeed featured two diffusion traces (see Figure S51, S52 and S53) which match the independently measured traces of **2** and **2´** (see Figure S49 and S50). The diffusion coefficient of **2** was found to be lower than the one determined for **2´**. Therefore, **2´** exhibits a smaller hydrodynamic surface, which supports its proposed structure. As expected, the diffusion coefficient of **1** was found to be very similar to the one of **2** (see Figure S54).

Table S2: Results of the DOSY NMR experiments.

	Diffusion coefficient [m²/s]	Hydrodynamic radius [Å]	Hydrodynamic diameter [Å]	Largest extent of molecule in X-ray structure [Å]
1	$5.71*10^{-10}$	7.10	14.20	20
2	$5.88*10^{-10}$	6.93	13.86	19
2´	$6.82*10^{-10}$	5.95	11.90	15[a]

[a] Data was obtained from the DFT optimised model (see Figure S60).

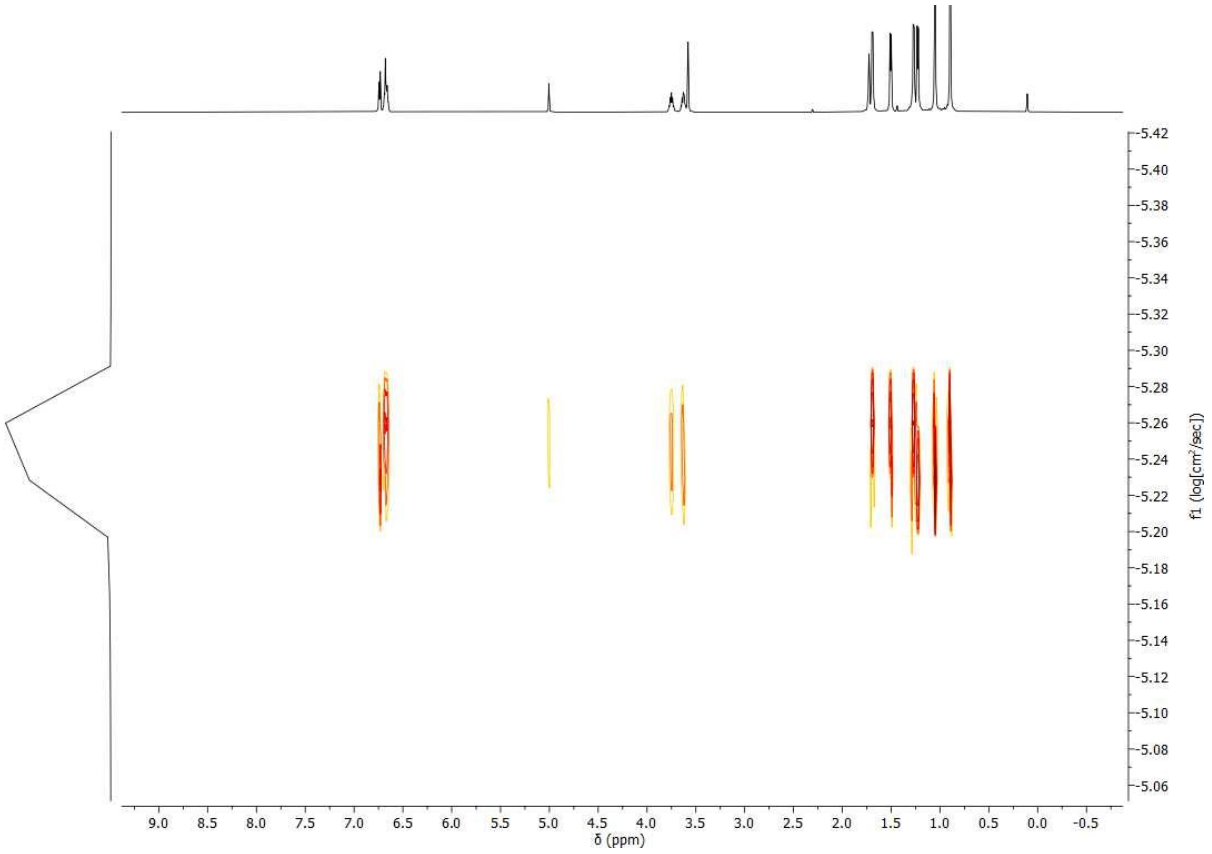

Figure S48: DOSY NMR spectrum (599.89 MHz, THF-d_8) of **1**.

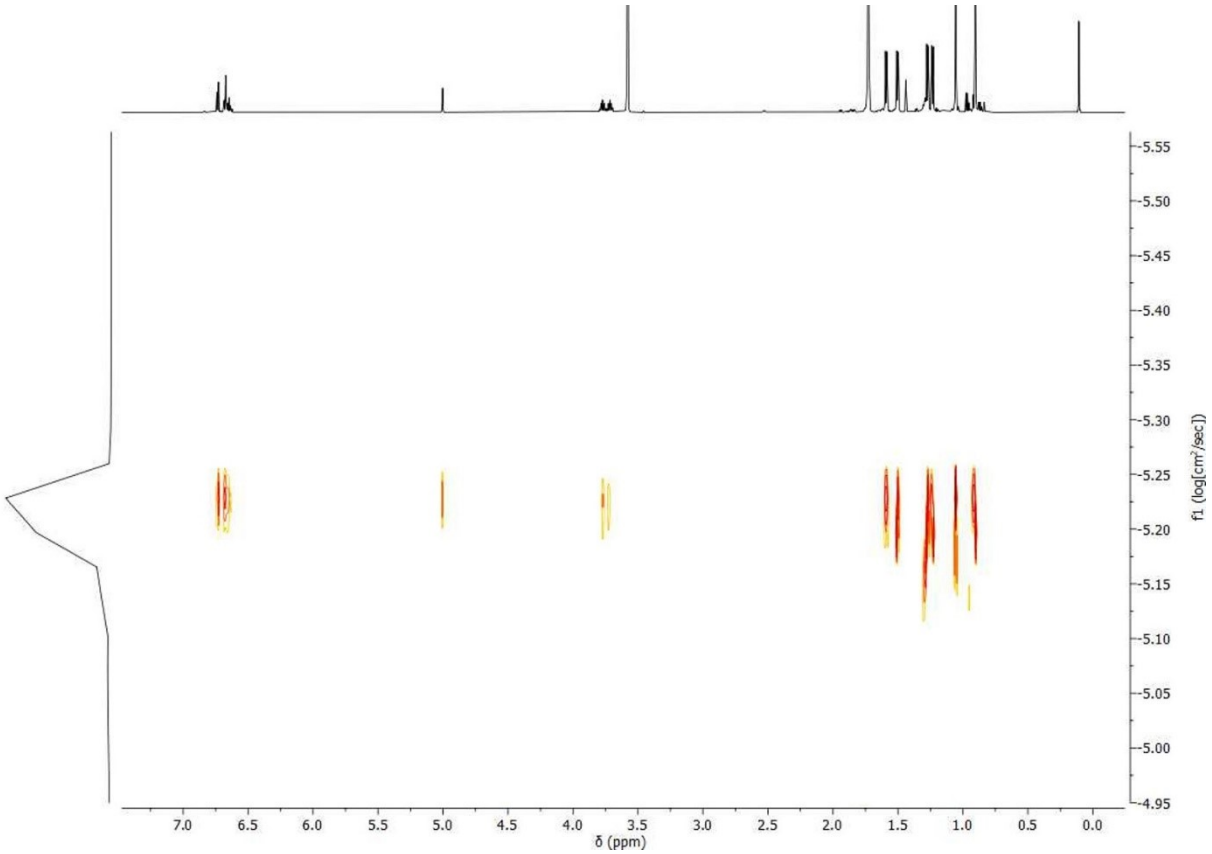

Figure S49: DOSY NMR spectrum (599.89 MHz, THF-d_8) of **2**.

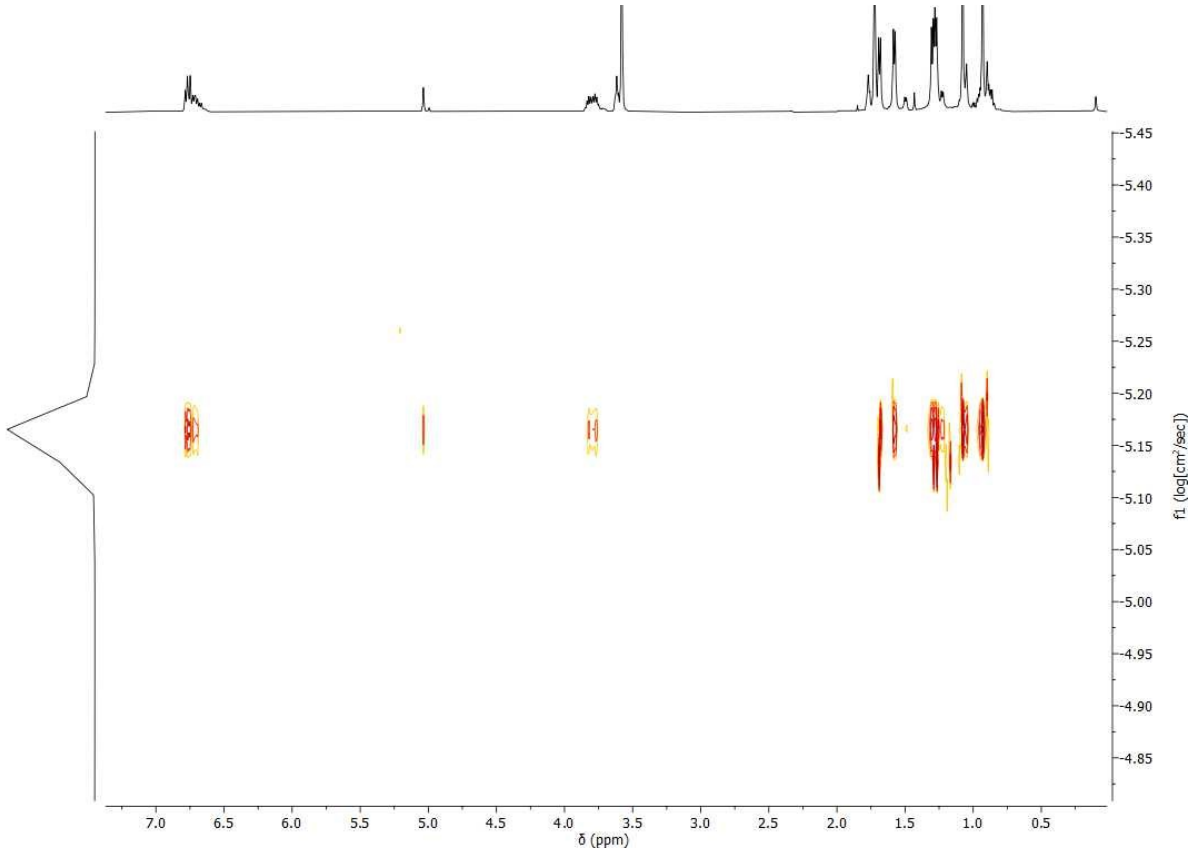

Figure S50: DOSY NMR spectrum (599.89 MHz, THF-d_8) of **2´** (93%). Concentration of **2** (7%) was too low to detect its diffusion traces under the chosen conditions.

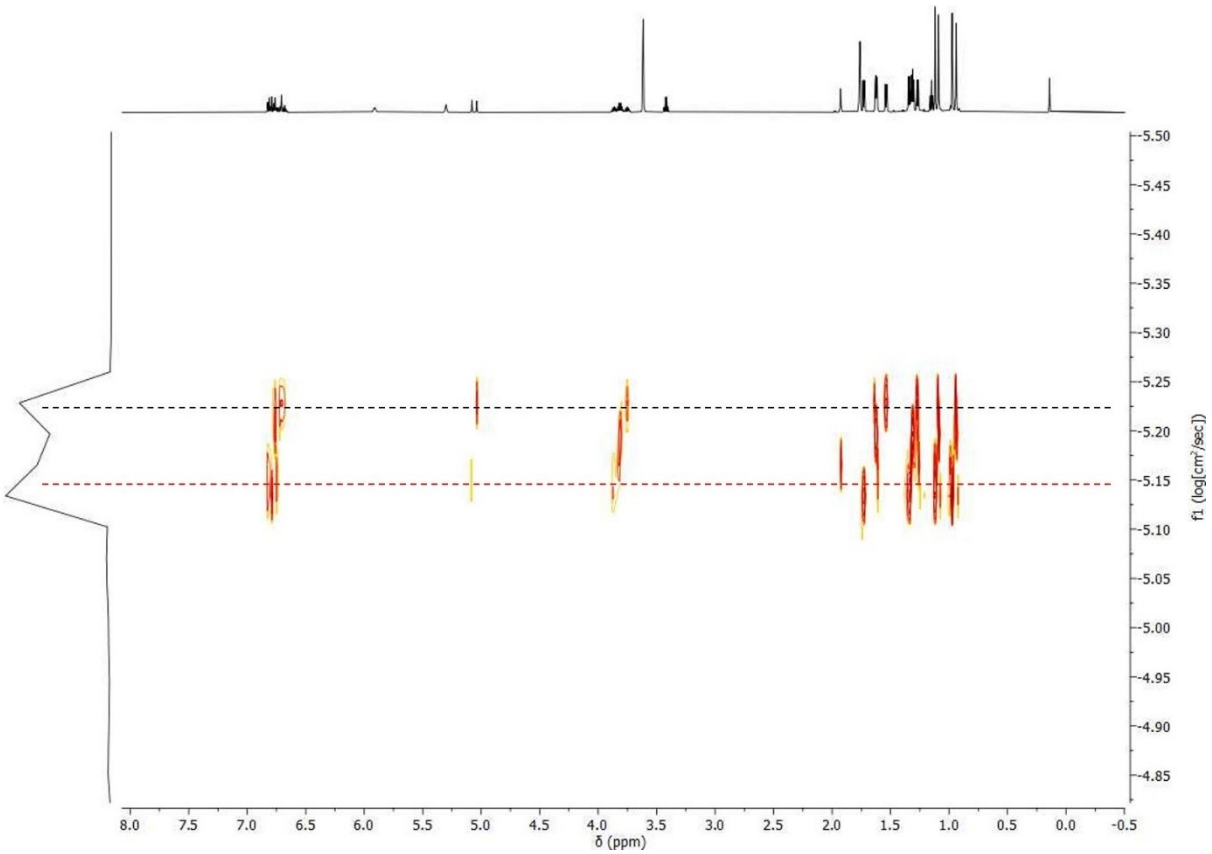

Figure S51: DOSY NMR spectrum (599.89 MHz, THF-d_8) of a mixture of **2´** (68%, marked by a red line) and $Ca(THF)_4[L^{tBu}NiCO_2]_2$ (32%, marked by a black line).

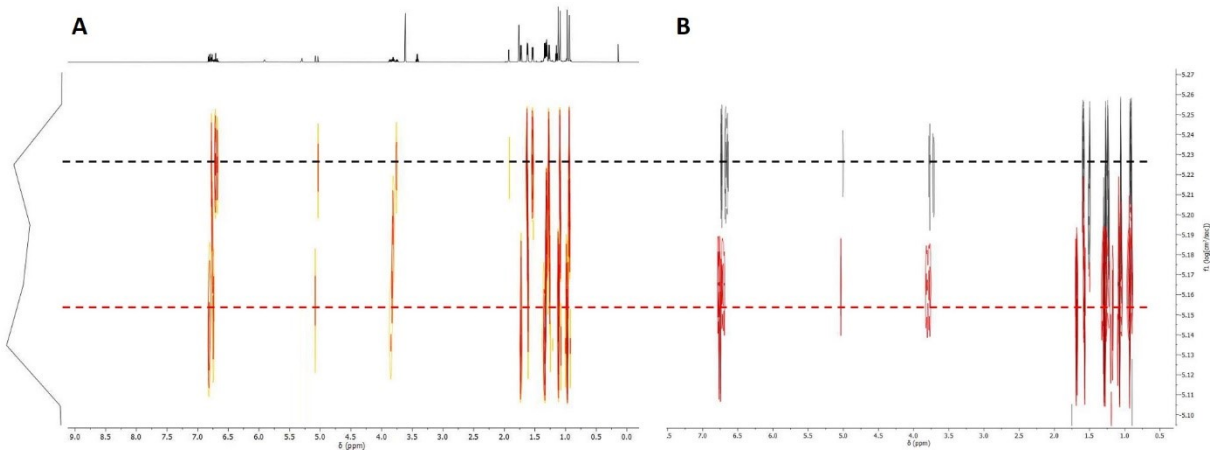

Figure S52: Comparison between the superimposed DOSY spectra (**B**) of **2´** (red line, see Figure S50) and **2** (black line, see Figure S49) and the DOSY spectrum of a mixture of both of them (**A**, see Figure S51).

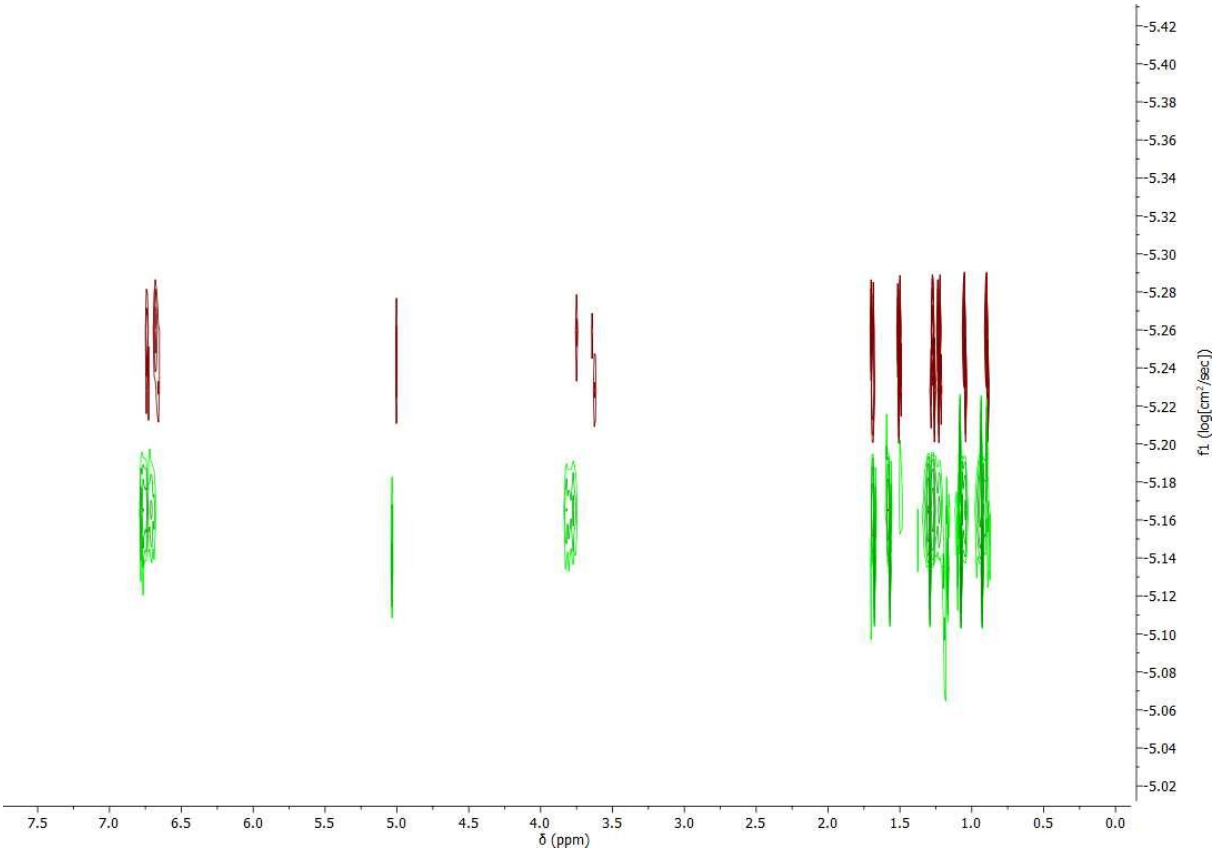

Figure S53: Superimposed DOSY spectra of **2´** (green trace, see Figure S50) and **1** (red trace, see Figure S48).

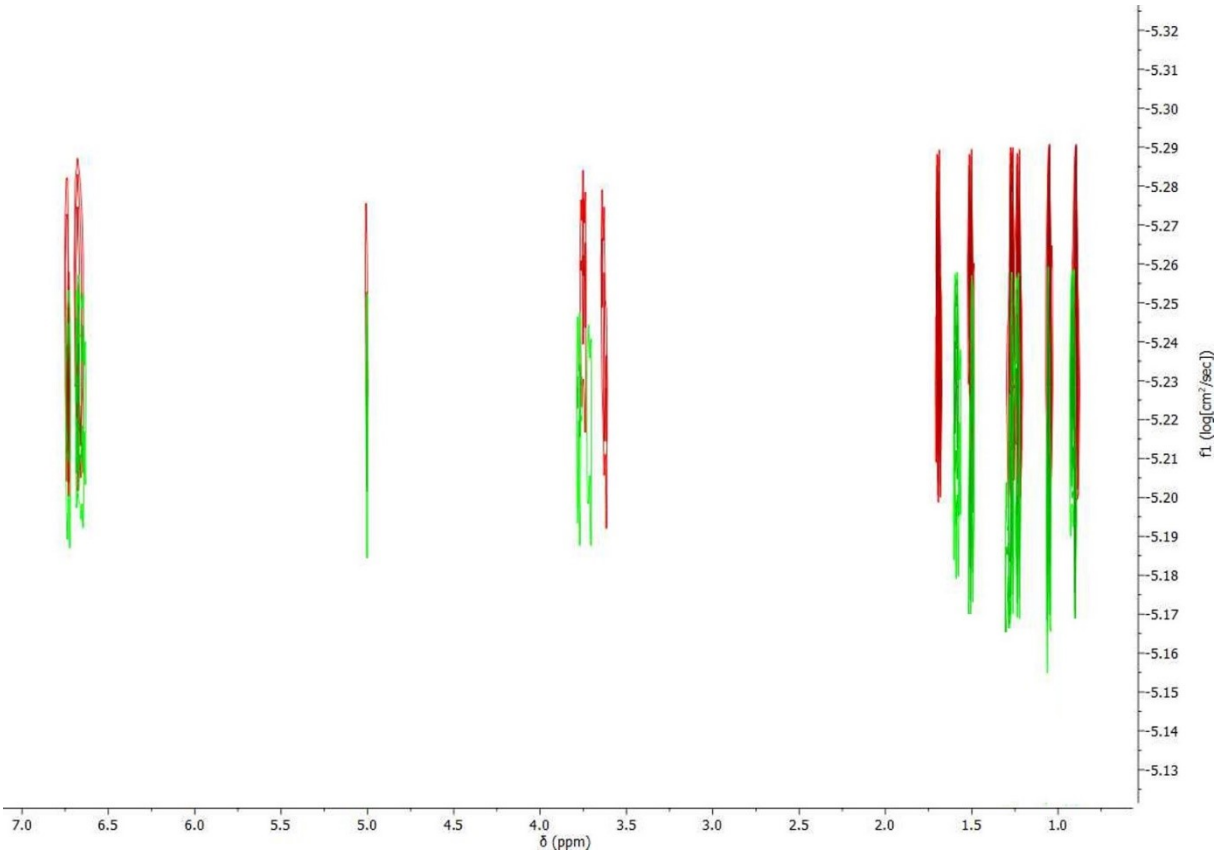

Figure S54: Superimposed DOSY spectra of **2** (green trace, see Figure S49) and **1** (red trace, see Figure S50).

4.1 Experiments for 3 and 4

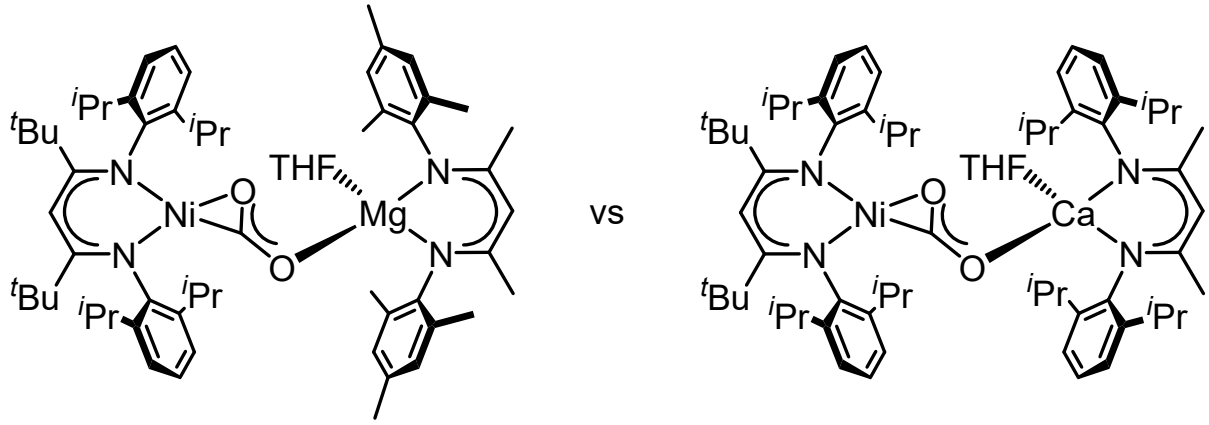

A sample containing **4** was prepared according to the procedure described in section 2.5. Although, the sample contained a mixture of up to four different compound the recorded DOSY trace could be assigned to ^{1}H NMR signals of **4** as the main component in the sample (see Figure S56). A DOSY measurement of a pure sample of complex **3** was used as reference (see Figure S55). Indeed, both complexes **3** and **4** were found to have similar hydrodynamic radii while the Ca derivative is slightly larger.

Table S3: Results of the DOSY NMR experiments.

	Diffusion coefficient [m²/s]	**Hydrodynamic radius [Å]**	**Hydrodynamic diameter [Å]**	**Largest extent of molecule in X-ray structure [Å]**
3	$6.84*10^{-10}$	5.94	11.88	15
4	$6.55*10^{-10}$	6.20	12.40	16[a]

[a] Data was obtained from the DFT optimised model (see Figure S63).

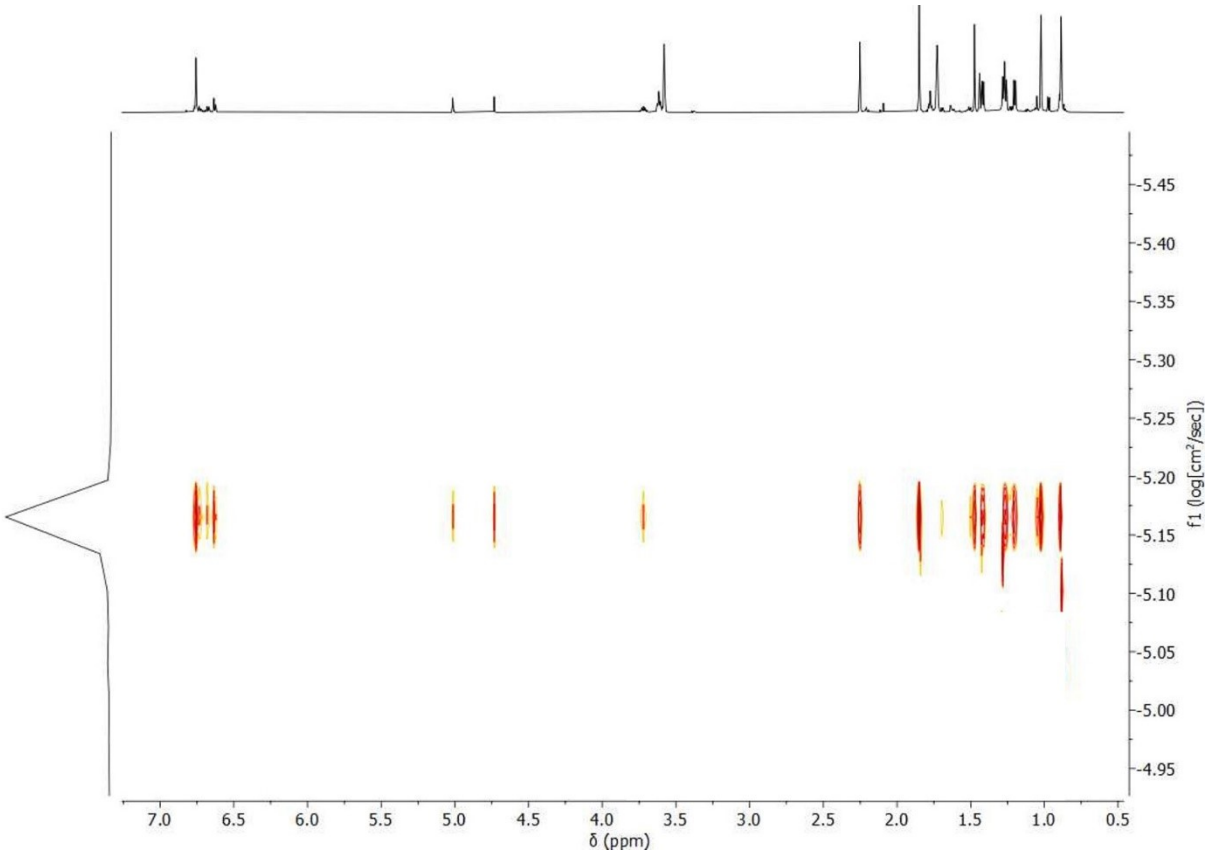

Figure S55: DOSY NMR spectrum (599.89 MHz, THF-d_8) of **3**.

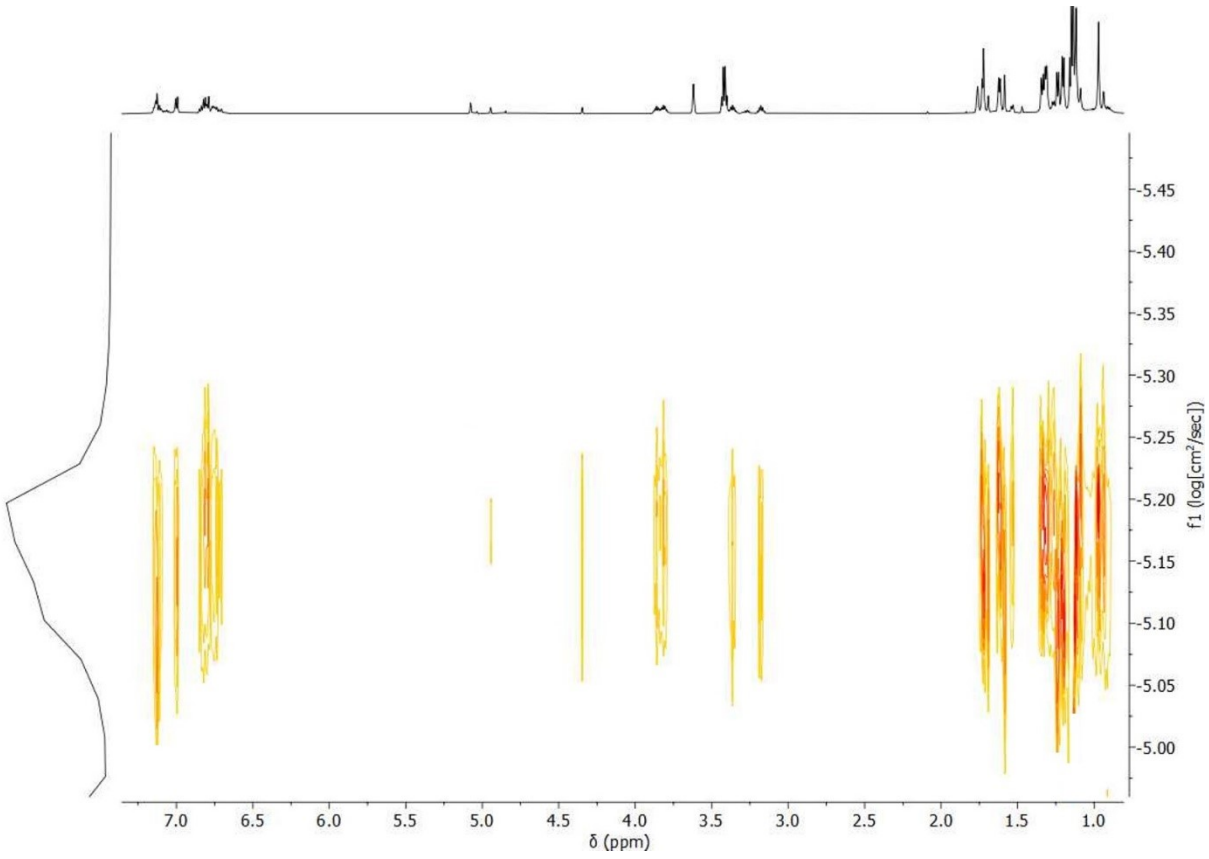

Figure S56: DOSY NMR spectrum (599.89 MHz, THF-d_8) of **4**.

5. Computational Details

Density functional calculations were performed in redundant internal coordinates without symmetry restrictions using the Gaussian 16[8] software package.

The molecular structures of the complexes **1** und **2** as determined by X-ray diffraction analyses were used as starting points for geometry optimizations. Starting points for species **1'** and **2'** were constructed using structural elements of **1** and **2**.

The B3LYP functional[9-11] was employed amended by the D3 version of Grimme's dispersion,[12] together with Def2-SVP basis set for C and H atoms, except for the C atoms which are part to the CO_2 units bound to the Ni atoms, for which the Def2-TZVP basis was used. The Def2-TZVP basis set was also used for all other atoms.[13-14]

The presence of the solvent tetrahydrofuran around the molecules was taken into consideration during calculations by means of the Polarizable Continuum Model (PCM). Vibrational frequencies for all molecules were computed analytically.

All molecular structures were optimised in different spin states and always the singlet state turned out to be the ground state.

For determination of reaction energies characterising the Schlenk equilibria of **1** and **2** (Scheme 4, identical to Scheme 2 in the main paper) structures of all reactants were optimised (figure S57-S61).

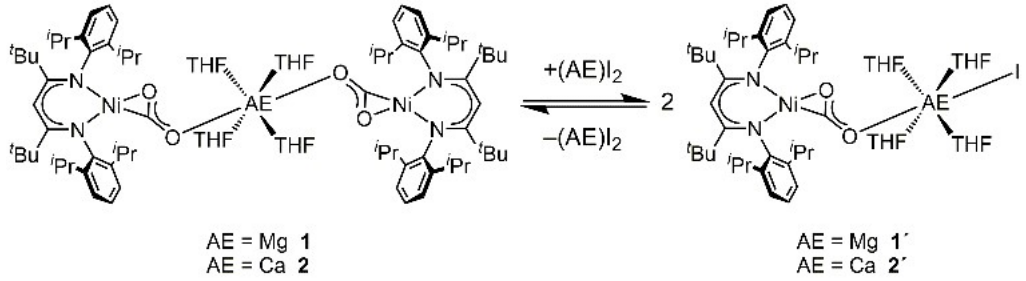

Scheme S4: Schlenk equilibrium of **1** or **2** when treated with $(AE)I_2$.

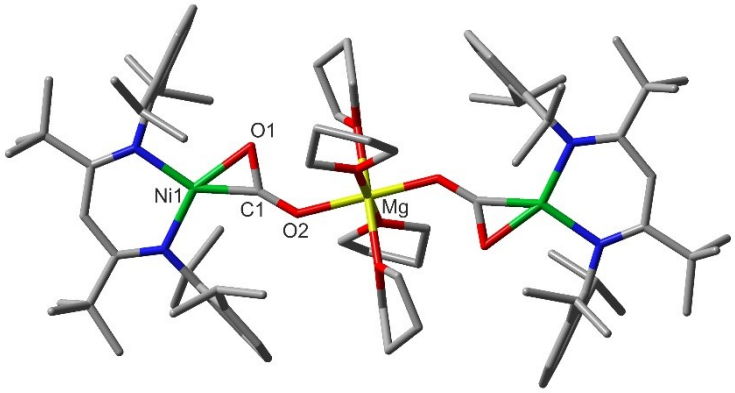

Figure S57: Optimised molecular structure of $[Mg(THF)_4(L^{tBu}NiCO_2)_2]$, **1**. Hydrogen atoms are omitted for clarity. Selected bond lengths (Å) and angles (°): Ni1-C1 1.822, Ni1-O1 1.979, C1-O1 1.273, C1-O2 1.244, O2-Mg 2.026, O1-C1-O2 129.5.

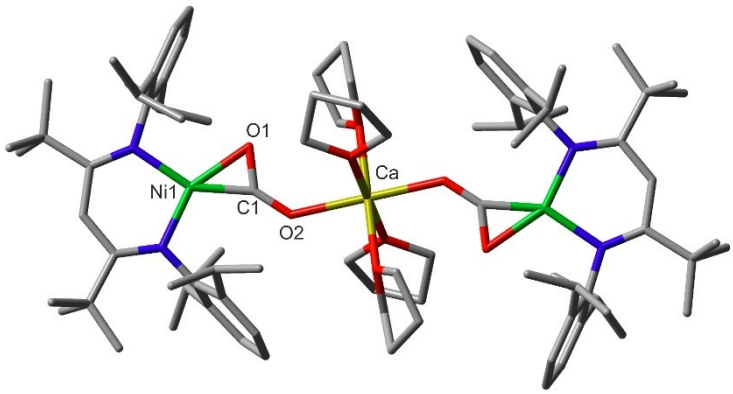

Figure S58: Optimised molecular structure of $[Ca(THF)_4(L^{tBu}NiCO_2)_2]$, **2**. Hydrogen atoms are omitted for clarity. Selected bond lengths (Å) and angles (°): Ni1-C1 1.808, Ni1-O1 2.006, C1-O1 1.273, C1-O2 1.241, O2-Ca 2.276, O1-C1-O2 129.8.

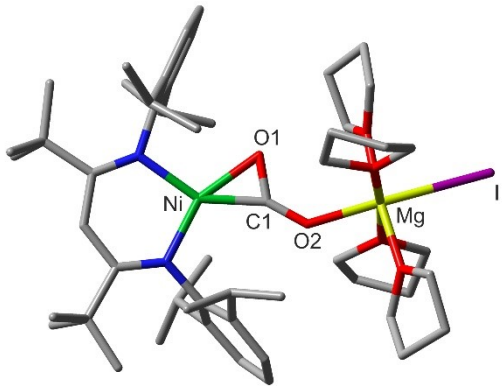

Figure S59: Optimised molecular structure of $[MgI(THF)_4(L^{tBu}NiCO_2)]$, **1´**. Hydrogen atoms are omitted for clarity. Selected bond lengths (Å) and angles (°): Ni-C1 1.823, Ni-O1 1.979, C1-O1 1.271, C1-O2 1.247, O2-Mg 2.023, Mg-I 3.033, O1-C1-O2 129.2.

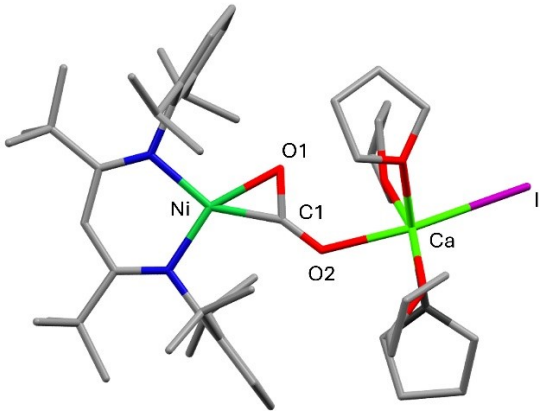

Figure S60: Optimised molecular structure of $[CaI(THF)_4(L^{tBu}NiCO_2)]$, **2´**. Hydrogen atoms are omitted for clarity. Selected bond lengths (Å) and angles (°): Ni-C1 1.821, Ni-O1 1.986, C1-O1 1.272, C1-O2 1.247, O2-Ca 2.306, Ca-I 3.154, O1-C1-O2 129.0.

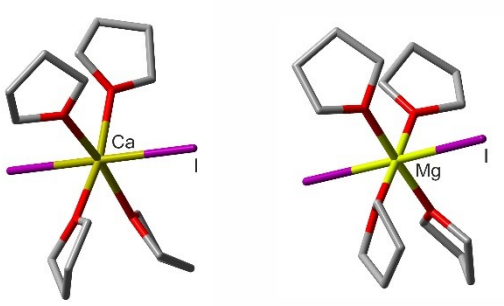

Figure S61: Optimised molecular structures of $[MgI_2(THF)_4]$ and $[CaI_2(THF)_4]$. Hydrogen atoms are omitted for clarity.

Using just simple molecules CaI_2 or MgI_2 as reactants lead formally to strongly exothermic reactions due to the neglection of lattice energy. For a more realistic description, $(AE)I_2(THF)_4$ units (see Figure S61) were used, assuming that a part of $(AE)I_2$ is already dissolved in THF before reaction with **1** or **2**.

The calculated reaction energies including corrections for zero-point vibrational energy are:

$$[Mg(THF)_4(L^{tBu}NiCO_2)_2] + [MgI_2(THF)_4] \rightleftarrows 2\,[MgI(THF)_4(L^{tBu}NiCO_2)] \qquad +\,2{,}7\ kJ/mol$$

$$[Ca(THF)_4(L^{tBu}NiCO_2)_2] + [CaI_2(THF)_4] \rightleftarrows 2\,[CaI(THF)_4(L^{tBu}NiCO_2)] \qquad -\,3{,}5\ kJ/mol$$

The molecular structure of the complex **3** as determined by X-ray diffraction analysis was used as starting point for a geometry optimization for the hypothetical complex **4**. The optimised molecules are shown in Figures S62 and S63.

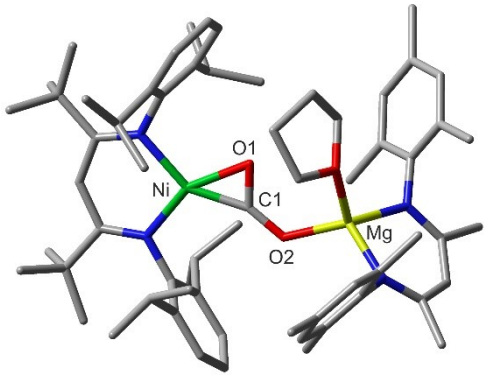

Figure S62: Optimised molecular structure of $[L^{tBu}NiCO_2Mg(THF)L^{Mes}]$, **3**. Hydrogen atoms are omitted for clarity. Selected bond lengths (Å) and angles (°): Ni-C1 1.829, Ni-O1 1.983, C1-O1 1.269, C1-O2 1.260, O2-Mg 1.959, O1-C1-O2 126.6.

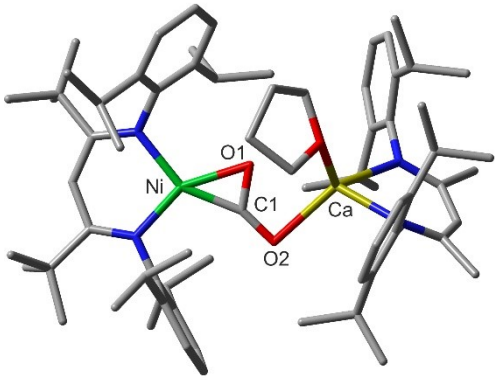

Figure S63: Optimised molecular structure of [$L^{tBu}NiCO_2Ca(THF)L^{Dipp}$], **4**. Hydrogen atoms are omitted for clarity. Selected bond lengths (Å) and angles (°): Ni-C1 1.818, Ni-O1 2.011, C1-O1 1.303, C1-O2 1.243, O2-Ca 12.361, O1-C1-O2 124.3.

Cartesian coordinates (Å) for the optimised theoretical structures (B3LYP-D3/Def2-TZVP&Def2-SVP) of the molecules shown above can be found in a separate xyz file.

6. Crystallographic Data

The data collections were performed with a BRUKER D8 VENTURE area detector with Mo-Kα radiation (λ = 0.71073 Å). Multi-scan absorption corrections implemented in SADABS[15] were applied to the data. The structures were solved by intrinsic phasing method (SHELXT-2013)[16] and refined by full matrix least square procedures based on F2 with all measured reflections (SHELXT-2014)[17] in the graphical user interface SHELXle[18] with anisotropic temperature factors for all non-hydrogen atoms. All hydrogen atoms were added geometrically and refined by using a riding model.

CCDC numbers 2346585 - 2346589 contain the supplementary crystallographic data for this paper. These data can be obtained free of charge from the Cambridge Crystallographic Data Centre via www.ccdc.cam.ac.uk/data_request/cif.

For compound **2** XRD measurements suggested that the complex crystallised in the space group $I4_1/a$. However, due to disorder around the carbonite ligands and to the high symmetry within the unit cell refinement of the structure was not successful and attempts to obtain crystalline material of higher quality failed. In order to show an image of the structure the data was solved in a triclinic space and isotropically refined (see Figure S64). Although **1** and **2** share a very similar constitution their solid-state structure exhibit slightly different geometrical arrangements: **1** exhibits a C_i symmetry with both ligand fragments being in plane while for **2** a C_{2v} symmetry is observed with both ligand fragments being perpendicular to each other.

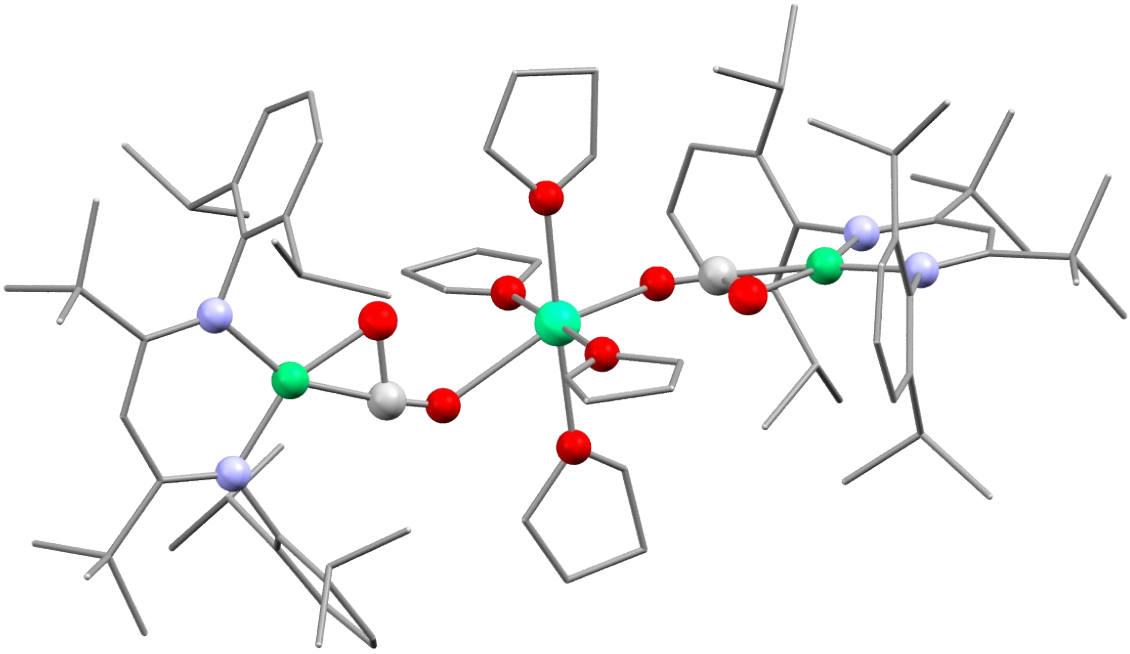

Figure S64: Molecular structure of **2** as determined by X-ray diffraction analysis.

Crystal structure	**$[Mg(THF)_4(L^{tBu}NiCO_2)_2]$, 1**	**$[Ca(18C6)(L^{tBu}NiCO_2)_2]$, 2-18C6**	**$[L^{tBu}NiCO_2Mg(THF)L^{Mes}]$, 3**
CCDC Depositon Nr	2346585	2346588	2346587
Chemical formula	$C_{88}H_{136}MgN_4Ni_2O_8 + C_6H_{14}$	$C_{84}H_{130}CaN_4O_{10} + 2\ C_4H_{10}O$	$C_{63}H_{90}MgN_4NiO_4 + C_4H_{10}O$
M_r/g*mol^{-1}	1605.90	1661.65	1108.51
Temperature/K	100(2)	100(2)	100(2)
Wave length/Å	0.71073	0.71073	0.71073
Crystal system	Triclinic	Monoclinic	Triclinic
Space group	P-1	P n	P-1
a/Å	10.331(1)	16.743(1)	11.787(1)
b/Å	12.155(2)	14.2680(1)	13.159(1)
c/Å	20.115(3)	20.019(1)	21.606(2)
α/°	85.509(5)	90	95.572(3)
β/°	76.039(5)	97.276(2)	101.159(3)
γ/°	68.417(5)	90	101.843(3)
Cell volume/ Å^3	2279.4(5)	4744.2(5)	3184.9(5)
Z	1	2	2
P_{calc}/g*cm^{-1}	1.170	1.163	1.156
μ(MoK_α)mm^{-1}	0.475	0.508	0.363
F(0 0 0)	874.0	1804.0	1204.0
Crystal size/mm	0.360*0.260*0.120	0.450*0.230*0.090	0.25*0.19*0.10
2θ area/°	2.29 - 25.485	2.500 – 26.420	1.984– 25.489
Measured reflexes	78371	239598	94354
Independent reflexes	9329	19500	11728
Parameters/ restrains	508/0	1189/1236	766/809
R_{int}	0.046	0.038	0.0560
R_1 (I>2σ(I))	0.0544	0.0374	0.059
wR_2 (all data)	0.1473	0.0985	0.1366
GooF (all data)	1.085	1.03	1.072
Flack-parameter	-	-	-
Max. u. min $\Delta\rho_{elect.}$ /e Å^{-3}	1.22 / -0.65	0.89 / -0.45	0.80 / -0.53
Absorption correction	Multi-scan	Multi-scan	Multi-scan
Max/min. transmission	0.745/0.6658	0.745/0.693	0.745/0.660

Crystal structure	**$[Ca(18C6)(L^{tBu}NiCO_3)_2]$, 5^{Ca}-18C6**	**$[Mg(THF)_4(L^{tBu}NiCO)_2]$, 6**	
CCDC Depositon Nr	2346586	2346589	
Chemical formula	$C_{84}H_{130}CaN_4Ni_2O_{12}$ + C_2H_3N	$C_{88}H_{138}MgN_4Ni_2O_6$ + 2 $C_4H_{10}O$	
M_r/g*mol^{-1}	1586.47	1637.98	
Temperature/K	100(2)	100(2)	
Wave length/Å	0.71073	0.71073	
Crystal system	Triclinic	Monoclinic	
Space group	P-1	$P2_1/c$	
a/Å	13.119(2)	28.041(4)	
b/Å	18.636(3)	14.697(2)	
c/Å	19.149(2)	24.348(4)	
α/°	81.507(5)	90	
β/°	86.676(5)	104.010(5)	
γ/°	74.077(5)	90	
Cell volume/ Å^3	4451.8(1)	9736(2)	
Z	2	4	
P_{calc}/g*cm^{-1}	1.184	1.118	
μ(MoK_α)mm^{-1}	0.539	0.446	
F(0 0 0)	1712.0	3576.0	
Crystal size/mm	0.12*0.07*0.05	0.45*0.19*0.11	
2θ area/°	1.923 - 26.397	2.039 - 26.440	
Measured reflexes	119060	627124	
Independent reflexes	18175	20019	
Parameters/ restrains	18175 / 984	1155/2309	
R_{int}	0.084	0.065	
R_1 (I>2σ(I))	0.040	0.065	
wR_2 (all data)	0.096	0.165	
GooF (all data)	1.03	1.05	
Flack-parameter	-	-	
Max. u. min $\Delta\rho_{elect.}$ /e Å^{-3}	0.83 / –0.38	0.98/-1.17	
Absorption correction	Multi-scan	Multi-scan	
Max/min. transmission	0.745/0.714	0.745/0.707	

Literature

[1] S. Wolff, V. Pelmenschikov, R. Müller, M. Ertegi, B. Cula, M. Kaupp, C. Limberg, *Chem. Eur. J.* **2024**, *30*, e202303112.

[2] P. Zimmermann, S. Hoof, B. Braun-Cula, C. Herwig, C. Limberg, *Angew. Chem.* **2018**, *130*, 7349-7353.

[3] S. J. Bonyhady, C. Jones, S. Nembenna, A. Stasch, A. J. Edwards, G. J. McIntyre, *Chem. Eur. J.* **2010**, *16*, 938-955.

[4] A. Tortajada, D. E. Anderson, E. Hevia, *Helv. Chim. Acta* **2022**, *105*, e202200060.

[5] L. Lochmann, J. Trekoval, *J. Org.Chem.* **1979**, *179*, 123-132.

[6] R. E. H. Kuveke, L. Barwise, Y. van Ingen, K. Vashisth, N. Roberts, S. S. Chitnis, J. L. Dutton, C. D. Martin, R. L. Melen, *ACS Cent. Sci.* **2022**, *8*, 855-863.

[7] P. Zimmermann, D. Ar, M. Rossler, P. Holze, B. Cula, C. Herwig, C. Limberg, *Angew. Chem. Int. Ed. Engl.* **2021**, *60*, 2312-2321.

[8] Gaussian 16, Revision A.03, M. J. Frisch, G. W. Trucks, H. B. Schlegel, G. E. Scuseria, M. A. Robb, J. R. Cheeseman, G. Scalmani, V. Barone, G. A. Petersson, H. Nakatsuji, X. Li, M. Caricato, A. V. Marenich, J. Bloino, B. G. Janesko, R. Gomperts, B. Mennucci, H. P. Hratchian, J. V. Ortiz, A. F. Izmaylov, J. L. Sonnenberg, D. Williams-Young, F. Ding, F. Lipparini, F. Egidi, J. Goings, B. Peng, A. Petrone, T. Henderson, D. Ranasinghe, V. G. Zakrzewski, J. Gao, N. Rega, G. Zheng, W. Liang, M. Hada, M. Ehara, K. Toyota, R. Fukuda, J. Hasegawa, M. Ishida, T. Nakajima, Y. Honda, O. Kitao, H. Nakai, T. Vreven, K. Throssell, J. A. Montgomery, Jr., J. E. Peralta, F. Ogliaro, M. J. Bearpark, J. J. Heyd, E. N. Brothers, K. N. Kudin, V. N. Staroverov, T. A. Keith, R. Kobayashi, J. Normand, K. Raghavachari, A. P. Rendell, J. C. Burant, S. S. Iyengar, J. Tomasi, M. Cossi, J. M. Millam, M. Klene, C. Adamo, R. Cammi, J. W. Ochterski, R. L. Martin, K. Morokuma, O. Farkas, J. B. Foresman, and D. J. Fox, Gaussian, Inc., Wallingford CT, 2016.

[9] A. D. Becke, *Phys. Rev. A* **1988**, 38, 3098–3100.

[10] C. Lee, W. Yang, R. G. Parr, *Phys. Rev. B* **1988**, 37, 785–789.

[11] A. D. Becke, *J. Chem. Phys*. **1993**, 98, 5648–5652.

[12] S. Grimme, S. Ehrlich, L. Goerigk, *J. Comp. Chem*. **2011**, 32, 1456–1465.

[13] F. Weigend, R. Ahlrichs, *Phys. Chem. Chem. Phys*. **2005**, 7, 3297.

[14] F. Weigend, *Phys. Chem. Chem. Phys.* **2006**, 8, 1057–1065.

[15] G. M. Sheldrick, SADABS 1996, University of Göttingen, Germany.

[16] G. M. Sheldrick, *Acta Crystallogr. A* **2015**, 71, 3.

[17] G. M. Sheldrick, *Acta Crystallogr. C* **2015**, 71, 3.

[18] C. B. Hübschle, G. M. Sheldrick, B. Dittrich, *J. Appl. Cryst.* **2011**, 44, 1281-1284.